UNIVERSITÉ DE MONTRÉAL

# VARIABLE CAPACITY MINI-SPLIT AIR SOURCE HEAT PUMP MODEL FOR TRNSYS

GUILLAUME ST-ONGE

DÉPARTEMENT DE GÉNIE MÉCANIQUE

ÉCOLE POLYTECHNIQUE DE MONTRÉAL

MÉMOIRE PRÉSENTÉ EN VUE DE L'OBTENTION

DU DIPLÔME DE MAÎTRISE ÈS SCIENCES APPLIQUÉES

(GÉNIE MÉCANIQUE)

NOVEMBRE 2018

© Guillaume St-Onge, 2018.

UNIVERSITÉ DE MONTRÉAL

ÉCOLE POLYTECHNIQUE DE MONTRÉAL

Ce mémoire intitulé :

VARIABLE CAPACITY MINI-SPLIT AIR SOURCE HEAT PUMP MODEL FOR TRNSYS

présenté par : ST-ONGE Guillaume

en vue de l'obtention du diplôme de : Maîtrise ès sciences appliquées

a été dûment accepté par le jury d'examen constitué de :

M. BERNIER Michel, Ph. D., président

M. KUMMERT Michaël, Doctorat, membre et directeur de recherche

M. VÉTEL Jérôme, Doctorat, membre

# DEDICATION

*To my wife and family:*

*thank you for your love,*

*support*

*and patience.*

*This document wouldn't exist without you.*

*I love you.*

# ACKNOWLEDGEMENTS

I'm extremely grateful to my professor and supervisor Michaël Kummert for his intelligence, his flexibility, his support and his love for MATLAB figures. You're right: it's so much nicer this way!

To Martin, Eric, Justin, Mathieu, John, Daniel, Bruno, Alexia, Amin and all my ex-colleagues at CanmetENERGY: merci de m'avoir si bien accueilli et supporté dans cet environnement de travail unique et stimulant. Votre passion est contagieuse!

In fact, thanks to everyone at CanmetENERGY (Natural Resources Canada) in Varennes, Québec, for their financial support on this project.

# RÉSUMÉ

Les pompes à chaleur sont des appareils efficaces qui ont la capacité d'extraire la majorité de leur énergie de sources renouvelables (air, sol, eau). Les pompes à chaleur air-air (PACAA), en particulier, sont utilisées depuis longtemps dans le secteur résidentiel canadien. Elles sont faciles à installer, leur coût en capital est moindre que les pompes à chaleur utilisant le sol (géothermie) et elles représentent une solution efficace de chauffage résidentiel qui peut jouer un rôle important dans les efforts internationaux pour diminuer les émissions de gaz à effet de serre.

Malgré ces avantages, les PACAA comportent leur part de contraintes qui limitent leur progression au pays. Elles sont reconnues pour multiplier les cycles marche/arrêt à charge partielle, ce qui affecte leur efficacité et cause de l'inconfort pour les usagers. Leurs performances chutent rapidement à basse température ambiante, au point où elles cessent complètement d'opérer dans les climats froids. Les économies sur les coûts peuvent alors devenir négligeables ou inexistantes dans certaines régions caractérisées par un climat froid et/ou un accès à de l'énergie abordable comme du gaz naturel.

De récents progrès technologiques ont favorisé la venue des compresseurs entraînés par des moteurs à fréquence variable (inverter-driven compressors) dans les pompes à chaleur air-air à capacité variable (PACAACV). Ces compresseurs permettent d'accroître la capacité de chauffage en maintenant un Coefficient de Performance (COP) supérieur à 1.0 à basse température ambiante, tout en offrant plus de confort et d'efficacité à charge partielle.

Cependant, certaines études rapportent que la technologie pourrait ne pas toujours livrer les performances (COP) annoncées sur le terrain. De plus, il y a présentement une pénurie de modèles de simulation disponibles pour aider les ingénieurs en bâtiment à mieux comprendre le comportement et estimer le potentiel d'économie énergétique des PACAACV.

Les objectifs principaux de ce projet sont donc d'effectuer des tests de laboratoire sur des pompes à chaleur air-air bibloc à capacité variable pour obtenir une cartographie de performance complète, et d'utiliser ces résultats pour créer un modèle de PACAACV simple et accessible pour utilisation dans le logiciel de simulation TRNSYS.

Des expériences détaillées ont été menées dans une chambre de test de contrôle climatique au laboratoire de CanmetÉNERGIE à Varennes. Le banc d'essai a pu soumettre l'unité à une variété

de charges de chauffage et de températures ambiantes définies par l'usager, tout en mesurant explicitement la fréquence du compresseur pour évaluer son impact sur la performance des PACAACV. Les tests ont été effectués de décembre 2016 à avril 2017 avec une PACAACV disponible sur le marché, dont la capacité nominale de chauffage et de climatisation s'élevaient respectivement à 4.0 kW (13,600 Btu/h) à 8.3 °C et 3.5 kW (12,000 Btu/h) à 35 °C.

Les résultats démontrent que le COP diminue généralement lorsque la vitesse du compresseur augmente et que la température ambiante diminue. Lorsque comparés aux données du manufacturier, ils montrent un bon accord en ce qui a trait à la capacité de chauffage. Toutefois, la puissance électrique consommée s'avère nettement supérieure aux attentes. Ceci mène à un COP significativement moindre que prédit par les données du manufacturier, particulièrement à basse fréquence de compresseur.

La mesure explicite de la fréquence de l'alimentation électrique du compresseur a permis de facilement représenter les résultats de tests sous la forme de régressions polynomiales multiples. En effet, une seule équation parvient à exprimer la capacité et la puissance électrique consommée en fonction de la température ambiante et de la fréquence du compresseur. Cette méthode s'avère la plus simple et efficace pour transférer les résultats des tests dans le nouveau modèle.

Un modèle spécifique aux PACAACV est développé en adaptant le type de pompe à chaleur air-air conventionnel existant dans TRNSYS (Type 954), de façon à ce que la performance modélisée de la PACAACV soit ajustée en fonction de la fréquence du compresseur au pas de temps actuel. Deux versions du modèle sont proposées pour prendre en considération l'effet des cycles de dégivrage : une première approche de déclassement en régime permanent, toute désignée pour les longs pas de temps (ex. horaires), ainsi qu'une approche originale qui modélise les cycles de dégivrage dynamiquement et qui s'avère de mise pour les pas de temps courts (ex. 1 min).

Les résultats de simulation révèlent un bon accord avec les mesures pour les deux versions du modèle (déclassement et dynamique). De plus, les fichiers de performance élaborés à partir des données de régression offrent des résultats de simulation plus précis que les fichiers de performance basés sur les données du manufacturier.

La suite des travaux devrait viser à valider les résultats et les courbes de performance avec d'autres systèmes de PACAACV (différents manufacturiers et tailles) et à procéder à davantage de simulations sous charge partielle. Une meilleure compréhension des cycles de dégivrage, des

mécanismes de protection et des performances en mode climatisation est également souhaitable, en route vers la création d'un modèle plus robuste qui pourrait offrir aux ingénieurs un outil de simulation fiable pour juger de la pertinence d'une adoption massive des PACAACV dans le secteur résidentiel canadien.

# ABSTRACT

Heat pumps are energy efficient devices that can extract the majority of their energy from a renewable cold source (air, ground, water). Air source heat pumps (ASHPs), in particular, have long been used in the Canadian residential sector. They are easy to install, their capital cost is lower than ground source heat pumps, and they represent an energy efficient space heating solution than can play a key role in international efforts to reduce GHG emissions.

Despite these advantages, ASHPs also have limitations that hinder their adoption in the country. They are known to cycle at part load, causing discomfort for users and reducing their efficiency. Their performance also decreases significantly with outdoor temperature, to the point where they stop operating in colder climates. Therefore, utility cost savings can become negligible or non-existent in some regions characterized by cold climate and/or access to affordable energy sources like natural gas.

Recent technological advancements have seen the use of inverter-driven compressors in variable capacity air source heat pumps (VCASHPs). Their benefit is to increase the heating capacity while maintaining an efficiency above 100 % at low ambient temperatures. They also maintain better comfort conditions at warmer temperatures by avoiding On/Off cycles.

However, some studies report that the technology may not always deliver the advertised improved efficiency in the field. Moreover, there is a lack of simulation models available for building designers to better understand VCASHP behaviour and estimate their energy saving potential.

The main objectives of this project are therefore to perform laboratory tests on a mini-split variable capacity air source heat pump to obtain a complete performance map, and use these results to create a simple and accessible VCASHP model in TRNSYS.

Detailed experiments were conducted in an environmental controllable test chamber at the CanmetENERGY-Varennes laboratory. The test bench can provide a variety of heating loads and user-defined ambient temperatures, while explicitly measuring compressor frequency to help establish its impact on VCASHP performance. Testing was conducted from December 2016 to April 2017 with a commercially available ductless VCASHP system with a rated heating and cooling capacity of 4.0 kW (13,600 Btu/h) at 8.3 °C and 3.5 kW (12,000 Btu/h) at 35 °C, respectively.

Results show that COP generally decreases at higher compressor speeds and lower outdoor temperatures. When compared to manufacturer data, they show good agreement for heating capacity, but measured power input proved to be much higher than expected. This leads to a measured COP significantly lower than predicted by manufacturer data, especially at lower compressor speeds.

Explicitly measuring the frequency of the compressor power allowed to conveniently represent test results with multiple polynomial regressions. Indeed, a single equation can express capacity and power input as a function of outdoor temperature and compressor frequency. This proved to be the simplest and most efficient way to export test results into the new model.

A VCASHP model is developed by adapting the existing conventional ASHP Type 954 in TRNSYS, so that the modeled performance of the VCASHP can be adjusted to the compressor frequency at the current timestep. Two versions of the model are proposed to take into account the effect of defrost cycles: a steady-state "derating" approach which is well adapted to long time steps (e.g. hourly), or an original approach that models the defrost cycles dynamically, which is well adapted to short time steps (e.g. 1 min).

Simulation results reveal good agreement with measurements for both versions of the model (derating and dynamic). The regression-based performance file yields better simulation results than the performance file based on manufacturer data.

Future work should aim at validating test results and performance curves with other ductless VCASHP systems (different manufacturers or sizes) and performing more simulations under part load conditions. A better understanding of defrost cycles, protection controls and performance in cooling mode should also be achieved, on the way to build a more robust model that could provide engineers a reliable simulation tool to assess the appropriateness of widespread adoption of VCASHPs in Canada's residential sector.

# TABLE OF CONTENTS

DEDICATION ..... III

ACKNOWLEDGEMENTS ..... IV

RÉSUMÉ ..... V

ABSTRACT ..... VIII

LIST OF TABLES ..... XIV

LIST OF FIGURES ..... XV

LIST OF SYMBOLS AND ABBREVIATIONS ..... XIX

LIST OF APPENDICES ..... XXIV

CHAPTER 1 INTRODUCTION AND LITERATURE REVIEW ..... 1

1.1 Heat pumps ..... 1

1.1.1 Performance of heat pumps (COP, EER, HSPF, SEER) ..... 3

1.1.2 Heat pumps worldwide ..... 4

1.1.3 Air source heat pumps ..... 6

1.1.4 Variable capacity air source heat pumps ..... 8

1.2 Testing ..... 12

1.2.1 Standardized tests for conventional heat pumps ..... 12

1.2.2 New standardized tests for variable capacity heat pumps ..... 13

1.2.3 Conventional heat pumps: test results ..... 14

1.2.4 Variable capacity heat pumps: laboratory results ..... 15

1.2.5 Variable capacity heat pumps: field results ..... 17

1.3 Modeling ..... 20

1.3.1 Software and conventional heat pump models ..... 20

1.3.2 Variable capacity heat pump models ..... 21

1.4 Conclusions of the literature review ..... 28
1.5 Objectives ..... 29
1.6 Thesis outline ..... 30
CHAPTER 2 METHODOLOGY ..... 31
2.1 Test bench ..... 31
2.1.1 The heat pump ..... 32
2.1.2 Fresh air fans and electric baseboards ..... 33
2.1.3 Instrumentation ..... 33
2.2 Calculating the heat output ..... 36
2.2.1 Refrigerant side ..... 36
2.2.2 Air side ..... 37
2.3 Fresh air fans control strategy ..... 39
2.3.1 Constant outdoor shed temperature ..... 39
2.3.2 Constant indoor shed heating load ..... 40
2.4 Approach ..... 42
CHAPTER 3 RESULTS ..... 43
3.1 Results overview ..... 43
3.2 Detailed analysis ..... 44
3.2.1 Normal operation ..... 44
3.2.2 Refrigerant side and defrost cycles ..... 46
3.2.3 Solar gains ..... 55
3.2.4 Short cycling ..... 57
3.2.5 Protection mechanisms ..... 58
3.3 Steady state results ..... 61

3.4 Comparison to manufacturer data ..... 62

3.4.1 Frequency bins ..... 62

3.4.2 How manufacturer data is obtained ..... 63

3.4.3 Analysis ..... 65

3.4.4 Coefficients of determination ..... 67

3.5 Multiple polynomial regressions ..... 68

3.6 Conditions that trigger defrost cycles ..... 69

3.7 Comparison with conventional heat pumps ..... 70

3.8 Uncertainty analysis ..... 73

3.9 Influence of indoor temperature ..... 76

CHAPTER 4 THE MODEL ..... 78

4.1 General approach ..... 78

4.2 New performance file ..... 79

4.2.1 Manufacturer data based VCHP performance file ..... 80

4.2.2 Regression-based VCHP performance file ..... 82

4.2.3 Fortran executable ..... 83

4.3 Two options to simulate defrost cycles ..... 83

4.4 Type 3254a – Dynamic model ..... 84

4.5 Type 3254b – Pseudo-steady-state model ..... 86

4.6 From Type 954 to Type 3254: modifications to the TRNSYS Proforma (tmf file) and Fortran code ..... 87

CHAPTER 5 SIMULATION RESULTS ..... 89

5.1 Type 3254a – Dynamic model ..... 90

5.2 Type 3254b – Pseudo-steady-state model ..... 95

CHAPTER 6 CONCLUSION AND RECOMMENDATIONS ..... 97

6.1 Contributions ..... 97

6.2 Limitations ..... 98

6.3 Recommendations for future work ..... 99

BIBLIOGRAPHY ..... 100

APPENDICES ..... 108

# LIST OF TABLES

Table 2-1: Detailed instrumentation list ..... 35

Table 2-2: Indoor unit outlet air speed and volumetric air flow equivalences (adapted from Mitsubishi Electric Corporation (2009a)) ..... 38

Table 2-3: PID signal values and corresponding fan voltage levels ..... 40

Table 3-1: Example of VCHP manufacturer data at a rated frequency of 52.5 Hz (Mitsubishi Electric Corporation 2009b) ..... 64

Table 3-2: Coefficients of determination for capacity and power input for every frequency bin.. 67

Table 3-3: Uncertainty of main instruments ..... 73

Table 4-1: Capacity and power input correction factor vs frequency ..... 81

Table 4-2: New parameters and inputs for Type 3254a ..... 87

Table 4-3: New parameters and inputs for Type 3254b ..... 88

# LIST OF FIGURES

Figure 1-1: Main components of a heat pump system (left) and the vapor compression refrigeration cycle (adapted from Manteufel (2014)) .....2

Figure 1-2: Heating capacity of a 1-ton conventional ASHP and the DOE load line with respect with outdoor temperature (adapted from Kegel & McDonald (2015)) .....7

Figure 1-3: Heating capacity of a 1-ton and a 2-ton conventional heat pump and the DOE load line with respect with outdoor temperature (adapted from Kegel & McDonald (2015)) .....8

Figure 1-4: Heating capacity of a VCASHP at selected compressor speeds with respect to outdoor temperature (adapted from Kegel & McDonald (2015)) .....9

Figure 1-5: Room temperature evolution of a typical conventional (left) and inverter (right) air source heat pump in heating mode (adapted from Gomes et al. (2013)) .....10

Figure 1-6: Typical mini-split ASHP installation (Energy Star 2018).....11

Figure 1-7: TRNSYS distributed approach VCGSHP model from Bouheret and Bernier (2017) 25

Figure 1-8: Effect of the defrost degradation coefficient on heating capacity (Filliard 2009) .....28

Figure 2-1: Test bench (Tardif et al. 2016) .....31

Figure 2-2: Testing sheds with indoor unit (1), outdoor unit (2), exhaust fans (3) and electric baseboards (4) .....32

Figure 2-3: Indoor (left) and outdoor (right) unit of the VCASHP (Tardif et al. 2016) .....32

Figure 2-4: Fresh air fans and louvers (Tardif et al. 2016) .....33

Figure 2-5: R-410A heat pump cycle p-h diagram (adapted from Tardif et al. (2016)) .....34

Figure 2-6: Schematic representation of instrumentation (Tardif et al. 2016).....34

Figure 2-7: Anemometer added to the test bench .....38

Figure 2-8: Exhaust fan speed PID voltage with respect to $(UA)_T$ for the indoor shed.....41

Figure 2-9: Range of possible heating load lines induced by the fresh air fans on the indoor shed .....42

Figure 3-1: Global performance results for heating capacity with respect to outdoor shed temperature ..... 43

Figure 3-2: Global performance results for COP with respect to outdoor shed temperature ..... 44

Figure 3-3: Typical evolution of indoor air temperature, compressor frequency, refrigerant mass flow rate and indoor heat exchanger inlet refrigerant temperature ..... 45

Figure 3-4: Heating capacity and indoor shed temperature over a typical night of testing (approximately $T_{outdoor_shed}$ = -15 °C) ..... 46

Figure 3-5: R-410A heat pump cycle p-h diagram in heating mode (adapted from Klein (2016)) 47

Figure 3-6: Measured refrigerant temperature at the condenser inlet ($T_4$) compared to the saturated vapour point ($T_{4,assump}$, in blue) ..... 48

Figure 3-7: Measured ($h_4$) and assumed ($h_{4,assump}$) refrigerant enthalpy at the condenser inlet ..... 49

Figure 3-8: Measured and assumed refrigerant heat output on refrigerant side ..... 50

Figure 3-9: Air Volumetric Flow Rate at the indoor HX outlet of the heat pump ..... 51

Figure 3-10: Supply and indoor temperatures, along with heat output calculated on air side ..... 52

Figure 3-11: Heat output measured (black) and assumed (blue) on refrigerant side compared to heat output measured on air side (red) ..... 53

Figure 3-12: Comparison of the indoor temperature profile (yellow) to the heat output measured on air side (red) and assumed on refrigerant side (blue) ..... 54

Figure 3-13: COP of steady-state (filled) and transient ('x') data points ..... 55

Figure 3-14: Measured ambient temperature (RTD) compared to reference (OMEGA) ..... 56

Figure 3-15: Evolution of the dry-bulb ambient temperature, indoor temperature and compressor frequency with the RTD ambient temperature probe under direct sunlight ..... 57

Figure 3-16: Short cycling heat output and frequency (McDonald & Kegel 2017) ..... 58

Figure 3-17: Discharge temperature ($T_2$) protection at full load ..... 59

Figure 3-18: Compressor outlet pressure ($P_2$) protection control ..... 60

Figure 3-19: Steady-state results for heating capacity with respect to outdoor shed temperature . 61

Figure 3-20: Steady-state results for power input with respect to outdoor shed temperature.....61

Figure 3-21: Steady-state results for COP with respect to outdoor shed temperature .....62

Figure 3-22: Polynomial linear regression for capacity vs outdoor shed temperature (50 Hz) .....63

Figure 3-23: Example of capacity (left) and power input (right) correction curves for frequency (Mitsubishi Electric Corporation 2009b) .....64

Figure 3-24: Steady state - Measured and manufacturer published heating capacity vs outdoor shed dry-bulb temperature for a variety of chosen frequencies.....65

Figure 3-25: Steady state - Measured and manufacturer published power input vs outdoor dry-bulb temperature for a variety of chosen frequencies .....66

Figure 3-26: Steady state - Measured and manufacturer published COP vs outdoor shed dry-bulb temperature for a variety of chosen frequencies.....66

Figure 3-27: Multiple polynomial regression for heat output vs outdoor shed temperature and compressor frequency .....68

Figure 3-28: Multiple polynomial regression for power input vs outdoor shed temperature and compressor frequency .....69

Figure 3-29: Influence of outdoor air and unit temperature (left) and timer (right) on defrost cycles .....70

Figure 3-30: Comparing heating capacity between different sizes of conventional ASHPs and a VCASHP at different compressor frequencies (adapted from Kegel & McDonald (2015)) .71

Figure 3-31: Comparing COP between different sizes of conventional ASHPs and a VCASHP at different compressor frequencies (adapted from Kegel & McDonald (2015)).....72

Figure 3-32: Evolution of enthalpy and refrigerant temperature at the indoor exchanger inlet and outlet.....74

Figure 3-33: Steady state - Measured (with uncertainty) and manufacturer published heating capacity vs outdoor shed dry-bulb temperature for a variety of chosen frequencies.....75

Figure 3-34: Measured (with uncertainty) and manufacturer published COP vs outdoor shed dry-bulb temperature for a variety of chosen frequencies.....76

Figure 3-35: COP of low frequency (30-50 Hz, 'o') and high frequency (90-112.5 Hz, '+') steady state data points with respect to outdoor shed dry-bulb temperature .....77

Figure 4-1: Typical ASHP model (left) compared to a typical new VCASHP model (right) .....78

Figure 4-2: Conventional ASHP (left) compared to new VCASHP performance file (right) .....80

Figure 4-3: Frequency correction factors vs normalized frequency curve fits for capacity (blue) and power (red) .....82

Figure 4-4: Reproducing the dynamics of defrost cycles with new variables $t_{cycle}$, $t_{recovery}$ and $t_{duration}$ .....84

Figure 4-5: Defrost simulation control strategy at every time step .....86

Figure 5-1: Ambient and outdoor shed temperature on April 4-5th, 2017 .....89

Figure 5-2: Type 3254a: Comparing measured (refrigerant and air side) to simulated heat output (manufacturer and regression performance table).....90

Figure 5-3: Type 3254a: Comparing measured to simulated supply temperature (manufacturer and regression performance table) .....91

Figure 5-4: Type 3254a: Comparing measured to simulated indoor temperature (manufacturer and regression performance table) .....92

Figure 5-5: Type 3254a: Comparing measured to simulated frequency (manufacturer and regression performance table) .....93

Figure 5-6: Type 3254a: Comparing measured to simulated power input (manufacturer and regression performance table) .....94

Figure 5-7: Type 3254a: Simulation of heat output with a timestep of 5 min .....94

Figure 5-8: Type 3254b: Comparing measured (refrigerant and air side) to simulated heat output (manufacturer and regression performance table).....95

Figure 5-9: Type 3254b: Comparing measured to simulated indoor temperature (manufacturer and regression performance table) .....96

# LIST OF SYMBOLS AND ABBREVIATIONS

| | |
|---|---|
| AHRI | Air-Conditioning, Heating, and Refrigeration Institute |
| ANSI | American National Standards Institute |
| ASHP | Air Source Heat Pump |
| ASHRAE | American Society of Heating, Refrigerating and Air-Conditioning Engineers |
| CapRatio | Normalized capacity ratio extracted from the VCASHP performance table |
| CCASHP | Cold Climate Air Source Heat Pump |
| CFC | Second generation refrigerant |
| CFM | Volumetric Flow Rate ($ft^3$/min) |
| COP | Coefficient Of Performance |
| $Cp_{air}$ | Specific Heat of Air (J/kg-K) |
| CSA | Canadian Standards Association |
| DefrostPnlty | Defrost penalty ratio of the simulated heat output, Pseudo-steady-state model |
| DOE | United States Department of Energy |
| $DOE_{load\ line}$ | Representative heating load line on a single-family detached home |
| DHP | Ductless mini-split Heat Pump |
| EEV | Electronic Expansion Valve |
| EER | Energy Efficiency Ratio ((Btu/h)/W) |
| EES | Engineering Equation Solver |
| EPRI | Electric Power Research Institute |
| $\delta\Delta h_{indoorHX}$ | Relative Error on Enthalpy difference at indoor HX inlet and outlet |
| $\delta\dot{m}_{ref}$ | Relative Error on Refrigerant Mass Flow Rate |
| $\delta\dot{Q}_{ref_side}$ | Relative Error on Rate of Heat Transfer, on Refrigerant Side |
| EWT | Entering Water Temperature, in a Ground Source Heat Pump (°C) |

| | |
|---|---|
| $f_i$ | Estimated dependent variable with the polynomial curve fit |
| freq | Frequency of the Heat Pump compressor power (Hz) |
| GHG | Greenhouse Gas |
| GSHP | Ground Source Heat Pump |
| $h_i$ | Refrigerant Enthalpy at a specific point of the refrigeration cycle (J/kg) |
| $h_{4,assump}$ | Refrigerant enthalpy at indoor HX inlet assumed at saturated vapour point (J/kg) |
| $\Delta h_{indoorHX}$ | Enthalpy difference of refrigerant between inlet and outlet of the indoor HX (J/kg) |
| HSPF | Heating Seasonal Performance Factor (Btu/Wh) |
| HX | Heat Exchanger |
| IDB | Intake Air Dry-Bulb Temperature (°F) |
| $\dot{m}_{inf}$ | Infiltration Air Flow Rate (kg/s) |
| $\dot{m}_{ref}$ | Refrigerant Mass Flow Rate (g/s) |
| $\dot{m}_{v_inlet}$ | Air Volumetric Flow Rate at the indoor HX inlet of the heat pump (kg/s) |
| $\dot{m}_{v_outlet}$ | Air Volumetric Flow Rate at the indoor HX outlet of the heat pump (kg/s) |
| NEEP | Northeast Energy Efficiency Partnerships |
| $P_i$ | Refrigerant Pressure at a specific point of the refrigeration cycle (kPa) |
| $\dot{Q}_{air_side}$ | Rate of Heat Transfer, on Air Side (W) |
| $Q_C$ | Heat extracted from a cold source |
| $\dot{Q}_{EQ}$ | Internal Gains from equipment (W) |
| $Q_H$ | Heat delivered to a hot source |
| $\dot{Q}_h$ | Total Heating Capacity (W) |
| $\dot{Q}_{h,ref}$ | Reference Total Heating Capacity (W) |
| $\dot{Q}_L$ | Internal Gains from lighting (W) |
| $\dot{Q}_P$ | Internal Gains from occupants (W) |

| | |
|---|---|
| $\dot{Q}_{ref_side}$ | Rate of Heat Transfer, on Refrigerant Side (W) |
| $\dot{Q}_{ref_side,assump}$ | Rate of Heat Transfer with enthalpy assumed at saturated vapour point (W) |
| $\dot{Q}_{sens}$ | Sensible Cooling Capacity (W) |
| $\dot{Q}_{sens,ref}$ | Reference Sensible Cooling Capacity (W) |
| $\dot{Q}_{solar}$ | Solar gains (W) |
| $\dot{Q}_{total}$ | Total cooling capacity (W) |
| $\dot{Q}_{total,ref}$ | Reference Total cooling capacity (W) |
| PID | Proportional–Integral–Derivative |
| $Power_c$ | Power consumption, in cooling (W) |
| $Power_{c,ref}$ | Reference Power consumption, in cooling (W) |
| $Power_h$ | Power consumption, in heating (W) |
| $Power_{h,ref}$ | Reference Power consumption, in heating (W) |
| PwrRatio | Normalized power ratio extracted from the VCASHP performance table |
| $R^2$ | Coefficient of determination (R-squared) of the linear regression |
| RatedCap | Rated Capacity (W) |
| RecovPnlty | Penalty factor for transient effects in indoor HX and outdoor HX after defrost |
| RPM | Frequency for rotation, in Revolutions Per Minute |
| RTD | Resistance Temperature Detector |
| SEEM | Simplified Energy Enthalpy Model |
| SEER | Seasonal Energy Efficiency Ratio (Btu/Wh) |
| $SS_{reg}$ | Sum of the squares of differences between measured and estimated curve-fit values |
| $SS_{tot}$ | Sum of the squares of differences between measured and mean of dependent var. |
| t | Current time step of the simulation (min) |
| $\tau$ | Recovery time constant of the heat pump (min) |

| | |
|---|---|
| $t_{cycle}$ | Duration of the heat pump cycle (min) |
| $t_{duration}$ | Duration of the defrost cycle of the heat pump (min) |
| $t_{recovery}$ | Duration of recovery period of the heat pump after defrost (min) |
| $T_{amb}$ | Ambient Dry-Bulb Air Temperature (°C) |
| $T_{db}$ | Entering Air Dry-Bulb Temperature (°C) |
| $T_i$ | Refrigerant Temperature at a specific point of the refrigeration cycle (°C) |
| $T_{4,assump}$ | Refrigerant Temperature at indoor HX inlet assumed at saturated vapour point (°C) |
| $T_{indoor_shed}$ | Air Temperature of the indoor shed (demand side), in °C |
| $T_{outdoor_shed}$ | Air Temperature of the outdoor shed (sink), in °C |
| $T_{ref}$ | Reference Temperature (283 K) |
| $T_{set}$ | Air Temperature Setpoint (°C) |
| $T_{supply}$ | Supply Air temperature at the indoor HX outlet of the heat pump (°C) |
| $T_{wb}$ | Entering Air Wet Bulb Temperature (°C) |
| $T_{w,in}$ | Entering Water Temperature (°C) |
| TC | Total Capacity of the Heat Pump ($x10^3$ Btu/h) |
| TESS | Thermal Energy System Specialists (Madison, Wisconsin) |
| TPC | Total Power Consumption of the Heat Pump (kW) |
| TRNSYS | System Simulation Tool |
| u ($\Delta h_{indoorHX}$) | Absolute uncertainty on indoor HX refr. enthalpy diff. between inlet/outlet (J/kg) |
| $U_TA_T$ | Heat Transfer Coefficient and Area over which heat transfer occurs (W/K) |
| $(UA)_T$ | Global Heat Loss and Infiltration Product (W/K) |
| $\dot{V}_{air}$ | Air Volumetric Flow Rate of a Water-to-Air Heat Pump |
| $\dot{V}_{air,ref}$ | Reference Air Volumetric Flow Rate of a Water-to-Air Heat Pump |
| $\dot{V}_w$ | Water Volumetric Flow Rate of a Water-to-Air Heat Pump |

| | |
|---|---|
| $\dot{V}_{w,ref}$ | Reference Water Volumetric Flow Rate of a Water-to-Air Heat Pump |
| VCASHP | Variable Capacity Air Source Heat Pump |
| VFD | Variable Frequency Drive |
| VRF | Variable Refrigerant Flow |
| $W_{in}$ | Work input at the compressor |
| $w_{inlet}$ | Humidity ratio at the indoor HX inlet of the heat pump (g of water / kg of dry air) |
| $w_{outlet}$ | Humidity ratio at the indoor HX outlet of the heat pump (g of water / kg of dry air) |

# LIST OF APPENDICES

APPENDIX A – COMPANION SOFTWARE PACKAGE.....108

# CHAPTER 1 INTRODUCTION AND LITERATURE REVIEW

The Canadian residential sector accounts for a significant part of the country's secondary energy use (17 %) and greenhouse gas emissions (14 %) (NRCan-OEE 2016). Heat pumps have been known to provide important environmental and economic benefits, and could potentially play a key role in helping the country meet the ambitious targets of the Paris Agreement.

This chapter defines the heat pump concept, details the factors that have hindered their widespread adoption in colder climates and summarizes the recent technological advancements that led to variable capacity air source heat pumps (VCASHPs). Then, current testing procedures and results are reviewed, along with available VCASHP models, to demonstrate their utility and identify their limitations. Finally, the objectives and scope of the project are presented, along with the thesis outline.

## 1.1 Heat pumps

Just like a pump can force a fluid in a specific direction, heat pumps are devices that have the ability to go against spontaneous heat transfer and move thermal energy from a cold to a hot source. They are used in residential, commercial and industrial applications as an efficient way to regulate space or water temperature, either in heating or cooling mode.

The origins of the heat pump can be traced back to the early 19th century, when Carnot exposed the vapor compression refrigeration concept. Fifty years later, Lord Kelvin is generally credited as the first to propose a practical heat pump system - also known as a "heat multiplier" - showing that a refrigeration machine could also be used in heating (Reay and Macmichael 1988). The increasing need for artificial refrigeration and the evolution of electric power transmission then contributed to the expansion of air conditioning in the 1930s (Janssen 1999). But the turning point truly came in the 1970's after the oil crisis, when the need for an alternative to fossil fuels identified heat pumps as a potential solution. However, these devices were not able to establish as a viable technology, and the market collapsed when oil prices went down in the 1980s (Quaschning 2010). Nowadays, technological advancement and international efforts to reduce GHG emissions has brought heat pumps back to the forefront.

The main components of a heat pump system (Aye 2007) and the vapor compression refrigeration cycle are shown in Figure 1-1.

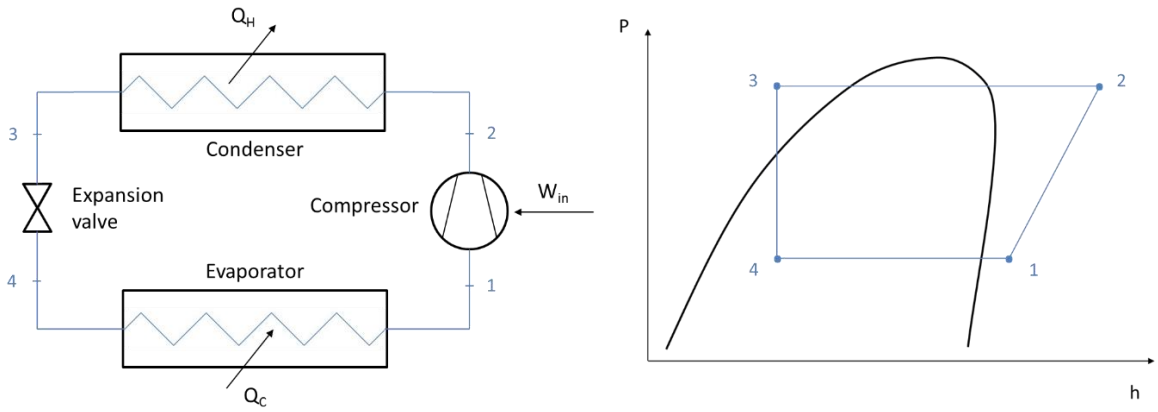


Figure 1-1: Main components of a heat pump system (left) and the vapor compression refrigeration cycle (adapted from Manteufel (2014))

Refrigerant: the fluid that circulates through the heat pump pipes. Its low boiling point (typically below -30 °C) allows to extract heat from the cold source - e.g. ambient air in heating mode - even under cold weather. Since the Montreal protocol (1987), second generation refrigerants (CFCs) like R-12 or R-22 have been replaced by new refrigerants that do not contribute to ozone depletion (e.g. R-134a or R-410A).

Compressor: mechanical device that increases the refrigerant pressure and temperature before sending it to the condenser. The electrical energy consumed by the compressor is generally much lower than the useful heat, which makes the heat pump a highly efficient device (more details will follow).

Evaporator: heat exchanger that removes heat from the cold source. Therefore, refrigerant temperature must be lower than the cold source. Refrigerant enters the evaporator in a cold liquid state and exits as cold vapor before being sent towards the compressor. The evaporator can either be the indoor unit (cooling mode) or the outdoor unit (heating mode).

Condenser: heat exchanger that rejects heat to the hot source. Therefore, refrigerant temperature must be higher than the hot source. Refrigerant enters the condenser in a hot vapor state and exits

as hot liquid before being sent towards the expansion valve. The condenser can either be the indoor unit (heating mode) or the outdoor unit (cooling mode).

Expansion valve: component that allows the refrigerant pressure and temperature to decrease before entering the evaporator, in order to complete the vapor compression cycle. Recent technology improvements brought Electronic Expansion Valves (EEVs), which can provide real-time adjustment of refrigerant flow to optimize the heat pump performance.

The heat pump type is determined by the medium used to exchange heat with the outdoor environment. Main heat pump types include air-source, ground-source and water-source heat pumps.

### 1.1.1 Performance of heat pumps (COP, EER, HSPF, SEER)

A few ratios exist to evaluate the performance of heat pumps, as described in (NRCan 2004).

The coefficient of performance (COP) is a dimensionless ratio equivalent to the heat pump's useful heat transfer divided by the total energy input. The useful heat movement is the extracted and supplied heat in cooling and heating mode, respectively (Equations (1.1) and (1.2)).

$$COP_{cooling} = Heat\ extracted\ (Wh)/\ Energy\ input\ (Wh) \tag{1.1}$$

$$COP_{heating} = Heat\ supplied\ (Wh)/\ Energy\ input\ (Wh) \tag{1.2}$$

The energy efficiency ratio (EER) is sometimes used to express the heat pump performance in cooling. The EER expresses the same ratio as the cooling COP, but it is not dimensionless, since the cooling capacity is expressed in Btu/h, as shown in Equation 1.3. Like the COP, it varies with outdoor and indoor temperatures.

$$EER_{cooling} = Cooling\ capacity\ (Btu/hr)/\ Power\ input\ (W) \tag{1.3}$$

To measure the heating performance of a heat pump over an entire season, the heating seasonal performance factor (HSPF) ratio is introduced. Equation (1.4) defines it as the total heat output in Btu (including auxiliary heat) over the entire heating season, divided by the total electrical energy

used (in watt-hour) by the heat pump and the auxiliary. Obviously, the weather data used has a strong impact on the HSPF calculation, and can lead to significant discrepancies (more details will follow).

$$HSPF_{heating} = Total\ heat\ output\ (Btu) / Total\ energy\ input\ (Wh) \qquad (1.4)$$

Finally, the seasonal energy efficiency ratio (SEER) is similar to the HSPF, but for cooling performance (Equation 1.5). This ratio is "based on a climate with an average summer temperature of 28°C" (NRCan 2004).

$$SEER_{cooling} = Total\ cooling\ (Btu) / Total\ energy\ input\ (Wh) \qquad (1.5)$$

To summarize, the COP of heat pumps is generally well above 1.0 (typically around 3.0 in heating, and 4.0 in cooling), meaning they perform significantly better than regular electric baseboards.

Moreover, Carnot's theorem sets the theoretical maximum COP in cooling and heating. The "lift" is defined as the difference between the hot and the cold source temperature (in Kelvin). As seen with Equations (1.6) and (1.7), a large lift can significantly decrease the maximum possible COP at a specific outdoor temperature.

$$COP_{max,cooling} = T_{cold} / (T_{hot} - T_{cold}) \qquad (1.6)$$

$$COP_{max,heating} = T_{hot} / (T_{hot} - T_{cold}), \qquad (1.7)$$

where temperatures are expressed in K.

### 1.1.2 Heat pumps worldwide

Air conditioners – a sub-category of heat pumps, only capable of operating in cooling mode – are well established worldwide (global market valued at US$ 92.6 billion), especially in warmer climates in Asia Pacific (BSRIA 2017). However, it proved difficult to obtain a clear picture of the current global market penetration of heat pumps. Despite growing interest for the technology in

China (IEA Heat Pumping Technologies Program 2017), it can safely be said that their adoption remains quite limited.

According to Nishihata (2013), heat pumps "are expected to account for between 5 % and 20 % of the [European Union]'s renewable energy target for 2020", which is set at 20 % final energy consumption from renewable sources (European Commission 2016). Moreover, recent data shows that heat pump systems can only be found in 2.5 % of Canadian households (Kegel et al. 2017).

Lapsaa et al. (2017) provide key insights about the situation in North America. Heat pump sales in the United States have been greatly affected by the 2006 housing crisis and have just recently got back to early 2000's levels. The residential sector accounts for the vast majority of the sales, and heat pumps remain significantly less popular than air-conditioners and furnaces in both US and Canada.

Many factors can explain this slow growth. The high capital cost remains a major hurdle, especially for ground source heat pumps (GSHPs). The disappointing performance of air source heat pumps (ASHPs) at lower ambient temperatures (more details will follow) have also hindered their widespread adoption in countries with colder climates like Canada.

Moreover, longer term economic benefits associated with heat pump adoption are affected by energy prices in a given region. In recent years, the extremely low natural gas rates in Ontario, for example, lead to an astronomical payback period of more than 40 years for any heat pump technology (Kegel et al. 2014).

The GHG emissions savings induced by a heat pump also depend on how the electricity is generated and which energy source they replace. In Québec - where hydroelectricity dominates, meaning that the $CO_2$ intensity of electricity generation is very low - the savings are negligible for residential heat pump systems since they often replace direct (resistance) electric heating.

On the contrary, in regions where the electricity is not generated from a clean energy source, the high coefficient of performance of heat pumps brings significant GHG emissions savings compared to resistance electric heating (but not necessarily compared to gas furnaces). Unfortunately, this link between GHG emissions savings and energy source is not always clearly understood. Nishihata (2013) reports that many countries do not consider heat pumps as renewable technologies, despite the fact that these devices extract the majority of their energy from a

renewable cold source like air or water. As a result, no incentives are allowed, which hinders their adoption.

Finally, current advertised heat pump performance often generates skepticism and confusion (more details will follow). According to Nishihata (2013), “defining international standards for heat pump efficiency” could contribute to increase their adoption.

### 1.1.3 Air source heat pumps

Air source heat pumps are currently the most prevalent type of heat pump on the market worldwide (European Commission 2016). They are easy to install, their capital cost is lower than ground source heat pumps, and as mentioned before, they can provide significant utility cost and GHG emissions savings in some regions.

Two main types exist: air-to-water heat pumps - used with hydronic heating systems - and far more widespread air-to-air heat pumps (NRCan 2004).

Despite their many advantages, ASHPs also have limitations that reduce their advantages in colder climates. Figure 1-2 shows that their heating capacity declines at colder outdoor temperatures. On the other hand, the heating load of the building increases with colder temperature. Indeed, the blue dashed line in Figure 1-2 displays a representative heating load for a single-family detached home. This alternative DOE load line from Rice et al. (2015) is obtained with Equation (1.8), where the outdoor temperature is in °F and the rated cooling load ($Q_c$) is set at 12 000 Btu/h for the tested unit.

$$DOE_{load\ line} = 1.15 * Q_c * \left[\frac{60 - T_{OA}}{60 - 5}\right] \tag{1.8}$$

The point where both curves (heat load and heat pump capacity) meet is called the “balance point”. Below the balance point, the heat output provided by the ASHP is not sufficient to entirely heat the space. Auxiliary heating must then be used to fill the gap, which affects the performance of the system because electric resistance heating is most often used, with a COP of 1.

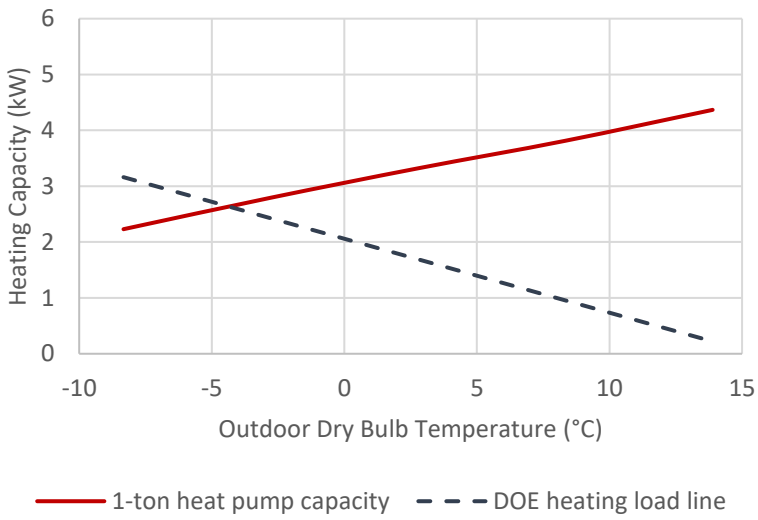


Figure 1-2: Heating capacity of a 1-ton conventional ASHP and the DOE load line with respect with outdoor temperature (adapted from Kegel & McDonald (2015))

Moreover, ASHPs stop to operate under very cold weather. A cutoff temperature (typically around -10 °C) is set to prevent extreme discharge refrigerant temperatures that could damage the heat pump (Messmer 2013). The system therefore has to rely entirely on auxiliary electrical heating at outdoor temperatures below the cutoff point, which also greatly penalizes the system performance and creates a clear economic disadvantage for homeowners in regions with access to affordable fossil fuel (Messmer 2013).

In theory, this problem could be partly solved by oversizing the heat pump – like with the 2-ton conventional heat pump in Figure 1-3 – to obtain a colder balance point (or no balance point at all in this case). However, Cummings et al. (2014) report that this strategy is not recommended by many heat pump standards. It is known to lead to excessive on/off cycling for conventional single-speed systems (Munk et al. 2014), which causes uncomfortable room temperature fluctuations and "inefficiencies that reduce the performances of units during the transient period" (Bagarella et al. 2013). Excessive cycling is also linked to humidity problems in cooling when the heat pump "ON" cycles are too short (Munk et al. 2014). In some extreme cases, it can even cause important ice accumulation on the evaporator because the heat pump may not operate long enough to trigger defrost cycles (SouthShore HVAC 2017).

Defrost cycles prevent long term ASHP performance from deteriorating by melting the ice that forms on the evaporator under certain conditions of humidity, outside temperature and outdoor heat exchanger temperature. During this 5-10 min period, the refrigerant cycle is reversed and, in most cases, the indoor fan stops, temporarily limiting (or reversing) heat transfer. In other words, even if the heat pump benefits from removing the ice in the long term, its short-term performance is affected and temporary discomfort - decrease in room temperature - is experienced by the user.

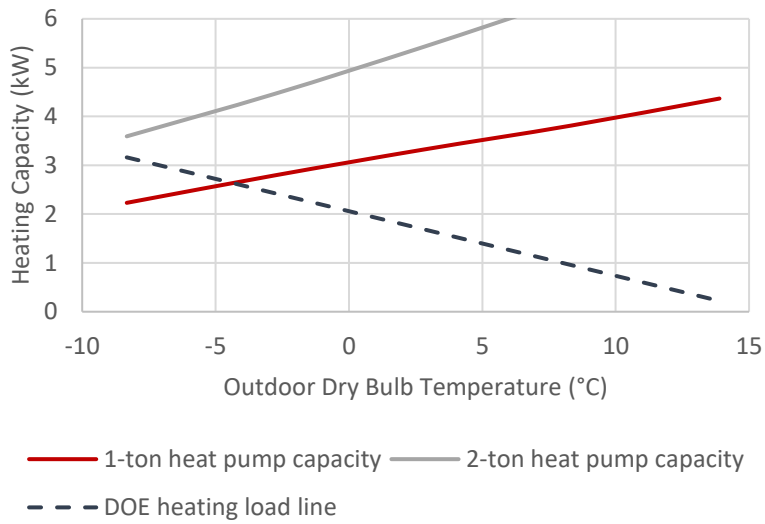


Figure 1-3: Heating capacity of a 1-ton and a 2-ton conventional heat pump and the DOE load line with respect with outdoor temperature (adapted from Kegel & McDonald (2015))

### 1.1.4 Variable capacity air source heat pumps

Variable capacity air source heat pumps (VCASHPs) are inverter-driven devices capable of adjusting their compressor speed to the current thermal load, which could offer solutions to most of the air source heat pump limitations outlined above.

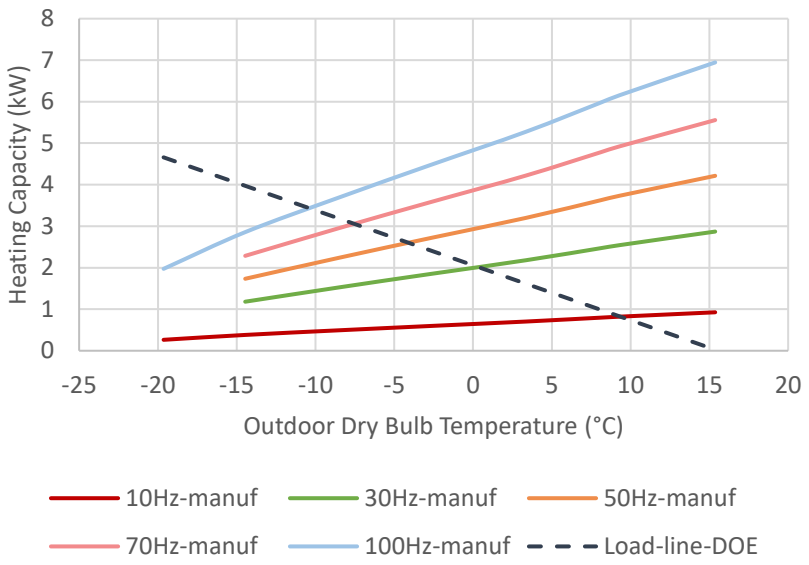


Figure 1-4: Heating capacity of a VCASHP at selected compressor speeds with respect to outdoor temperature (adapted from Kegel & McDonald 2015)

Figure 1-4 shows that at an outdoor temperature of 0.0 °C, the VCASHP does not need to cycle. It can continuously meet the load by setting its compressor frequency to only 30 Hz.

Minimizing cycling - or eliminating it in this case - has many benefits, as shown in Figure 1-5. It provides better comfort to the user by reducing temperature fluctuations at part load. Heat pump performance is also increased by avoiding cycling losses and consuming just the right amount of electrical power to maintain the indoor setpoint. In addition, operation at reduced compressor speed is roughly equivalent to the operation of a heat pump with oversized heat exchangers (condenser and evaporator), reducing the temperature differences across these heat exchangers and improving the machine COP.

Moreover, VCASHP higher compressor speeds are crucial. They allow to reach the indoor setpoint faster, and offer increased heat output at lower outdoor temperatures, which reduces the dependence on electric resistance heat (Rice et al. 2015). In the example of Figure 1-4, the balance point at 100 Hz is around -12 °C, instead of -8 °C at the nominal frequency of 70 Hz.

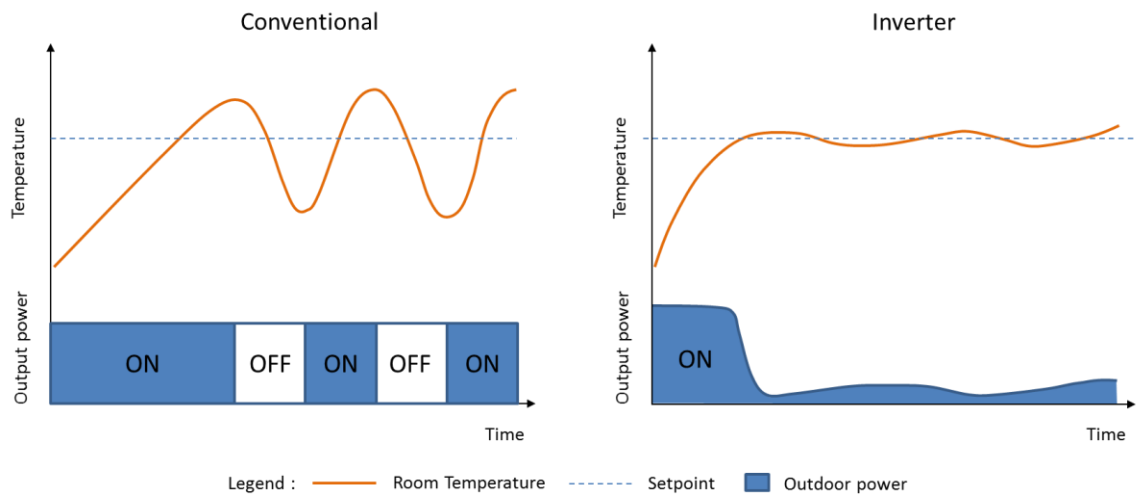


Figure 1-5: Room temperature evolution of a typical conventional (left) and inverter (right) air source heat pump in heating mode (adapted from Gomes et al. 2013)

These characteristics, combined to a better control strategy (including an electronic expansion valve and lower discharge temperatures), enable VCASHPs to operate at much lower outdoor temperatures than conventional ASHPs. Some of these VCASHPs have been known to provide heat at outdoor dry-bulb temperatures below -25 °C, while still maintaining a COP above 1.0 (Sager et al. 2014).

Oversizing can also be considered with inverter-driven heat pumps, since the variable speed compressor prevents the unit from cycling at low load, also providing sufficient latent cooling capacity to avoid humidity problems in cooling (Munk et al. 2014). While the benefits of this strategy still need to be confirmed by tests (more details will follow), it could further reduce the need for auxiliary heating at very low outdoor temperatures.

VCASHPs can be seen as an evolution of fixed speed and two-stage air source heat pumps (Davis and Larson 2016). Also known as Cold Climate Air Source Heat Pumps (CCASHPs), their capital cost is significantly higher than conventional ASHPs (Kegel et al. 2012).

The inverter-driven technology was introduced on the North American market in 2006 (Ecotope Inc. 2014). It was first made available for ductless systems, and eventually was incorporated in ducted heating systems (Larson et al. 2013). In the latter, the indoor coil is included inside the ductwork where a fan pushes the warm air across the building. The former is often referred to as

“split” or “mini-split”, since the indoor coil is placed “inside an ‘indoor unit’ mounted on the wall or ceiling to individually heat and cool a space” (Kegel et al. 2017).

Figure 1-6: Typical mini-split ASHP installation (Energy Star 2018)

As seen in Figure 1-6, refrigerant lines represent a simple and interesting retrofit solution for buildings without ductwork, and "the absence of air ducts (...) permits the use of a fan with much less power consumption than their ducted counterparts" (Howard Cheung and Braun 2014). Many indoor units can be combined with the outdoor unit to serve different zones. While these systems are generally quieter than ducted heat pumps, they might cause aesthetic issues for some homeowners and become quite expensive if the number of indoor units is too important (Winkler 2011).

In conclusion, VCASHPs seem to be a promising solution to ASHP limitations. However, their operation is still not fully understood since manufacturers are reluctant to reveal their control strategies. Therefore, while VCASHP are “advertised as being efficient, their actual performance is still largely unknown” (Kegel et al. 2017). Their potential has to be confirmed by tests and specific simulation tools need to be developed to justify their higher capital cost and increase market adoption.

## 1.2 Testing

The evolution of heat pumps from fixed to variable speed technology calls for an update on test procedures. Conventional heat pump testing standards and their limitations are first reviewed, followed by new standardized test methods for VCHPs. Relevant laboratory and field test results are also presented, to determine if they match the expectations and if they provide sufficient data to build a VCHP model.

### 1.2.1 Standardized tests for conventional heat pumps

Rating procedures have long been used to standardize testing for the different heat pump manufacturers. Performance data is obtained at specific outdoor conditions to determine a heating seasonal performance factor (HSPF) and a seasonal energy efficiency ratio (SEER) in cooling to facilitate comparisons between the numerous heat pumps available on the market.

Major standards (Standards Council of Canada (2006); ANSI/AHRI Standard 210/240 (2012); Air-Conditioning & Refrigeration Institute (ARI) (2005); U.S. Department of Energy (1979)) adopt a similar approach. The Canadian standard CSA C656-05, for example, uses the heat pump performance and the building load at outdoor temperatures of 8 °C, 1.7 °C and -8.3 °C to calculate the HSPF.

However, current limitations of the HSPF are exposed by Francisco et al. (2004). It is shown that climatic conditions and building load can have a significant effect - up to 3-4 ratings points - on calculated HSPF values. Nonetheless, manufacturers ignore this variation and only publish the HSPF rating for one combination: climate zone IV and minimum building load. In other words, a heat pump with a lower certified HSPF could actually perform better than a higher HSPF heat pump in climate zone V at maximum building load. Francisco et al. (2004) also mention that other default values included in Air-Conditioning & Refrigeration Institute (ARI) (2005), like the ‘degradation coefficient’, the ‘c-factor’ - accounting for thermal storage - and the ‘house heating balance point’ may be misadapted for current constructions, which can also lead to an overestimation or an underestimation of the heat pump performance in a specific context.

Finally, equipment sizing, duct losses and the heat pump control strategy (Francisco et al. 2004) - including the cut-off temperature at which the auxiliary starts to operate (Le Lostec and Nouanegue 2014) - also have an effect on heat pump performance that is not taken into account by the HSPF metric.

### 1.2.2 New standardized tests for variable capacity heat pumps

The limitations previously exposed for conventional heat pump testing procedures remain valid when they are used for VCHPs. In fact, the HSPF metric is even less adapted for inverter-driven heat pumps and the extended outdoor temperature ranges under which they can operate. Sager et al. (2014) consider that "existing test standards for air source heat pumps (CSA C656-05) do not include COP results at cold temperatures suitable to Canadian climates, leaving the market unsure of their performance at low temperatures".

Northeast Energy Efficiency Partnerships (NEEP) (2017a) expresses similar concerns, adding that manufacturer data at cold outdoor temperatures is "not standardized or consistent" and that the HSPF metric "assumes the use of electric resistance elements, and tests in steady-state operation (as opposed to allowing modulation)", which is too restrictive for the possibilities offered by the inverter-driven technology. Moreover, field data obtained by Le Lostec & Nouanegue (2014) confirmed that the HSPF metric overestimated VCHP performance.

Rice et al. (2015) explain that the VCHP test standard adopted by the industry was proposed by Domanski (1988). However, this simple approach developed for the VCHPs available at the end of the 1980's is not entirely suitable for recent units.

Many studies therefore propose new rating test procedures better suited for VCHPs.

ANSI/AHRI Standard 210/240 (2012) includes specific test conditions for VCHPs. They consist of 5 required points (-8.33 °C at maximum speed, 1.67 °C defrost test at intermediate speed, 8.33 °C at maximum and minimum speed, 16.7 °C at minimum speed) and 3 optional points. These rather rigid specifications can be hard to apply for some recent VCHPs. For example, if a unit operating at minimum speed has a balance point around 0 °C, it might be impossible to obtain the intermediate speed defrost point, which can cause extrapolation errors (Rice et al. 2015). Moreover, the standard does not consider VCHP control strategies that often restrict the compressor speed range (e.g. no low compressor speed available at very low outdoor temperature), which might also

lead to an overestimation of the HSPF. To overcome these issues, Rice et al. (2015) suggest a new load line closer to the ANSI/AHRI Standard 210/240 (2012) maximum design heating requirement that better fits the EnergyPlus residential building loads.

Similarly, US DOE (2016) recommends a new test procedure for VCHPs in heating mode, along with a revised load line equation. A recent report by the Northeast Energy Efficiency Partnerships (2017a) focuses on cold climate performance. Their proposed standard adds a low outdoor temperature test point (-15 °C) for which a minimum COP is required (2.0 for ductless, 1.75 for ducted systems) at maximum capacity operation. The objective is to motivate manufacturers to keep on improving the VCHP technology, and help customers identify which commercially available units can effectively operate in cold climates. Canadian Standards Association (2017) suggests new tests for a wider range of outdoor temperatures (as low as -26 °C) and heating loads, in addition to climate-based ratings to clarify which performance should be expected depending on the location.

Finally, Christensen et al. (2011) present a field-monitoring protocol specifically for mini-split heat pumps, intended to "provide a consistent methodology for performance measurement" of these units.

All these promising test procedures for VCHPs still have not been adopted by the manufacturers and the scientific community. Until HSPF values and manufacturer data are more consistent, it therefore remains important to perform laboratory and field tests to validate the manufacturer claims about the benefits of this new technology.

### 1.2.3 Conventional heat pumps: test results

Before getting to VCHPs, a few recent test results for conventional heat pumps are worth mentioning.

Waddicor et al. (2016) confirm that cycling losses are not negligible at startup and during short cycling for fixed-speed water-to-water heat pumps.

Moreover, Corberán et al. (2013) show that the only non-negligible contributor to COP degradation of conventional water-to-water heat pumps is the power drawn during the OFF period.

These results suggest that a multi-stage heat pump with appropriate control could improve the efficiency of these systems by minimizing on/off cycling at part load.

### 1.2.4 Variable capacity heat pumps: laboratory results

Recent VCHP laboratory test results are reviewed to validate the claimed performances of this new technology and understand how they could eventually be used to develop a VCHP model.

Karlsson et al. (2006) evaluate 12 VCHPs and compare the results with previous tests conducted on VCHPs (2001) and conventional heat pumps (1991). Results show that the VCHP performance steadily improves over the years, and that defrost control strategies generally get more elaborate. Nakos et al. (2014) confirmed this trend, despite the significant performance variation between the current market available units.

Karlsson (2007) performs tests on variable speed ground-source heat pump prototypes connected to hydronic heating systems, explicitly stating that the key learnings could apply to other types of heat pumps. While it seems that the VCHPs are capable of improving their COP at part load, Kegel & McDonald (2015) wish the detailed results from this study would have been made available and expressed as a performance map to facilitate their analysis. Nevertheless, Karlsson (2007) also rightly underlines the importance of considering the transient behaviour of VCHPs before comparing their performance to single-speed heat pumps.

Hunt et al. (2015) ran tests focusing on the VCHP dynamics. A 2-ton ducted split residential VCHP is separated in two distinct thermal chambers for the indoor and the outdoor unit, which allows to modify the load or the setpoint in the indoor zone without affecting the constant air conditions in the outdoor zone. It is first shown that the VCHP is capable of tracking the increasing load over a 4-hour period to maintain the indoor setpoint (21 °C) under a constant outdoor temperature (8 °C). Then, when the setpoint is suddenly increased from 20 °C under steady-state operation to 22.2 °C, the VCHP immediately answers by ramping up to maximum capacity. On the way to reach the new setpoint, the ‘heat pump only’ mode shows a much better COP than the ‘heat pump + auxiliary’ mode (3.8 vs 1.4), since the power consumption of the former is substantially lower. However, modeling based on test data shows that “the ‘heat pump only’ mode would take significantly more time to cause a 2.2 °C setpoint increase” because the heat output is obviously smaller than the ‘heat pump + auxiliary’. While these results obviously provide great insights, the tests are only

performed at one outdoor temperature (8 °C). Additional tests using this approach for a wide range of outdoor temperature are still required to get a complete VCHP performance map that would facilitate the comparison with field data and help to build a dedicated model.

Winkler (2011) also made an important contribution on this matter. Qualitatively monitoring the compressor speed allows to get performance curves at various outdoor temperatures for two market available mini-split ductless heat pumps (Fujitsu and Mitsubishi). Moreover, a state of the art test bench collected key metrics - including indoor unit fan speed and humidity - to enable air side and refrigerant side heat output calculations. Results show that both units present a better COP at part load, but a lower COP at full load when compared to a two-stage high SEER forced air system. Moreover, variations in fan speed only seem to have a small effect on the COP, and the theoretical minimum capacities could not be reproduced since short-cycling started to occur at a higher load than anticipated. One important limitation of this study is that the compressor speed is not explicitly measured and only estimated as maximum, intermediate and minimum. As underlined by the authors, an “intermediate” frequency is pretty vague and makes it harder to compare results with manufacturer data since the real compressor speed may not necessarily be aligned with the rated frequency of both units. An exact measure of the frequency would also help to build a more precise performance map and VCHP model.

Kegel et al. (2017) and Kegel & McDonald (2015) conduct similar testing and seem to agree on many results. In both cases, the ductless VCHP are able to produce heat down to an outdoor temperature of -25 °C. Also, they both consider manufacturer data difficult to interpret, especially at outdoor temperatures below -15 °C, and the measured performance data appears to be systematically below manufacturer data. While the defrost cycles seem timed depending on outdoor temperature, it was not possible to understand their exact control strategy.

Moreover, Kegel et al. (2017) report that the VCHP is not able to maintain the 21 °C indoor setpoint at an outdoor temperature below -15 °C. This seems to be caused by a protection control that prevents the unit to remain at maximum speed more than 20 min, even when the indoor setpoint is not met. Higher compressor speeds than expected are also recorded at an outdoor temperature close to 0 °C because of frequent defrost cycles after which the compressor systematically ramps up at maximum speed.

Kegel & McDonald (2015) find that the tested VCHP unit performs better than a conventional heat pump (assisted by an electric heat auxiliary) at outdoor temperatures between -25 °C and -15 °C. However, at warmer outdoor temperatures (5 °C or more), the VCHP shows a lower COP than a single-speed ductless split system. Comparison with previous results (Winkler 2011) show a significantly lower COP at outdoor temperatures below 0 °C, and a much lower heat output at warmer temperatures. This can partly be explained by the fact that the testing facility is still incomplete, and unable to control the heating load or maintain an indoor setpoint. Therefore, no performance map could be obtained under these conditions.

The previous laboratory tests have shown that VCHPs generally perform better than conventional heat pumps. However, important discrepancies exist between studies and many results do not match the expectations set by manufacturer data. This emphasizes the need to further validate VCHP performance with field results.

### 1.2.5 Variable capacity heat pumps: field results

Field data is also crucial to VCHP testing. As stated by Winkler (2011), “laboratory experimentation provides controlled and accurate performance data against which installed performance from real homes can be compared (...)”. Factors like occupancy, use of setbacks, interaction of the heat pump with auxiliary heat are difficult to test in a lab setting and can have a strong impact on results (Larson et al. 2013). They should ideally be considered through a field monitoring study before eventually using the dataset to build a VCHP model.

Larson et al. (2013) perform field tests during eight weeks with six ducted VCHP in six different houses in Oregon. In heating mode, VCHPs are able to increase the COP by 25-30 % compared to single-speed units. These results are aligned with previous lab results obtained with a similar VCHP, leading the authors to consider that “performance curves of the heat pump itself can largely be developed from the lab data alone”. However, Rice et al. (2015) note that the modelled annual efficiencies based on VCHP field performance for this study is on average 25 % lower than the HSPF announced by manufacturers, while the difference for baseline single-speed heat pumps is only 5 %. It would be interesting to see how VCHP field results compare to an updated HSPF calculated with the alternative load line suggested by Rice et al. (2015). The mild weather also does not allow to collect enough field data at very low outdoor temperatures (lower than -5 °C) to confirm the VCHP performance under these conditions.

Munk et al. (2013) conducted field tests in Tennessee and Georgia in 4 homes retrofitted with ducted VCHPs. All but one VCHP show improved heating performance - lower capacities and longer period without cycling - compared to the baseline single-speed heat pumps. But once again, Rice et al. (2015) point out that the field performance is up to 36 % lower than the advertised HSPF for one the VCHPs, and outdoor temperatures are too high to gather relevant performance data for cold climates.

EPRI (2014) suggests an interesting approach to evaluate the benefits of VCHPs. A simulated-occupancy research home in Knoxville is retrofitted with two ducted variable speed heat pump systems. The results are compared with prior years' data obtained from the same home, which was then equipped with single-speed heat pumps (EPRI 2014). For similar outdoor temperature bins, it is found that the VCHPs drew 17 to 38 % less power during heating than the single-speed heat pumps. Unfortunately, the VCHPs are tested under milder weather than what the single-speed heat pumps have seen during the previous years, meaning that no VCHP performance data could be obtained below an outdoor temperature of -10 °C.

A report by Ecotope (2014) is related to a previously discussed laboratory test (Winkler 2011). Both publications are part of a major project piloted by the Northwest Energy Efficiency Alliance to better understand the new generation of ductless mini-split heat pumps. A total of 95 homes took part in the study, and field results are found to be reasonably aligned with laboratory results and manufacturer ratings (HSPF). Tests are conducted both in heating and cooling with an average seasonal COP of 3.0, under daily average outdoor temperatures as low as -17.8 °C.

Concordance with laboratory tests is generally less obvious for field tests conducted in even colder climates. Kegel et al. (2017) are able to obtain performance data at very low outdoor temperatures for a centrally ducted VCHP installed in a testing house in Ottawa, Canada. Results show COP values of 1.5 at -21 °C, confirming that the VCHP is capable of operating more efficiently than a single-speed heat pump (and an electric auxiliary) under these conditions. On the other hand, important discrepancies are found with the laboratory performance obtained for the ductless mini-split VCHP presented in the same study, especially at outdoor temperatures below -10 °C. Operation at lower capacity is also found to be problematic, as the system started to cycle on/off under insufficient load. Finally, it is found that the electric resistance auxiliary heaters account for an important part of the energy consumption of the system during defrost cycles.

In fact, an appropriate control strategy for the backup heat appears to be crucial for the performance of the system. While Schoenbauer et al. (2016) obtained space energy savings from 39 to 65 % for 3 ducted VCHPs installed in Minnesota homes, it is shown that for higher heating loads, the system controls prioritizes backup heating over higher frequencies of the heat pump, which prevents to gather crucial performance data under these conditions. In other words, a cut-off temperature lower than -10 °C would have allowed to better understand the behaviour of the CCASHP at very cold outdoor temperatures. Insufficient backup heat can also affect the VCHP performance. Sager et al. (2014) installed two ductless split systems in two highly instrumented houses, where occupancy is simulated by computer. Results show that mini-splits and their gas fireplace backup maintain a COP greater than 2.0 at outdoor temperatures below -15 °C. However, the system is unable to maintain the indoor setpoint at lower outdoor temperatures since the gas fireplace "was set to operate at too low a temperature". Once again, this underlines the need for better integration of VCHP and their auxiliary, in order to find the optimal backup heat control strategy to maximize comfort and system performance.

The sizing of the VCHP is also crucial. Le Lostec & Nouanegue (2014) perform a pilot-project on 22 test sites in Québec, Canada equipped with different ASHP technologies (ducted single-speed, ducted variable capacity and ductless mini-split heat pumps). Compared to the heating demand, they offer savings of 28 %, 45 % and 25 %, respectively. These somewhat disappointing ductless mini-split results can probably be explained by the fact that their rated capacity (1.5 ton) is significantly lower than the ducted single-speed (2.5 ton) and variable speed (3 ton). As mentioned by Le Lostec & Nouanegue (2014), it "would be relevant to analyze the energy savings of ductless heat pump (sic) with regards to their sizing, and to compare them with the savings generated by central cold climate heat pumps of a similar size".

In fact, many studies like Munk et al. (2013) consider oversizing as a viable option for VCHPs. Hunt et al. (2014) show that oversizing a VCHP reduces the power consumption and the need for backup heat. Cummings et al. (2015) believe that oversized heat pumps should be encouraged, and that standards should be modified accordingly (Cummings and Withers 2014).

Others are less categorical. Larson et al. (2013) insist on the importance to properly size, while Davis & Larson (2016) warn users against the risk of undersizing, which can affect VCHP performance, as seen previously with Le Lostec & Nouanegue (2014). Northeast Energy Efficiency

Partnerships (NEEP) (2017b) has even issued a guide called “Sizing and selecting ASHPs in cold climates” to provide a sizing framework for this issue. One of their recommendations is to make sure the VCHP minimum capacity is not over 115 % of the cooling load and to keep in mind that “grossly oversizing (...) can lead to excessive cycling, low efficiency and ineffective summer dehumidification”. These slightly different point of views on oversizing underline the fact that a proper VCHP model could eventually help stakeholders to get more clarity on this issue.

Since field results often differ from laboratory results and manufacturer data, and since the previously shown studies generally offer interesting but incomplete results, additional testing is required to obtain a complete VCHP performance map. This data will then be used to develop a VCHP model that could use manufacturer data and experimental results to predict “real life” performance of VCHPs.

## 1.3 Modeling

Modeling is crucial to evaluate heat pump performance. Indeed, laboratory and field testing is expensive and time-consuming, and models can be an alternative “(...) needed by building designers to evaluate different system options to identify the most economically attractive approaches” (Howard Cheung and Braun 2014). Moreover, creating models can contribute to improve heat pump design by facilitating the study of their performance (Hamam and Rocaries 1983).

The main conventional heat pump models and their limitations are first reviewed, followed by currently available and relevant VCHP models.

### 1.3.1 Software and conventional heat pump models

Many simulation software programs already offer components for (air-source) heat pumps. The list includes Transient System Simulation Tool (TRNSYS), EnergyPlus, Simplified Energy Enthalpy Model (SEEM) and Pleiades+COMFIE. However, as it is the case for TRNSYS (Transsolar 2012) and the TESS library (TESS 2012), available components are often designed for conventional air-source heat pumps only and are not able to reproduce the load-matching behavior of the variable capacity heat pump.

Similarly, the ASHRAE secondary toolkit (Brandemuehl et al. 1993) and the DOE-2 model (Winkelmann et al. 1993) are valuable references for conventional heat pump models, but are not suited for VCHPs.

Blervaque et al. (2016) confirm that recent improvements in heat pump technology - including inverter-driven variable capacity - and building envelope triggered the need for a new modeling approach adapted to this reality.

### 1.3.2 Variable capacity heat pump models

The main challenge is to use laboratory and/or field test results as a starting point to create a VCHP model. US DOE (2017, chap. 22) presents two methods: a performance table, and a performance curve.

The former can be convenient, for example, when the table is provided by the manufacturer, which can spare the user from having to represent the performance data in the form of an equation. Interpolation is used by the simulation software to obtain performance data for conditions that fall between the values included in the table. However, this method can be less accurate than regression performance curves and less adapted to extrapolate outside data limits (US DOE 2017, chap. 22). Moreover, manufacturer data for VCHPs is often available only at rated frequency, which makes it difficult to obtain a complete performance table for a variable capacity model.

The curve-fit smoothing associated with the performance curve can compensate for erroneous values in the performance data. In some cases, it can also be simpler for the user to just enter a few coefficients than to provide a whole performance table. For example, Tang (2005) proposed non-dimensional curve-fit heat pump models. This interesting approach allows to model the heat pump performance with a limited number of curves. Indeed, the equation-fit model for Water-to-Air heat pump (US DOE 2017, chap. 17.5.5) in EnergyPlus (object names Coil:Cooling:WaterToAirHeatPump:VariableSpeedEquationFit and Coil:Heating:WaterToAirHeatPump:VariableSpeedEquationFit) derived from Tang (2005) uses only five equations (three in cooling, two in heating), as shown below in Equations (1.7) to (1.11), where $A_i$ , $B_i$ , $C_i$ , $E_i$ and $F_i$ are equation fit coefficients.

Cooling mode :

$$\frac{Q_{total}}{Q_{total,ref}} = A1 + A2\left[\frac{T_{wb}}{T_{ref}}\right] + A3\left[\frac{T_{w,in}}{T_{ref}}\right] + A4\left[\frac{\mathrm{V}_{air}}{\mathrm{V}_{air,ref}}\right] + A5\left[\frac{\mathrm{V}_{w}}{\mathrm{V}_{w,ref}}\right] \tag{1.7}$$

$$\frac{Q_{sens}}{Q_{sens,ref}} = B1 + B2\left[\frac{T_{db}}{T_{ref}}\right] + B3\left[\frac{T_{wb}}{T_{ref}}\right] + B4\left[\frac{T_{w,in}}{T_{ref}}\right] + B5\left[\frac{\mathrm{V}_{air}}{\mathrm{V}_{air,ref}}\right] + B6\left[\frac{\mathrm{V}_{w}}{\mathrm{V}_{w,ref}}\right] \tag{1.8}$$

$$\frac{Power_c}{Power_{c,ref}} = C1 + C2\left[\frac{T_{wb}}{T_{ref}}\right] + C3\left[\frac{T_{w,in}}{T_{ref}}\right] + C4\left[\frac{\mathrm{V}_{air}}{\mathrm{V}_{air,ref}}\right] + C5\left[\frac{\mathrm{V}_{w}}{\mathrm{V}_{w,ref}}\right] \tag{1.9}$$

Heating mode :

$$\frac{Q_h}{Q_{h,ref}} = E1 + E2\left[\frac{T_{db}}{T_{ref}}\right] + E3\left[\frac{T_{w,in}}{T_{ref}}\right] + E4\left[\frac{\mathrm{V}_{air}}{\mathrm{V}_{air,ref}}\right] + E5\left[\frac{\mathrm{V}_{w}}{\mathrm{V}_{w,ref}}\right] \tag{1.10}$$

$$\frac{Power_h}{Power_{h,ref}} = F1 + F2\left[\frac{T_{db}}{T_{ref}}\right] + F3\left[\frac{T_{w,in}}{T_{ref}}\right] + F4\left[\frac{\mathrm{V}_{air}}{\mathrm{V}_{air,ref}}\right] + F5\left[\frac{\mathrm{V}_{w}}{\mathrm{V}_{w,ref}}\right] \tag{1.11}$$

These equations are non-dimensional, which generates a smaller range of coefficients values (US DOE 2017, chap. 17.5.5), aside from requiring “less computation time and are more robust than parameter estimation based models” (Tang 2005). It is important to mention that the models proposed in his study are meant for quasi-steady state operation and have not been validated for part load operation.

A few other EnergyPlus models use performance curves to approach VCHP modeling. For US DOE (2017, chap. 16.2.11), the Single-Speed Electric Heat Pump DX Air Heating Coil (object name Coil:Heating:DX:SingleSpeed) serves as a starting point. This component requires the performance at rated conditions and 6 performance curve fits – similar to Equations (1.7) to (1.11) – for which the user enters the coefficients (Big Ladder Software LLC 2014). These modifier curves account for the effect of outdoor, indoor dry-bulb temperature and the air flow rate across the heating coil. The curves also consider the effect of cycling losses and defrost cycles. The Multi-Speed Electric Heat Pump DX Air Heating Coil (object name

Coil:Heating:DX:MultiSpeed) uses a similar approach, but allows the modeling of 2-4 discrete compressor speeds. For compressor speeds that fall between these specified compressor frequencies, the component "linearly interpolates the performance at two consecutive speeds (n-1 and n) as needed to meet the heating load, with the fraction of time at each speed established by the speed ratio" (US DOE 2017, chap. 16.2.13). For more accuracy, the Variable Speed DX Air Heating Coil (object name Coil:Heating:DX:VariableSpeed) can incorporate up to 10 discrete compressor speeds. However, as explained by Nyika et al. (2014), manufacturer data is often only presented at rated frequency and is hardly available for other compressor speeds.

It should be noted that US DOE (2017, chap. 17.5.10) describes a similar model, adapted for the reality of water-to-air heat pumps, while US DOE (2017, chap. 17.5.5) extends the single-speed DX air heating coil to a more general approach. Instead of representing the heat pump as a coil, the Unitary Air-to-Air Heat Pump (input object AirLoopHVAC:UnitaryHeatPump:AirToAir) is modelled as a virtual component that includes the fan, the DX cooling and heating coil and the auxiliary heating coil to help "properly coordinate the operation of the various system components" (US DOE 2017, chap. 17.5.5.2). This model can be particularly useful in cases where heating or cooling is provided in multiple zones. Its multispeed counterpart can accept up to 4 discrete compressor speeds.

Furthermore, the Variable Refrigerant Flow Cooling Coil (US DOE 2017, chap. 16.2.23) adapts the Single-Speed Electric Heat Pump DX Air Cooling Coil (object name Coil:Cooling:DX:SingleSpeed) to account for the change in the coil's apparatus dew point and sensible heat ratio at part-load when the refrigerant flow is reduced.

Finally, the System Curve based Variable Refrigerant Flow (VRF) model (US DOE 2017, chap. 17.7) "varies the refrigerant flow rate using variable speed compressor(s) in the outdoor unit, and the electronic expansion valves (EEVs) located in each indoor unit". Many indoor units can be managed with a single outdoor unit, and the system curve based model can manage heat recovery, i.e. simultaneous heating and cooling in different zones (more details will follow). The particularity of this model is that it offers the possibility to represent the performance data by two curves (one for low, and one for high outdoor temperatures). These curves are separated by a boundary curve that delimits the transition that can occur at a different outdoor temperature on the different indoor temperature performance curves (US DOE 2017, chap. 17.7.1.7).

Other studies use performance curves and regression models. The simplicity of multiple polynomial regressions is also perfectly suited for studies related to the impact of VCHPs on the grid. Indeed, Kim et al. (2016) model the compressor power of a variable capacity air-to-water heat pump as a function of the steady-state ambient temperature, water return temperature and compressor frequency with impressive accuracy. Filliard (2009) uses a steady-state empirical modeling approach to characterize the performance of heat pumps for which the outdoor unit is placed in a temperate-space attic. It consists of 3 models that account for full-load, part load and defrost cycle operation, and that are integrated in the thermal simulation tool Pleiades+COMFIE. The first model shows good agreement with manufacturer data, while the part-load and the defrost model were not validated with experimental data. Larson et al. (2013) works with Ecotope to build separate equations for capacity and power input from field data for use in SEEM. Unfortunately, not much details are revealed for this model, apart from the fact that the inputs are the outdoor temperature, the air handler flow, and the return air temperature. It is also said that the simulation "implements a simple 'load following' algorithm to have the heat pump change its output to track the house heating load" (Larson et al. 2013). In other words, the load is compared to the equipment specification to see if the heat pump is OFF (load below minimal heating capacity), at part-load (load between minimum and maximum capacity), at full load or if the auxiliary resistance is required (load larger than maximum capacity). Nyika et al. (2014) use an empirical model developed by Cheung et al. (2011) to propose a method to generalize a model for a family of similar heat pump equipment. The model from Cheung et al. (2011) is based on 8 multiple polynomial equations in heating mode. The required inputs are the indoor temperature, outdoor temperature and volumetric flow rate while the parameters are the maximum heat output, power input and volumetric flow rate. Generalized performance maps are found to be less accurate than the specific counterpart for each equipment. Nonetheless, generalized performance maps remain helpful in cases where insufficient data is available from a specific model of the same family.

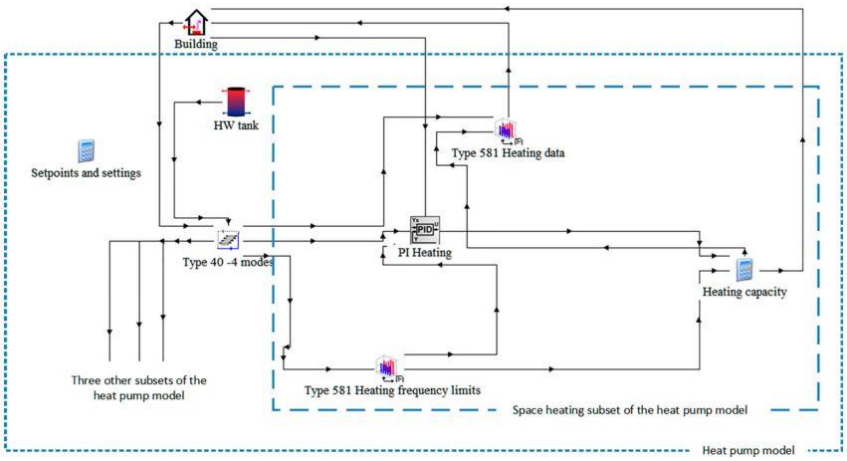


Figure 1-7: TRNSYS distributed approach VCGSHP model from Bouheret and Bernier (2018)

A good example of a performance table based model is certainly the variable capacity water-to-air heat pump model proposed by Bouheret & Bernier (2018). It is developed for variable capacity ground-source heat pumps (VCGSHPs), but large parts of this approach remain relevant for ASHPs. To our knowledge, it is one of the very few models that have been developed for VCHPs in TRNSYS. The model is not a new type, but a distributed approach of existing components. It offers four operating modes, including space heating. The modeling approach shown in Figure 1-7 can be summarized in 6 steps:

1- Controllers receive the indoor temperature from the building and compare it to setpoints and settings to determine the operating mode and the required heat pump frequency.

2- At the same time, two types rely on performance data sourced from an external file. The first, “high frequency limits”, provides minimum and maximum frequency and capacity for the current conditions (EWT, source ΔT, air flow rate).

3- A linear relationship expressing the heating capacity as a function of frequency is determined.

4- The model uses this relationship and the required heat pump frequency provided by the controller in step 1 to calculate the heat output sent to the building.

5- A second type sourcing performance data from an external file also receives the heat output calculated in step 4 and determines - at the current conditions (EWT, source ΔT, air flow rate) - the power input and water pressure drop.

6- The indoor temperature of the building is updated, and the same cycle is repeated.

In verification tests, the model shows the ability to adequately switch between the four existing modes and to reproduce manufacturer data, but no comparison is made with measured performance.

Other VCGSHP models are worth mentioning. Madani et al. (2011) presented a more complex strategy that consists on a series of semi-empirical sub-models of heat pump components (compressor, heat exchangers, expansion valve, heat source, storage tank, etc.) that are assembled in TRNSYS and EES to perform a co-solving technique. While the results are satisfying (less than 15 % deviation for all key metrics when compared to measurement), a simpler approach is probably desirable to help building energy stakeholders better understand the variable-speed technology. Moreover, for their study of a chiller combined with a water-source heat pump, Jeon et al. (2010) choose the simple multiple polynomial curve-fit approach developed by Tang (2005) over the parametric model proposed by Jin & Spitler (2002), arguing that the former offered better results.

Some variable capacity models have also been specifically developed for ductless heat pumps. According to Cheung & Braun (2014), ductless heat pumps “have complicated control algorithms (...)” and “(...) very little work has been done in the development of empirical models (...)”. Nonetheless, Hunt et al. (2015) suggest a very simple yet interesting approach. The maximum and minimum heating output are obtained experimentally, along with the corresponding power consumption values. Then, comparing the measured heat output at part load to these maximum and minimum values allows to interpolate the power consumption of the unit. Results show that the predicted power values match the measured power consumption of the unit within 10 %. It must be noted that these tests are only performed at one outdoor temperature (8 °C) and that the results should be validated for a variety of outdoor temperatures. Cheung & Braun (2014) present a more elaborate strategy that combines five empirical models for maximum, minimum, part-load, defrost operation (more details will follow) and indoor unit power. The first two consist of a set of conditional equations that adjust the maximum/minimum heat output and outdoor unit power consumption based on the current outdoor and indoor temperatures. The part-load model uses the

heat output and the fan operation mode as inputs to evaluate the outdoor unit power consumption at intermediate compressor speeds, while the indoor unit power model is represented by a second order polynomial equation function of the fan operation mode. When compared to measurements, the first two models seem significantly more accurate than the part-load and the indoor unit power consumption models. An explicit measure of the compressor frequency - instead of a rather vague "intermediate" frequency - could probably help close the gap on the part-load model, while defrost cycles have affected the indoor unit power consumption measures.

Certain studies focus on the dynamic - or transient - aspect of VCHP modeling. Gomes et al. (2013) present an original method based on the fact that VCHPs are known to operate at high (maximum) speed when activated, or when the indoor temperature is far from the setpoint. The authors define simple rules based on the current difference between the indoor temperature and setpoint to determine when the unit operates in this so-called "instability mode". The model closely tracks the power variation and shows impressive accuracy with deviation values of less than 2 % when compared to measured power consumption in both heating and cooling. US DOE (2017, chap. 17.7) suggests a way to adjust the cooling capacity when heat pump systems with multiple indoor units go from 'cooling only' mode to 'heat recovery mode', i.e. when the outdoor unit redistributes the heat to provide simultaneous cooling and heating in different zones. This period is characterized by a substantial time delay before the available cooling capacity is back to steady-state. A convenient exponential multiplier is used to describe the evolution of available cooling during this transition period.

Defrost cycles are specific to air source heat pumps and certainly represent the most important transient challenge in VCHP modeling. Indeed, Cheung & Braun (2014) underline the fact that before 2014, "no experimentally validated heat pump models (...) that simulate both heating and defrost operation" have been presented for ductless heat pumps. Certain models, however, focus exclusively on defrost operation. Blervaque et al. (2016) adapt a conventional ASHP empirical relationship by Mueller & Serber (1980) to the new reality of VCHP. The estimated amount of time between two defrost cycles is a function of the outdoor temperature and the relative humidity. This new model could not be validated experimentally. Similarly, the Variable Speed DX Air Heating Coil (US DOE 2017, chap. 16.2.14) reverse-cycle defrost modeling strategy is adapted from its single-speed counterpart, which uses a modifier curve "multiplied by the heating coil capacity, the fractional defrost time period and the runtime fraction of the heating coil to give the

defrost power at the specific temperatures at which the coil is operating". The only difference with the single-speed DX coil is that the heating capacity is set to the maximum compressor speed value during defrost cycles. The System Curve based Variable Refrigerant Flow model (US DOE 2017, chap. 17.7.1) adopts a similar approach, and accounts for the additional heating load caused by defrost. Filliard (2009) suggests a static approach and applies a degradation coefficient to the heating capacity each time the outdoor temperature is below 6 °C. The effect of this degradation is shown in Figure 1-8.

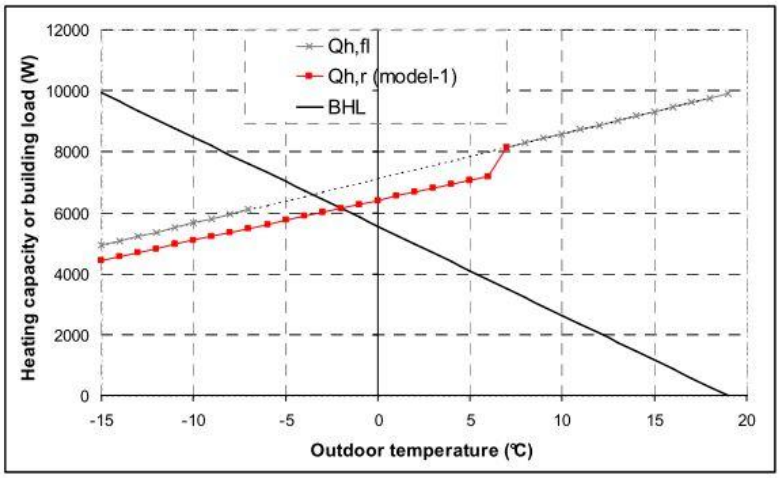


Figure 1-8: Effect of the defrost degradation coefficient on heating capacity (Filliard 2009)

In defrost mode, Cheung & Braun (2014) adjust the models previously presented for maximum, minimum, part-load operation and indoor unit power to account for the performance degradation. This complex modeling strategy accounts for many factors like the reduced indoor fan power consumption ("off" during defrost cycles), startup, shutdown and potential on/off cycling during defrost. These corrections are modeled by a series of linear empirical equations, which generally show good agreement with measured heat output and power consumption during a defrost cycle.

## 1.4 Conclusions of the literature review

In conclusion, some of the aforementioned VCHP models seem promising. However, many of them are often incomplete, too simple or complex and hardly accessible. Therefore, the fact

remains that there currently is a lack of VCHP models to help stakeholders evaluate the real potential of this technology.

This is especially true for ductless mini-split heat pumps. Cheung & Braun (2014) deplore that despite their recent progression in the North American market, “the tools available for modeling their performance within building simulation programs have not kept pace”.

A dedicated component able to dynamically simulate VCHP performance – including defrost cycles – and compatible with different modeling strategies (performance map, regression) could be especially helpful in a simulation software like TRNSYS. To our knowledge, this kind of model currently does not exist.

The development of this model strongly depends on performance testing. As seen previously, VCHPs test procedures and manufacturer data are not considered reliable, and show important discrepancies with laboratory and field test results. Moreover, it proved difficult to obtain a complete performance map from these tests and/or a complete set of manufacturer data needed to build a variable capacity model. Additional testing is therefore recommended (Kegel and McDonald 2015) to develop these simulation models and complement these previous studies that have shown the limitations of VCASHPs.

## 1.5 Objectives

The objectives of this thesis are presented below.

- Perform adequate testing to obtain more data and validate Variable Capacity Heat Pump (VCHP) performance while...
    - Focusing on Ductless mini-split Heat Pumps (DHPs)
    - Obtaining a complete performance map by:
        - Varying the heating load on a large scale of outdoor temperatures
        - Performing tests in cold climate conditions (well below -10 °C)
        - Explicitly measuring compressor speed

- Create a VCHP model:
    - Using the test results obtained in step 1
    - That is incorporated in TRNSYS as a new component
    - That is able to dynamically model their performance, including defrost cycles.

## 1.6 Thesis outline

Four chapters compose this thesis. This first chapter introduced the subject and presented the literature review. The second one presents the testing methodology that led to characterize the performance of one variable capacity mini-split air source heat pump. The third chapter provides the detailed test results and their analysis. The fourth chapter focuses on the methodology that allowed to use these test results to create the new VCASHP model. The fifth chapter presents the simulation results and their analysis for the two versions of the proposed VCASHP model. The thesis ends with conclusions and recommendations.

# CHAPTER 2 METHODOLOGY

This chapter focuses on the testing methodology. The reader can find more information about the modeling methodology in “Chapter 4 - The model”.

While the test bench can also be used in cooling, experiments for this project are limited to the heating mode.

## 2.1 Test bench

To develop a simulation strategy to better predict the performance of VCASHP systems, detailed experiments are conducted in a controllable environmental test chamber. The testing facility shown in Figure 2-1 was built prior to the testing phase by the CanmetENERGY team at the Varennes laboratory. It is essentially similar to the one described in Kegel et al. (2017), Kegel & McDonald (2015) and Tardif et al. (2016). It can provide a variety of heating loads and user-defined ambient temperatures, while explicitly measuring compressor frequency to help establish its impact on VCASHP performance.

Figure 2-1: Test bench (Tardif et al. 2016)

The test bench consists of two insulated 3.6 m wide x 4.9 m long x 3.6 m high sheds equipped with variable speed exhaust fans and intake louvers. The ductless mini-split variable capacity air source

heat pump indoor unit is set in the first shed representing the “demand side”, while the outdoor unit is encapsulated in the second (Figure 2-2).

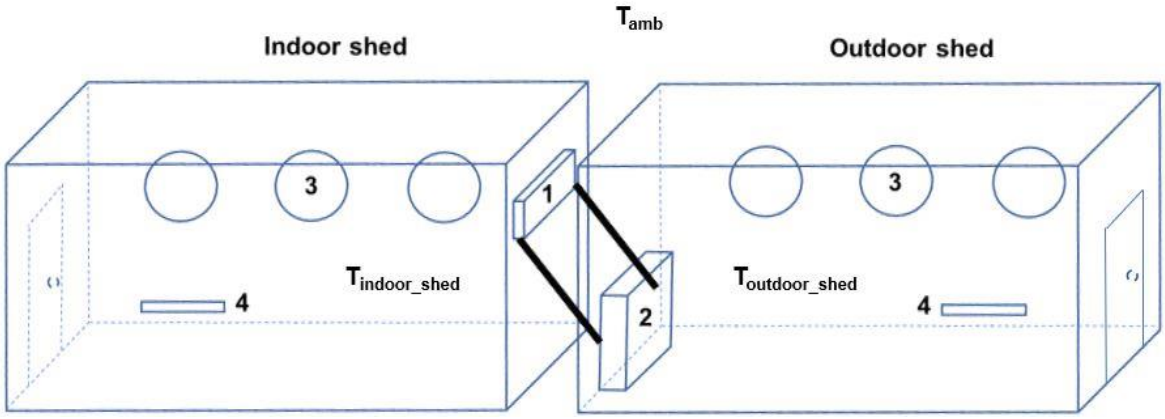


Figure 2-2: Testing sheds with indoor unit (1), outdoor unit (2), exhaust fans (3) and electric baseboards (4)

### 2.1.1 The heat pump

Testing was conducted from December 2016 to April 2017 on a commercially available ductless VCASHP system with a rated heating and cooling capacity of 4.0 kW (13,600 Btu/h) at 8.3 °C and 3.5 kW (12,000 Btu/h) at 35 °C, respectively (Mitsubishi Electric Corporation 2009a). The mini-split unit operates on a R-410A refrigerant closed loop heat pump cycle. Figure 2-3 presents the indoor and outdoor units of the heat pump. A 4-way reversing valve allows to toggle refrigerant flow between heating and cooling modes.

Figure 2-3: Indoor (left) and outdoor (right) unit of the VCASHP (Tardif et al. 2016)

### 2.1.2 Fresh air fans and electric baseboards

Six centrifugal variable speed sidewall exhaust fans and four intake louvers are used to induce a heating load and regulate the temperature of the testing chambers (Figure 2-4).

Figure 2-4: Fresh air fans and louvers (Tardif et al. 2016)

A Raspberry Pi computer allows to control the speed of the central exhaust fans in both sheds and adjust their air flow rate depending on the variations of ambient temperature during the course of a test. More details on this topic can be found in section 2.3 – “Fresh air fans control strategy”.

When needed, additional heating can be provided by electric baseboards in both sheds.

### 2.1.3 Instrumentation

As described in Kegel & McDonald (2015), the main observed variables are the refrigerant temperature, pressure and mass flow rate at numerous key points of the VCASHP cycle. These key locations are shown on the R-410A heat pump cycle p-h diagram in Figure 2-5. Note that the cycle and the points are theoretical (pressure losses on both heat exchangers are assumed negligible).

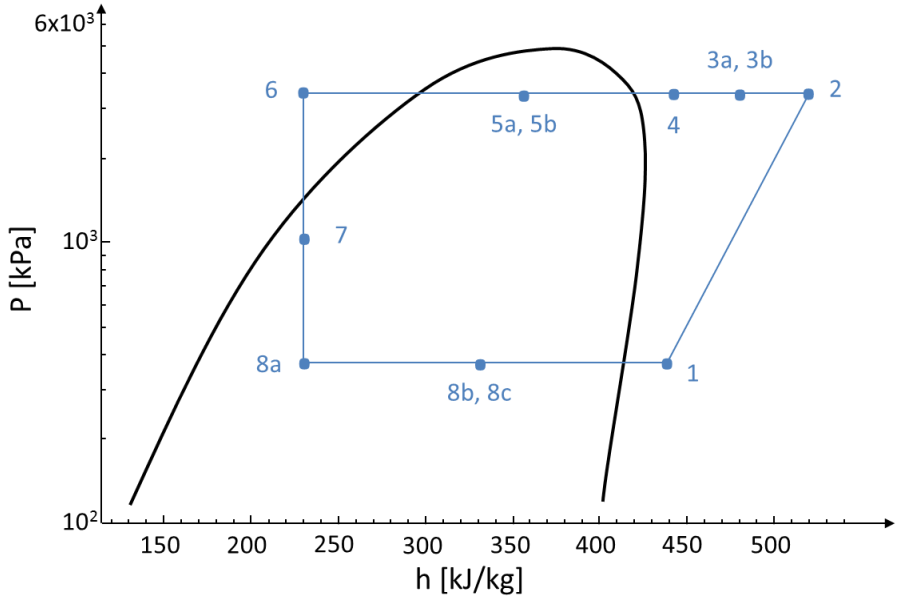


Figure 2-5: R-410A heat pump cycle p-h diagram (adapted from Tardif et al. 2016)

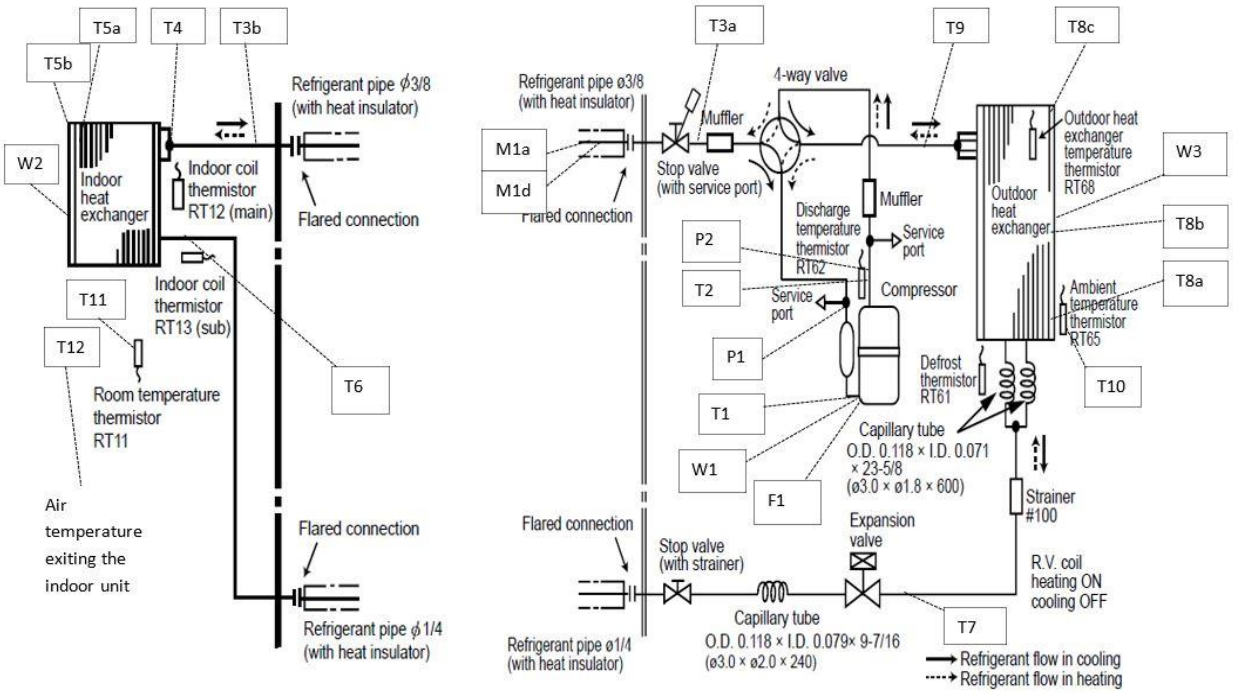


Figure 2-6: Schematic representation of instrumentation (Tardif et al. 2016)

Moreover, air temperature, power input and compressor RPM (frequency) are measured.

Figure 2-6 presents a schematic representation of the test bench instrumentation, which consists of thermocouples (T), pressure transducers (P), a PC8 DC Watt transducer and a WattNode Pulse kWh transducer (W) as well as a Coriolis refrigerant mass flow measuring system (M). The current through the compressor is also obtained from a current transformer (CT) and a passive low pass filter, which provides the compressor RPM and frequency (F). The numbers displayed on Figure 2-6 are aligned with those from Figure 2-5 and the detailed instrumentation list in Table 2-1.

Table 2-1: Detailed instrumentation list

| **Abbrev.** | **Value** | | **Abbrev.** | **Value** | |
|---|---|---|---|---|---|
| T1 | Compressor inlet temp. | | P1 | Compressor inlet pressure (evaporating) | |
| T2 | Compressor outlet temp. (superheat) | | P2 | Compressor outlet pressure (condensing) | |
| T3a-b | Compressor outlet temp. (desuperheat) | | M1a | Refrigerant mass flow rate | |
| T4 | Indoor unit inlet temp. | | M1d | Refrigerant mass flow direction | |
| T5a-b | Indoor unit temp. (condensing) | | W1a | Compressor power (DC Watt Transducer Phase A) | |
| T6 | Indoor unit outlet temp. (subcool) | | W1b | Comp. power (idem, Phase B) | |
| T7 | Outdoor exp. valve inlet | | W1c | Comp. power (idem, Phase C) | |
| T8a-b-c | Outdoor unit temp. (evaporating) | | W2 | Indoor (fan and unit) power (AC WattNode Pulse kWh transducer) | |
| T9 | Outdoor unit outlet temp. | | W3 | Outdoor fan power (Watt Transducer Phase A) | |
| T10 | Outdoor shed air temp. | | W4 | Drain pan heater power (AC WattNode Pulse kWh transducer) | |
| T11 | Indoor shed air temp. | | F1 | Compressor frequency (CT and passive low pass filter) | |
| T12 | Supply air temp. exiting the indoor unit | | $T_{amb}$ | Ambient temperature (not shown) | |

Refrigerant temperature is estimated by installing the shielded type T thermocouples on the copper tubing surface at each of the previously indicated locations.

Ambient temperature is also monitored by an RTD probe to avoid the occasional interference encountered between the original ambient temperature thermocouple and the electrical equipment when the machine went into defrost mode. The thermocouple measuring the supply air temperature (T12) should not be installed too close to the heat exchanger to avoid the effects of radiation that can lead to an overestimation of this temperature.

The compressor power is measured by a PC8 DC transducer located within the DC circuit in the compressor Variable Frequency Drive (VFD). The VFD converts the incoming AC to DC, before generating AC with a different frequency. It was deemed easier in this particular case to measure the power at the DC step. The indoor fan and main unit power consumption are measured directly on AC using a WattNode Pulse kWh transducer.

Data is obtained every minute and recorded on a datataker DT-85 data acquisition system. Tests are mostly conducted at night to avoid the effect of solar gains (more details can be found in section 3.2.3 – "Solar gains"). Humidity is not monitored, and the indoor unit fan speed is set at "high" for the entire testing phase.

The gathered data will allow to obtain the heating capacity, the power consumption and the COP of the tested unit for a variety of outdoor temperatures and heating loads.

## 2.2 Calculating the heat output

The two methods used to calculate the heat output are presented below.

### 2.2.1 Refrigerant side

Refrigerant temperature is measured at key locations previously indicated in Figure 2-5 and enthalpies at the various points are calculated from temperature and pressure using MATLAB (The MathWorks Inc 2016) along with the CoolProp add-on (Bell et al. 2014).

System performance is calculated on the refrigerant side using the enthalpies, refrigerant mass flow rate and electrical power input measured during testing.

Heat output of the VCASHP is calculated with Equation (2.1), using indoor unit inlet ($h_4$) and outlet ($h_6$) enthalpies.

$$\dot{Q}_{ref_side} = \dot{m}_{ref} * (h_4 - h_6) \tag{2.1}$$

Refrigerant at indoor unit inlet (point 4) is assumed to be entirely vapor. However, since transient effects occur (more details will follow) and R-410A refrigerant temperature is measured on the outside of the tubing wall, this condition is not always obtained. In some instances, measured refrigerant temperature and pressure correspond to point 4 being on the left (subcooled, liquid) side of the dome (Figure 2-5). Temperature of point 4 is then adjusted and taken at the saturated vapor point at the compressor outlet pressure to reflect the initial assumption (more details will follow in section 3.2.2 – "Refrigerant side and defrost cycles").

### 2.2.2 Air side

Validation of the refrigerant side heat output with measurements on air side was only introduced at the end of the testing phase. Indeed, it was originally assumed that measuring the indoor fan air volumetric flow could be avoided by leaving the indoor unit fan speed at "high" for all the test phase and taking the rated air flow value under these conditions (399 CFM) to estimate heat output on air side with Equation (2.2).

$$\dot{Q}_{air_side_approx} = \dot{m}_{v_outlet} * Cp_{air} * (T_{12} - T_{11}) \tag{2.2}$$

However, large discrepancies with heat output on refrigerant side and previous studies (Winkler 2011) revealed that the indoor unit fan air flow at "high" speed was probably significantly lower than the rated value. Therefore, an attempt was made to measure the volumetric air flow rate during the last week of testing (Figure 2-7).

Figure 2-7: Anemometer added to the test bench

Under these circumstances, air flow could not be measured according to the standard method tracking the pressure drop through a calibrated nozzle (Alexander et al. 1987). Instead, the air flow is estimated by fixing the anemometer perpendicular and as close as possible to the vanes to measure the air speed (the uncertainty of the measurements is estimated at 20 %). Then, this value is compared to the equivalences in Table 2-2 to estimate the airflow by a simple proportional calculation. The heat output on air side is calculated using Equation (2.2), as described previously.

Table 2-2: Indoor unit outlet air speed and volumetric air flow equivalences (adapted from Mitsubishi Electric Corporation (2009b))

| Model | Mode | Function | Air flow (CFM) | Air speed (ft/s) | Coverage (ft) |
|---|---|---|---|---|---|
| **MSZ-FE09NA** | HEAT | Dry | 381 | 19.2 | 27.7 |
| | COOL | Dry | 339 | 17.1 | 24.7 |
| | | Wet | 307 | 15.5 | 22.4 |
| **MSZ-FE12NA** | HEAT | Dry | 420 | 21.2 | 30.4 |
| | COOL | Dry | 381 | 19.2 | 27.7 |
| | | Wet | 350 | 17.6 | 25.4 |

It is also assumed that humidity can be neglected in the air side heat output calculations, which leads to Equation (2.3).

$$\dot{Q}_{air_side_real} = \dot{m}_{v_outlet} * (h_{12} - h_{11}) \quad (2.3)$$

Indeed, a simple EES (Klein 2016) script compares the difference between Equation (2.2) (with a constant $Cp_{air}$ value of 1.01 kJ/kg-K) and Equation (2.3) for ambient temperatures from -20 °C to 20 °C, and for a relative humidity of 0 % to 100 %. Relative error between the two methods always remains less than 1 %, suggesting that heat output on air side can be properly estimated by (2.2).

## 2.3 Fresh air fans control strategy

The ability to control the fresh air fan speed in both sheds with a Raspberry Pi computer provides flexibility, stability and makes it easier to reproduce similar conditions from one test to the other.

To better characterize the performance map of the tested VCASHP unit, tests are generally performed at a constant outdoor shed temperature and under a constant indoor shed heating load for the entire night (approximately 16 hours).

### 2.3.1 Constant outdoor shed temperature

The outdoor unit is encapsulated in a testing shed to have better control over the ambient temperature "seen" by the unit (thereafter named "outdoor shed temperature"). Indeed, variations in ambient temperature over the course of a test can be compensated by adjusting the fresh air fan speed so that the outdoor unit is exposed to a constant outdoor shed temperature.

For example, a test can be conducted at a constant outdoor shed temperature of -20 °C when the ambient temperature is -10 °C. The heat pump will start to operate, extract the heat from the outdoor shed and move it to the indoor shed until the outdoor shed temperature drops below -20 °C. Then, the fresh air fan will start and/or raise its speed until the outdoor shed temperature is stabilized at -20 °C. If during that night, the ambient temperature drops to -25 °C (colder than the outdoor shed temperature), the electric baseboards can be used to maintain the outdoor shed temperature at -20 °C.

### 2.3.2 Constant indoor shed heating load

Maintaining the indoor shed heating load at a constant value over the course of a test is key to evaluate the VCASHP performance. Once again, this can be achieved by adjusting the fresh air intake according to variations in ambient temperature; warmer weather results into higher fresh air fan speeds (and vice versa), so that the heating load remains constant.

The control strategy is first based on an accurate thermal characterization of the indoor shed. A global heat loss and infiltration product $(UA)_T$ is obtained for every indoor exhaust fan speed or voltage. Indeed, the Raspberry Pi computer is used as a Proportional-Integral (PI) micro controller for fan voltage levels (0 – 10 V). Table 2-3 shows the correspondence between PID signal values and fan voltage levels.

Table 2-3: PID signal values and corresponding fan voltage levels

| **Voltage (V)** | < 1.9 (off) | 3 | 4 | 5 | 6 | 7 | 8 | 9 | 9.9 |
|---|---|---|---|---|---|---|---|---|---|
| **PID** | 500 | 1000 | 1329 | 1665 | 1995 | 2330 | 2665 | 3000 | 3325 |

The 700 CFM-rated exhaust fan is operated at different speeds by sending a signal between 0 – 10 V to the controller. For each speed, the heat pump is shut off and heating is entirely assumed by two 750 W baseboard heaters and one 1221 W portable heater, until a steady-state indoor temperature is reached. Equation (2.4) is used to determine $(UA)_T$ for each fan speed. Internal gains essentially come from equipment - tests conducted at night - and are estimated at 100 W.

$$(UA)_T = \sum \dot{Q} \ / \ (T_{set} - T_{amb}) \tag{2.4}$$

$$@\ 3\ V\ (PID = 1000): (UA)_T = \frac{(1221 + 750 + 750 + 100)\ W}{\big(21 - (-4)\big)\ °C} = 112.8\ W/\ K$$

Figure 2-8 expresses PID signal values with respect to $(UA)_T$ for a variety of exhaust fan speeds, which leads to the following simple linear regression model (Equation 2.5).

$$PID = 14.901 * (UA)_T - 821.28 \tag{2.5}$$

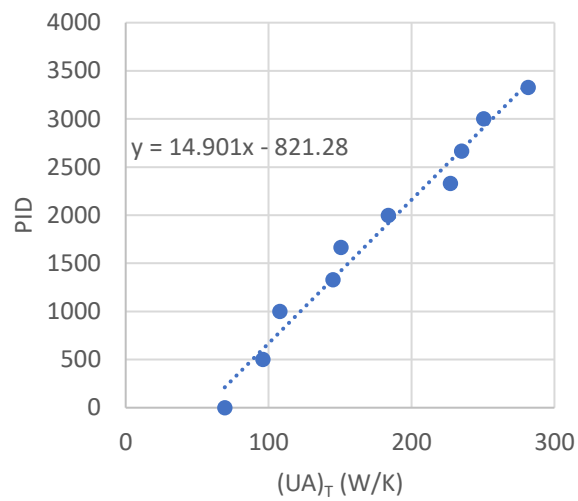


Figure 2-8: Exhaust fan speed PID voltage with respect to $(UA)_T$ for the indoor shed

This model then allows to perform constant load tests on the indoor shed. For a constant indoor shed temperature and heating load seen by the heat pump (last term of Equation 2.6), $(UA)_T$ – equivalent to the sum of $U_TA_T$ and $\dot{m}_{inf} * Cp_{air}$ – remains the only unknown in (2.6). It is recalculated at every time step, and the corresponding PID is used by the Raspberry Pi to modulate the fresh air intake according to variations in ambient temperature ($T_{amb}$).

$$U_T A_T * (T_{indoor\ shed} - T_{amb}) + \dot{m}_{inf} * Cp_{air} * (T_{indoor\ shed} - T_{amb}) - \dot{Q}_L - \dot{Q}_P - \dot{Q}_{EQ} - \dot{Q}_{solar} - \dot{m}_v * Cp_{air} * (T_{supply} - T_{indoor\ shed}) = 0 \quad (2.6)$$

In summary, this control strategy allows to reproduce a wide variety of constant heating loads and building UAs. Figure 2-9 displays the range of possible heating load lines for the indoor shed from the maximum to the minimum exhaust fan speed (OFF). These load lines were obtained with Equation (2.5) and (2.6), for every fan voltage level (PID) shown in Table 2-3. Therefore, a load line similar to the DOE standard (Equation 1.8) can be reproduced by adequately selecting the exhaust fan voltage (3V, in this case).

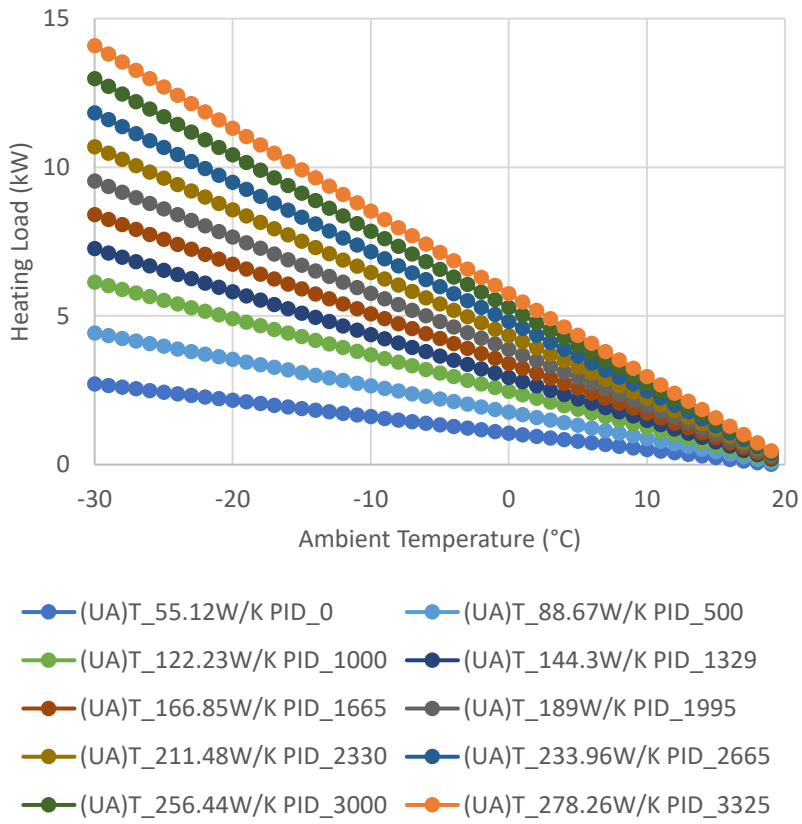


Figure 2-9: Range of possible heating load lines induced by the fresh air fans on the indoor shed

## 2.4 Approach

The key feature of this testing bench is the ability to explicitly measure the compressor operating speed. Therefore, particular attention is paid to varying heating loads at each outdoor shed temperature in order to obtain the widest possible range of frequencies and sufficient amount of data for each of these conditions. These results will then be used to compare the heat pump performance to manufacturer data and build a model to obtain better understanding of ductless VCASHPs.

# CHAPTER 3 RESULTS

## 3.1 Results overview

Global performance results are given in Figure 3-1, showing the heating capacity with respect to outdoor shed dry-bulb temperature and compressor frequency for the entire set of tests held between Dec 7 th, 2016 and Apr 5th, 2017. The indoor temperature setpoint and the indoor unit fan operation are maintained constant at 21 °C and "high speed", respectively. Although their variation can affect the heat pump performance, these impacts are not discussed and all presented plots and equations are limited to one indoor temperature and fan speed operation.

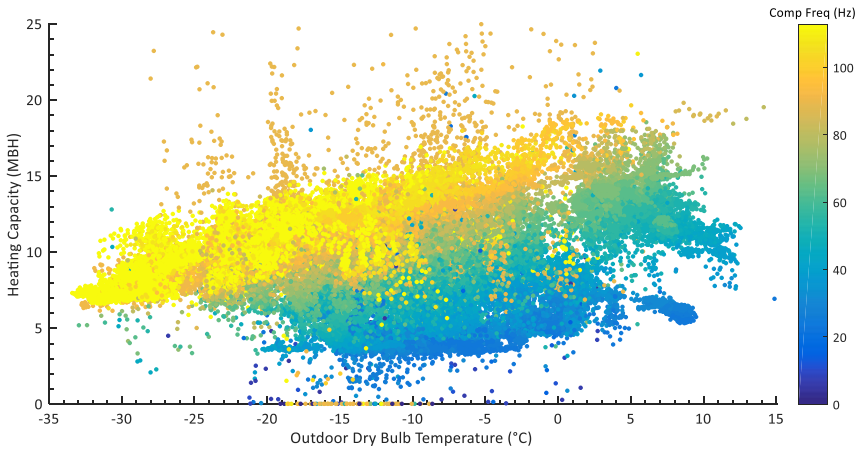


Figure 3-1: Global performance results for heating capacity with respect to outdoor shed temperature

The 1-ton commercially-available ductless VCASHP is able to operate at very low outdoor shed temperatures. The inverter-driven compressor also shows the ability to modulate frequency for different outdoor shed temperatures and heating loads. The maximum capacity generally increases with outdoor shed temperature and remains below the advertised 21 000 Btu/h mark. Frequency range also seems partially limited. At very low outdoor shed temperatures, compressor is mostly at high or maximum speed. At mild outdoor shed temperatures, compressor frequencies higher than 75 Hz are rarely obtained, which might limit the maximum heating capacity. Moreover, compressor frequencies lower than 20 Hz do not occur under any conditions.

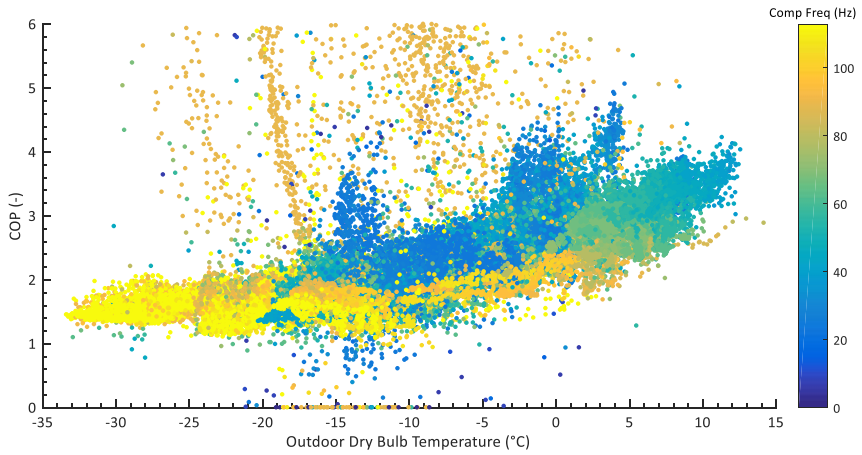


Figure 3-2: Global performance results for COP with respect to outdoor shed temperature

Measured COP is also found to be greater than 1.0 for every heating load and for the entire range of outdoor shed temperatures (outliers will be discussed below). Figure 3-2 displays the COP with respect to outdoor shed dry-bulb temperature and compressor frequency for the same set of tests. As expected, COP is greater at lower compressor frequencies and generally increases with outdoor shed temperature. Below -15 °C, compressor frequency is generally high and the COP stabilizes between 1.5 and 2.0, even under low frequencies. Moreover, a significant number of data points show suspiciously high or low COP values and need closer attention (more details will follow).

## 3.2 Detailed analysis

Manufacturer data curves for the tested unit are given at steady state. Therefore, results obtained under transient conditions need to be removed from the global dataset before comparing the unit measured performance to the manufacturer data.

First, a validation of the normal operation control strategy - as defined in the service manual - is performed. A review of the exceptions that disqualify some data points follows.

### 3.2.1 Normal operation

VCHP manufacturers are generally reluctant to reveal their exact control strategy. However, the tested unit's contractor guide contains the following general guidelines: a change in indoor

temperature triggers a change in compressor frequency and refrigerant mass flow rate, which results in a variation of the indoor heat exchanger temperature, which in turn causes a variation of the indoor temperature (Mitsubishi Electric 2013).

These guidelines are validated by measurements. Indeed, Figure 3-3 shows the evolution of indoor air temperature, compressor frequency, refrigerant mass flow rate and indoor heat exchanger inlet refrigerant temperature.

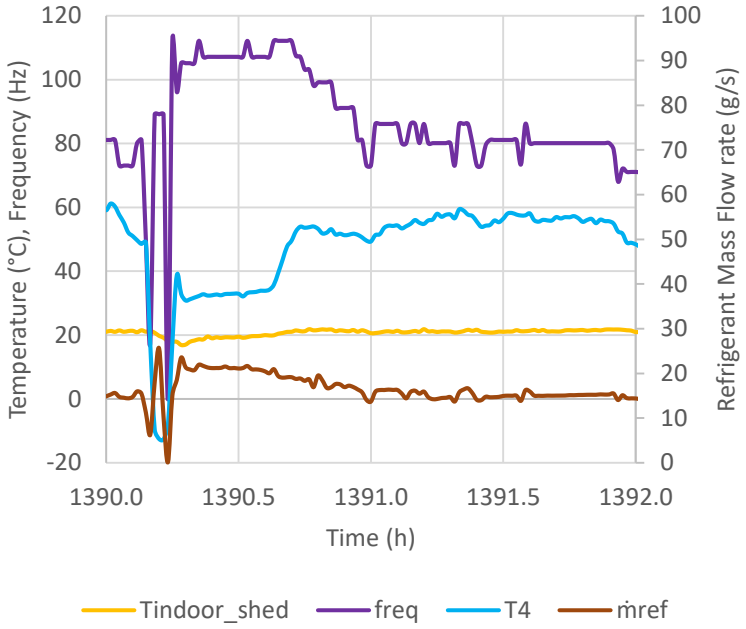


Figure 3-3: Typical evolution of indoor air temperature, compressor frequency, refrigerant mass flow rate and indoor heat exchanger inlet refrigerant temperature

At 1390.2h, the indoor air temperature ($T_{indoor_shed}$) decreases during a defrost cycle. The compressor frequency (freq) and the refrigerant mass flow rate ($\dot{m}_{ref}$) ramp up, which eventually causes the indoor heat exchanger inlet refrigerant temperature ($T_4$) to rise and contributes to the increase of the indoor temperature. Both compressor frequency and refrigerant mass flow rate then slightly decrease until the indoor temperature is stabilized at the setpoint (21 °C). This rather long recovery period after the defrost cycle is discussed in the next section.

### 3.2.2 Refrigerant side and defrost cycles

The methodology chosen to perform heat output calculations seems to induce errors during the 30-min period after defrost cycles.

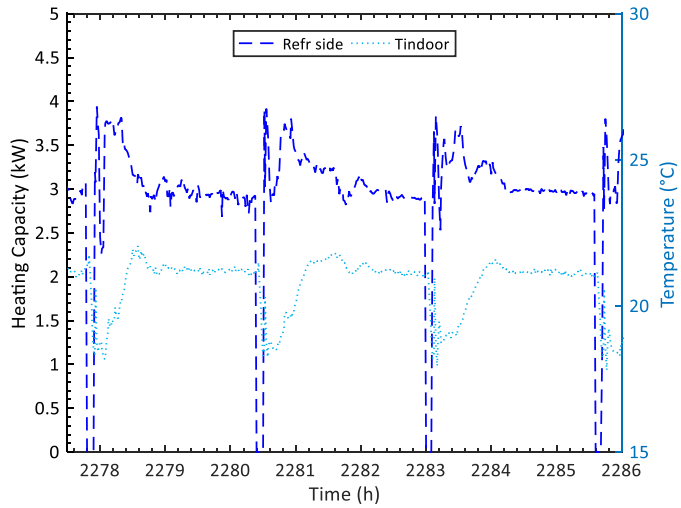


Figure 3-4: Heating capacity and indoor shed temperature over a typical night of testing (approximately $T_{outdoor_shed}$ = -15 °C)

Figure 3-4 shows the heating capacity and the temperature of the indoor shed measured over a typical night of testing (approximately $T_{outdoor_shed}$ = -15 °C), with data points collected every minute. Under these conditions, defrost cycles occur approximately every 2.5 hours (2277.8 h, 2280.4 h, etc.) and last 6 min.

At 2277.8 h, the compressor stops, the 4-way valve reverses the cycle and the compressor restarts. With indoor and outdoor fans closed, the VCASHP is temporarily in cooling mode to allow the ice to melt on outdoor heat exchanger coils. Heat output is therefore zero and indoor temperature drops.

At 2277.9 h, defrost ends. The compressor stops, the 4-way valve reverses the cycle and the compressor restarts once again. Indoor and outdoor fans resume, and the VCASHP is back in heating mode.

As described earlier, the test bench is designed to perform heat output calculations on refrigerant side (Equation 2.1, in the Methodology chapter). Figure 3-5 shows the theoretical pressure-

enthalpy diagram of the refrigerant in heating mode. At the condenser inlet (point 4,assump), refrigerant is assumed to be 100 % vapor.

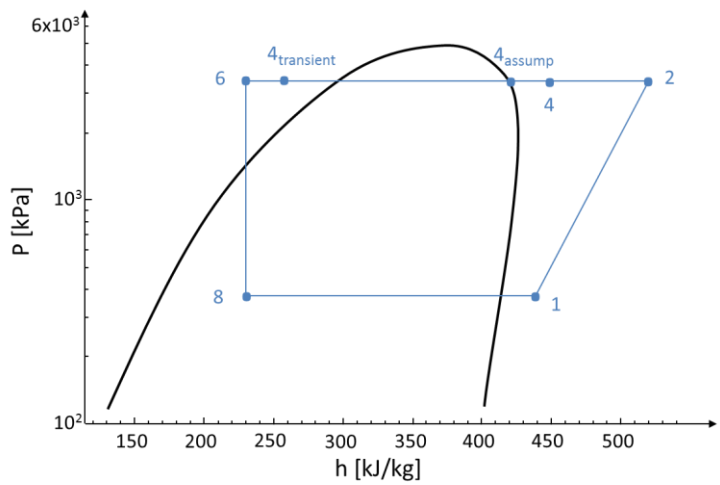


Figure 3-5: R-410A heat pump cycle p-h diagram in heating mode (adapted from Klein 2016)

However, during the 30-min period after defrost, measured refrigerant temperature ($T_{4,transient}$) is significantly below the saturated vapor point ($T_{4,assump}$, in blue), as seen in Figure 3-6 (note that in steady-state, $T_{4,assump}$ is considered equal to $T_4$ for clarity of exposition). The 100% vapor assumption does not consider the transitory effects that occur on both heat exchangers and on the refrigerant cycle after defrost, temporarily limiting heat output and indoor temperature.

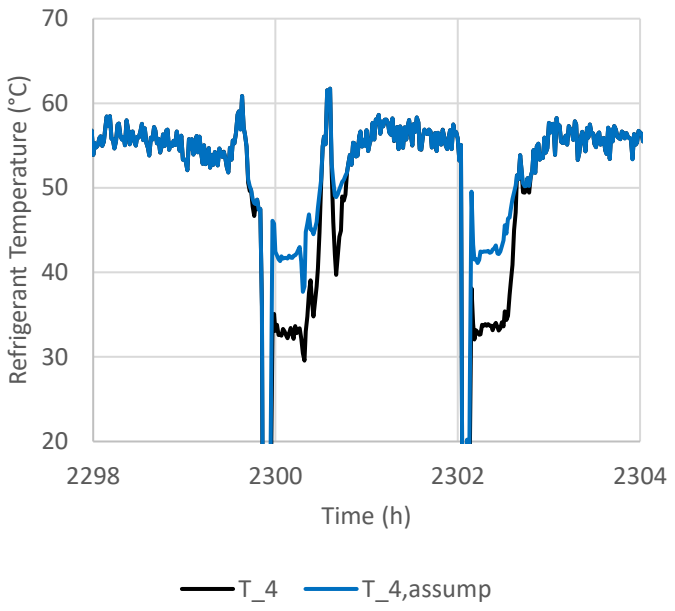


Figure 3-6: Measured refrigerant temperature at the condenser inlet ($T_4$) compared to the saturated vapour point ($T_{4,assump}$, in blue)

This creates large discrepancies between assumed ($h_{4,assump}$) and measured enthalpy ($h_4$) under transient conditions ($h_{4,transient}$), as seen in Figure 3-7 (as explained previously, note that in steady-state when $T_4$ is greater than $T_{4,assump}$, $h_{4,assump}$ is considered equal to $h_4$ for clarity of exposition).

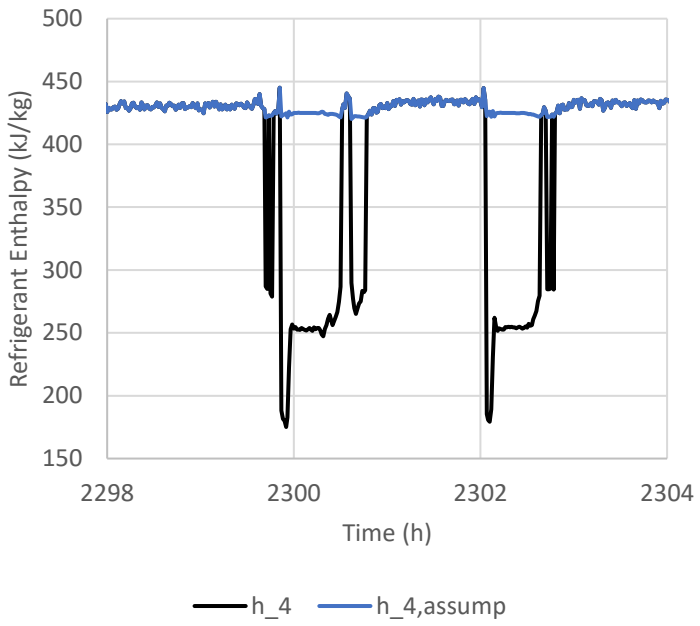


Figure 3-7: Measured ($h_4$) and assumed ($h_{4,assump}$) refrigerant enthalpy at the condenser inlet

Indeed, a measured refrigerant temperature below the saturated vapor point pushes point 4 in the subcooled region - on the left side of the dome – on Figure 3-5, which seems highly unlikely at the condenser inlet.

In other words, heat output calculations on refrigerant side during this 30-min period after defrost are largely based on an assumption that seems to be in contradiction with measurements. Figure 3-8 displays the large heat output discrepancies between the measurements ($\dot{Q}_{ref_side}$) and the 100 % vapor assumption during these periods ($\dot{Q}_{ref_side,assump}$).

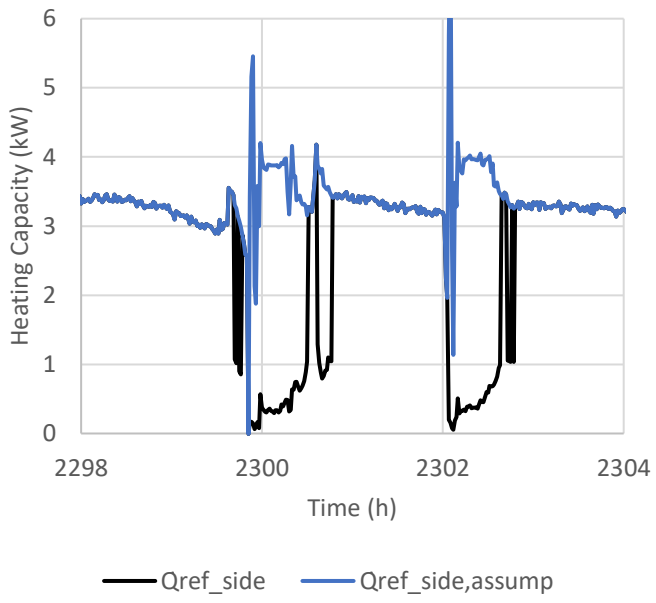


Figure 3-8: Measured and assumed refrigerant heat output on refrigerant side

Therefore, validation with heat output calculated on air side seems crucial for this period. As explained previously, an anemometer was added to the lab during the last week of testing. Figure 3-9 presents the recorded indoor unit outlet air flow, which displays a mostly constant profile at approximately 300 CFM. Though largely below rated high fan speed (399 CFM), this estimated airflow is rather close to values measured (338 CFM) in other experiments with the same heat pump model (Winkler 2011).

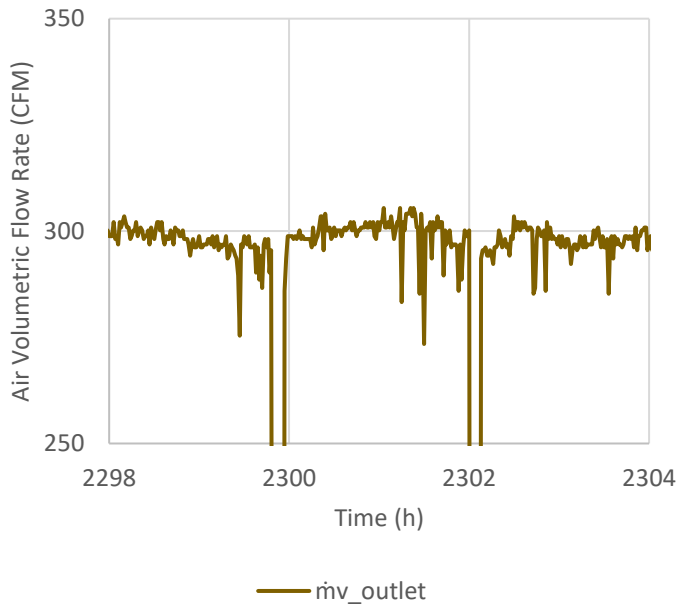


Figure 3-9: Air Volumetric Flow Rate at the indoor HX outlet of the heat pump

Figure 3-10 displays the supply and indoor air temperatures, along with the heat output calculated on air side (using Equation 2.2). The supply air temperature (gray) and the heat output on air side (red) seem to display a similar profile. Indeed, at 2297.5 h, a sudden increase in the supply temperature has the same effect on heat output (air side) and indoor temperature.

Figure 3-10: Supply and indoor temperatures, along with heat output calculated on air side

Figure 3-11 compares heat output on air side and refrigerant side (measured and assumed). The two methods yield similar results at steady state. However, significant discrepancies exist during the 30-min period after defrost cycles. Heat output on air side is comprised between the measured and assumed refrigerant side heat output.

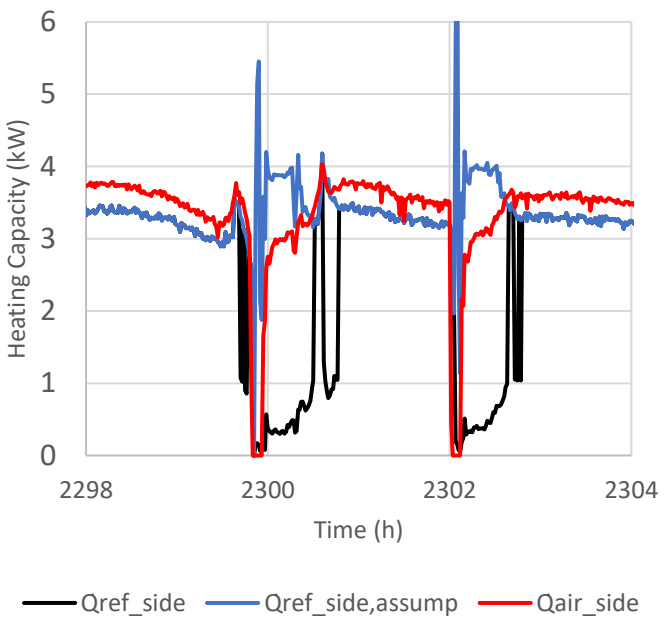


Figure 3-11: Heat output measured (black) and assumed (blue) on refrigerant side compared to heat output measured on air side (red)

Furthermore, Figure 3-12 shows that the indoor temperature curve profile seems to better match the heat output calculated on air side. Indeed, it seems unlikely that the refrigerant side heat output local maxima - @ 2300 h, 2302 h - would coincide with indoor temperature local minima.

Figure 3-12: Comparison of the indoor temperature profile (yellow) to the heat output measured on air side (red) and assumed on refrigerant side (blue)

In summary, the 100 % vapor assumption leads to an overestimation of the heat output during the 30-min period after defrost cycles. This assumption does not consider the transient effects that occur on both heat exchangers and on the refrigerant cycle after defrost, temporarily limiting heat output and indoor temperature.

Consequently, the air side method seems better suited to evaluate the capacity during these periods. However, airflow monitoring was only introduced at the very end of the testing phase, meaning that refrigerant side is the only heat output available for most of the data points.

This leaves exclusion as the only viable option to adjust the refrigerant side heat output values. Figure 3-13 displays the COP of the entire set of results. The difference with Figure 3-2 is that transient results - data points captured during defrost cycles and up to 30 min after - are identified with a cross ('x'). It appears clear that the vast majority of outliers come from transient results. Once again, this suggests that COP might be overestimated during and 30 min after defrost cycles.

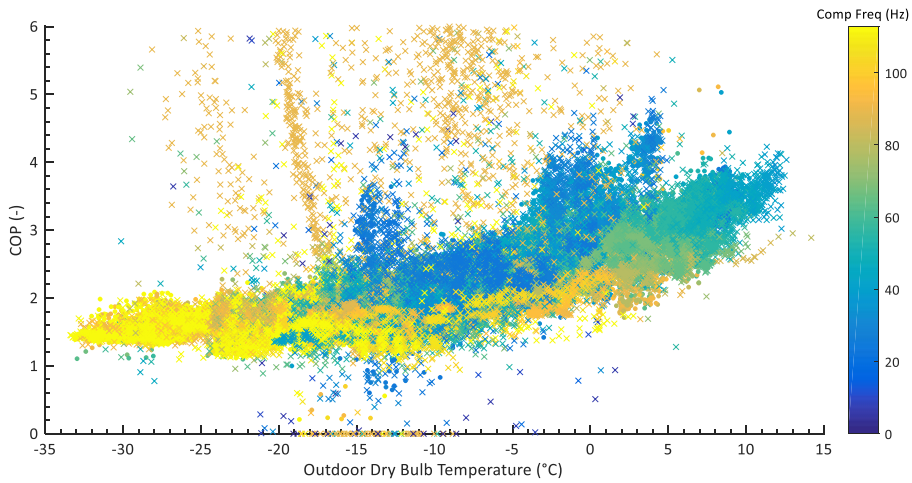


Figure 3-13: COP of steady-state (filled) and transient ('x') data points

Therefore, the data points obtained during defrost cycles and up to 30 min after defrost cycles are removed from the steady state dataset used to compare results to manufacturer data and build the VCASHP model in the following sections.

### 3.2.3 Solar gains

Some data points obtained during daytime yield inconsistent results. Two factors seem to cause them: the poor performance of the RTD ambient temperature probe under direct sunlight, and the inappropriate indoor fresh air fan control strategy under these conditions (described previously in Chapter 2).

Figure 3-14 shows that RTD ambient temperatures obtained when the sun hit the west facade of the test shed – 1836 h, 1860 h - are inconsistent and up to 10 °C over the reference.

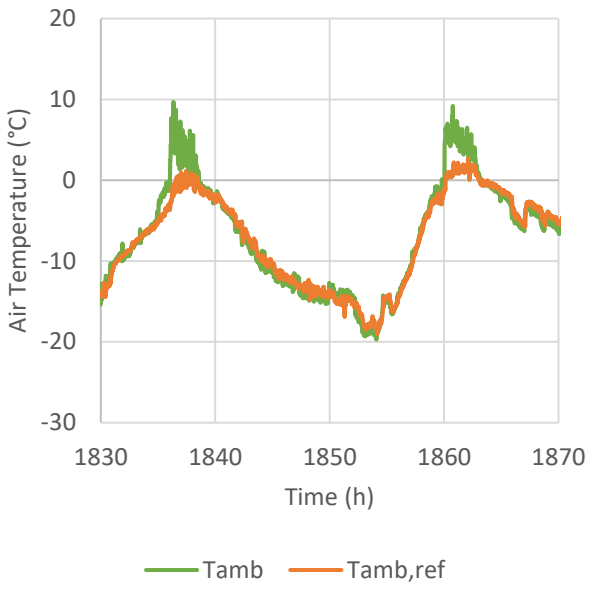


Figure 3-14: Measured ambient temperature (RTD) compared to reference (OMEGA)

This temporary overestimation of the ambient temperature also affects the indoor fresh air fan operation. Indeed, the fan speed is increased according to the overestimated ambient temperature, leading to much larger heating loads than planned. The evolution of the dry-bulb ambient temperature, the indoor temperature and the compressor frequency are presented in Figure 3-15.

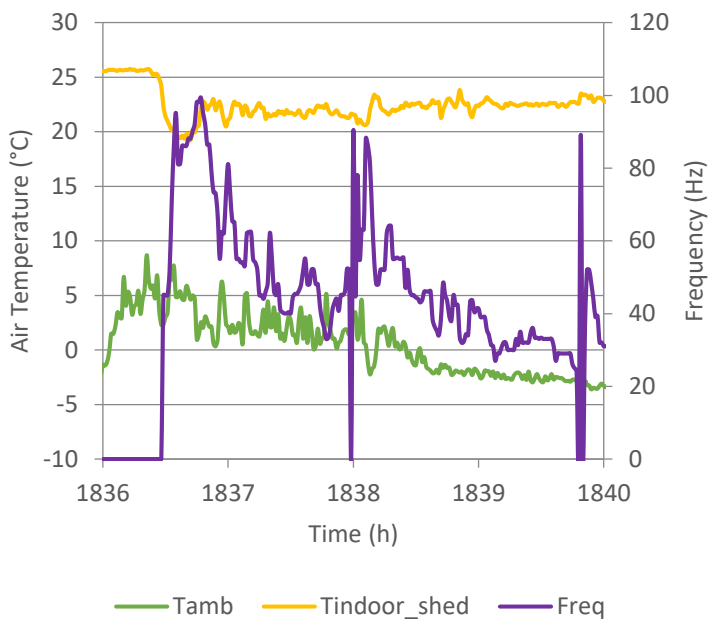


Figure 3-15: Evolution of the dry-bulb ambient temperature, indoor temperature and compressor frequency with the RTD ambient temperature probe under direct sunlight

At 1836 h, the small load combined to the solar gain contribution (not monitored) leads to an indoor temperature of more than 25 °C, which causes the VCHP compressor to stop. The sudden decrease of the indoor temperature at 1836.5 h is caused by the triggering of the indoor fresh air fans, influenced by the overestimated ambient temperature. For the next hours, the heating load increases systematically and the VCHP compressor operates at a much higher speed than what would normally be needed.

In summary, since transient effects can be induced by the sun, all data points obtained during daytime are removed from the steady state dataset.

### 3.2.4 Short cycling

Short cycling occurs when the heating load is below the minimal heating capacity of the VCHP. The heat pump stops, which eventually causes the indoor temperature to decrease. The VCHP then resumes at maximum speed, as dictated by the heat pump control strategy. Quickly, the VHCP overshoots the indoor setpoint and stops again. The same cycle is then repeated.

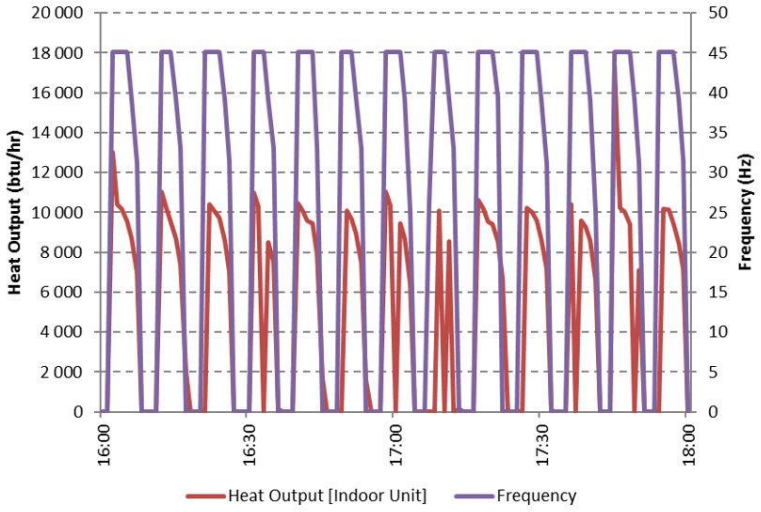


Figure 3-16: Short cycling heat output and frequency (McDonald and Kegel 2017)

VCHP manufacturers claim that the ability of their compressors to operate at very low speeds can prevent this ineffective operation. However, measurements reveal that short cycling occurs with heating loads of approximately 6000 Btu/h (Figure 3-16), which is well over the claimed minimum capacity of 3000 Btu/h. This also confirms what had been previously reported by Winkler (2011).

Data points obtained under transient short cycling conditions are also removed from the steady state dataset.

### 3.2.5 Protection mechanisms

Various protection mechanisms regulate VCHP performance. As explained previously, they prevent extreme refrigerant temperatures that can potentially damage the heat pump (Messmer (2013); Bertsch & Groll (2008); Kegel et al.(2017)).

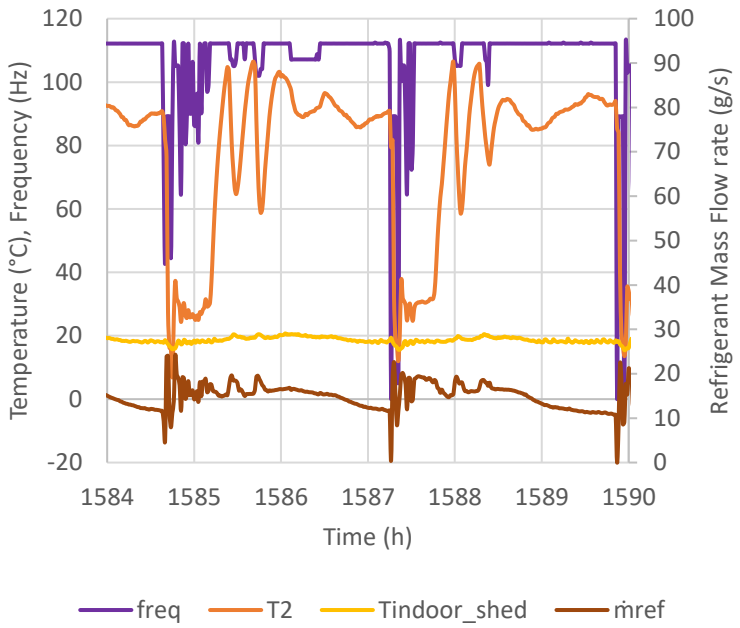


Figure 3-17: Discharge temperature ($T_2$) protection at full load

The first one concerns discharge temperature (compressor outlet, $T_2$) and is well documented in the manufacturer service manual (Mitsubishi Electric Corporation 2009a). Figure 3-17 displays compressor frequency, compressor outlet temperature, indoor air temperature and refrigerant mass flow rate at a near-maximal capacity infiltration load of 12 500 Btu/h. After defrost cycles at 1584.7 h and 1587.2 h, frequency (freq) ramps up to maximum (112.5 Hz) and refrigerant mass flow rate ($\dot{m}_{ref}$) is increased until compressor outlet temperature ($T_2$) raises around 30 min later. However, peaks and valleys occur every time $T_2$ reaches over 100 °C, suggesting a limit might be imposed. After two or three attempts, this seems to lead to an eventual decrease of $T_2$, $\dot{m}_{ref}$ and indoor air temperature ($T_{indoor_shed}$) for the remaining time before the following defrost cycle, even when the compressor operating frequency is maximal. Note that the compressor outlet pressure, the heat output and the power input are not shown on Figure 3-17, but also show a decrease for the remaining time before the following defrost cycle.

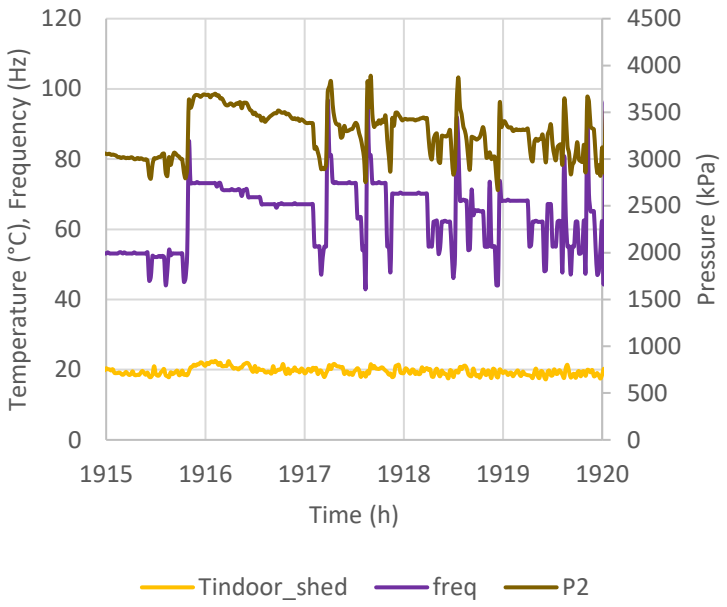


Figure 3-18: Compressor outlet pressure ($P_2$) protection control

A similar protection control seems implemented for compressor outlet pressure ($P_2$), as shown in Figure 3-18. At 1915.8 h, high and constant values of $P_2$ help maintain the indoor setpoint (21 °C). However, $P_2$ soon decreases and cycling starts at 1917.2 h, often bringing $T_{indoor_shed}$ below 20 °C. Recurrent levels of peaks and valleys for $P_2$ suggest there might be a pressure limit around 3750 kPa to protect the heat pump, as documented in Mitsubishi Electric Corporation (2009a). Thus, the system's control strategy and protection controls could explain why compressor frequencies higher than 75 Hz could not be maintained at mild outdoor shed temperatures, and why the indoor setpoint and the heating load were hardly met.

It could be helpful to remove results affected by these protection controls. Indeed, for similar tests conditions (e.g. same heating load and outdoor shed temperature), VCHP performance can vary significantly depending if the protection mechanisms have intervened or not. Unfortunately, the control strategy and the implications of these protection mechanisms are not fully understood at this stage. Therefore, data points obtained under protection mechanisms have to remain part of the dataset labeled as "steady state results" that will be compared to manufacturer data.

In summary, steady state results include data points affected by protection mechanisms, but exclude measurements during defrost cycles (and the 30-min period following them), daytime and short

cycling conditions. The global results of approximately 90 000 data points are reduced to 41100 data points.

## 3.3 Steady state results

Steady state results for heating capacity, power input and COP are presented in Figure 3-19, Figure 3-20 and Figure 3-21. Data is collected every minute.

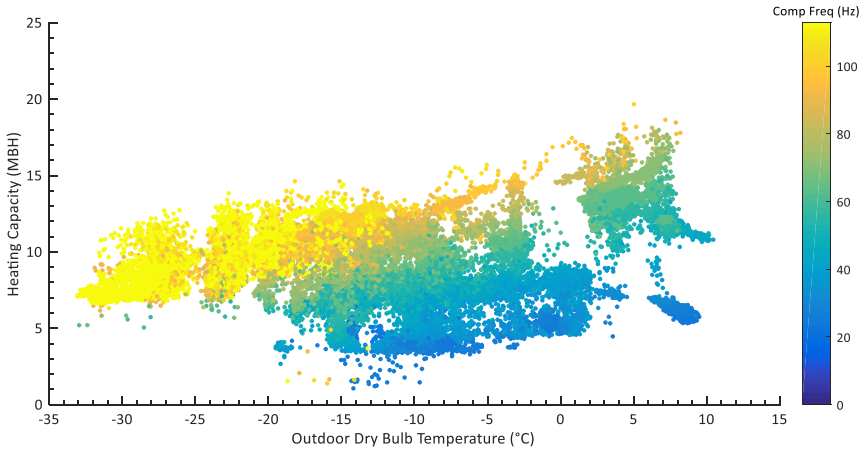


Figure 3-19: Steady-state results for heating capacity with respect to outdoor shed temperature

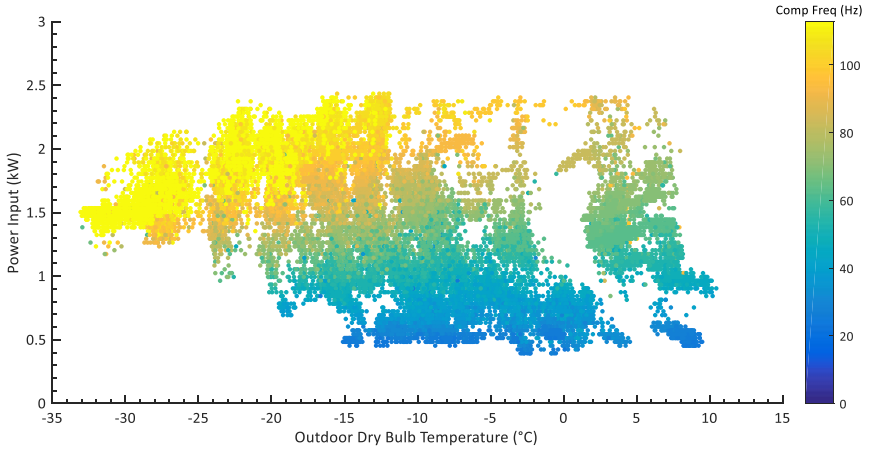


Figure 3-20: Steady-state results for power input with respect to outdoor shed temperature

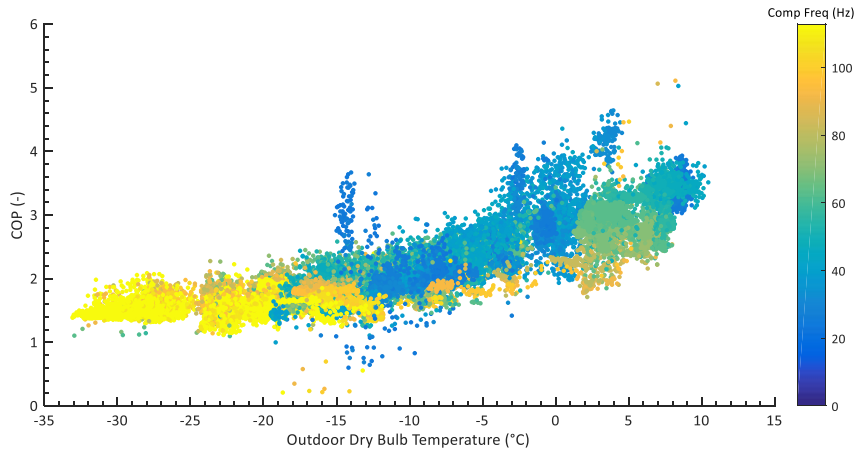


Figure 3-21: Steady-state results for COP with respect to outdoor shed temperature

In general, steady state results display a similar profile than the previously presented global results. As expected, the suspiciously high (and low) capacity and COP data points found in global results have disappeared.

Results also show a lack of higher frequency data points around 0 °C (Figure 3-19 and Figure 3-20). Future work should focus on imposing high heating loads at this outdoor shed temperature to complete this part of the performance map, keeping in mind that defrost cycles probably happen more frequently under these conditions. Therefore, if defrost cycle data points - and those from the 30 min period following - are excluded from steady state results, this might not leave much time to collect steady state data before the next defrost cycle.

To facilitate comparison with manufacturer data curves, regression is performed using only steady state results.

## 3.4 Comparison to manufacturer data

### 3.4.1 Frequency bins

The previous steady state results are broken down into 5 Hz wide frequency bins from 20 Hz to 115 Hz. Figure 3-22 shows the polynomial linear regression curve that can be extracted for capacity

with respect to outdoor shed temperature at 50 Hz. A similar linear regression curve is obtained for every frequency bin.

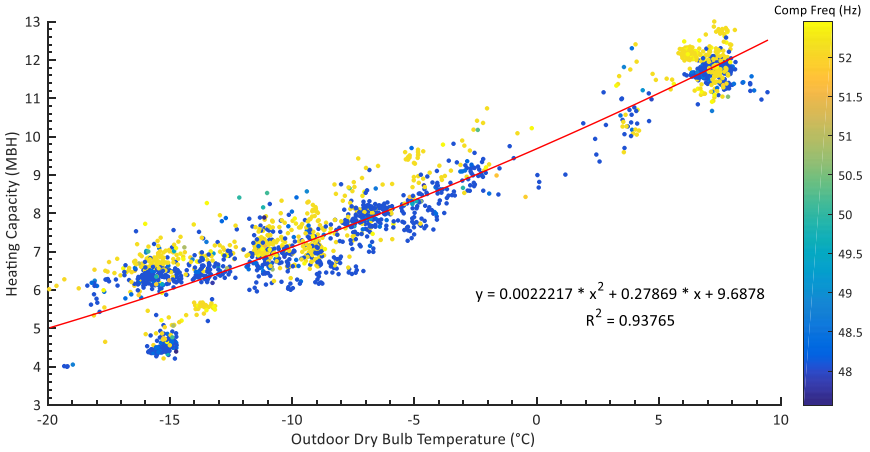


Figure 3-22: Polynomial linear regression for capacity vs outdoor shed temperature (50 Hz)

### 3.4.2 How manufacturer data is obtained

An example of VCHP manufacturer data is first presented at rated frequency (52.5 Hz) in Table 3-1. The capacity and power consumption of the VCHP vary depending on the outdoor shed conditions and the indoor air temperature. Relative humidity is assumed constant at an arbitrary value (75 %) to convert the wet-bulb outdoor temperatures provided by the manufacturer to dry-bulb temperatures before entering them in the model performance table.

Table 3-1: Example of VCHP manufacturer data at a rated frequency of 52.5 Hz (Mitsubishi Electric Corporation 2009a)

| Model | Indoor air IDB (°F) | Outdoor intake air WB temperature (°F) | | | | | | | | | | | | | |
|---|---|---|---|---|---|---|---|---|---|---|---|---|---|---|---|
| | | 5 | | 15 | | 25 | | 35 | | 43 | | 45 | | 55 | |
| | | TC | TPC | TC | TPC | TC | TPC | TC | TPC | TC | TPC | TC | TPC | TC | TPC |
| **MUZ-FE09NA** | 75 | 4.8 | 0.44 | 6.3 | 0.56 | 7.9 | 0.66 | 9.4 | 0.73 | 10.6 | 0.77 | 11.0 | 0.78 | 12.4 | 0.81 |
| | 70 | 5.2 | 0.42 | 6.7 | 0.54 | 8.2 | 0.64 | 9.6 | 0.71 | 10.9 | 0.75 | 11.2 | 0.77 | 12.7 | 0.80 |
| | 65 | 5.5 | 0.41 | 6.9 | 0.52 | 8.6 | 0.62 | 10.0 | 0.69 | 11.2 | 0.73 | 11.6 | 0.74 | 13.0 | 0.78 |
| **MUZ-FE09NAH** | 75 | 4.8 | 0.57 | 6.3 | 0.69 | 7.9 | 0.79 | 9.4 | 0.73 | 10.6 | 0.77 | 11.0 | 0.78 | 12.4 | 0.81 |
| | 70 | 5.2 | 0.55 | 6.7 | 0.67 | 8.2 | 0.77 | 9.6 | 0.71 | 10.9 | 0.75 | 11.2 | 0.77 | 12.7 | 0.80 |
| | 65 | 5.5 | 0.54 | 6.9 | 0.65 | 8.6 | 0.75 | 10.0 | 0.69 | 11.2 | 0.73 | 11.6 | 0.74 | 13.0 | 0.78 |
| **MUZ-FE12NA MUZ-FE12NA1** | 75 | 6.0 | 0.58 | 7.9 | 0.73 | 9.9 | 0.86 | 11.8 | 0.96 | 13.3 | 1.00 | 13.7 | 1.02 | 15.5 | 1.06 |
| | 70 | 6.5 | 0.55 | 8.4 | 0.71 | 10.2 | 0.84 | 12.0 | 0.93 | 13.6 | 0.98 | 14.0 | 1.00 | 15.8 | 1.04 |
| | 65 | 6.8 | 0.53 | 8.6 | 0.68 | 10.7 | 0.81 | 12.4 | 0.91 | 14.0 | 0.96 | 14.4 | 0.97 | 16.2 | 1.02 |
| **MUZ-FE12NAH** | 75 | 6.0 | 0.71 | 7.9 | 0.86 | 9.9 | 0.99 | 11.8 | 0.96 | 13.3 | 1.00 | 13.7 | 1.02 | 15.5 | 1.06 |
| | 70 | 6.5 | 0.68 | 8.4 | 0.84 | 10.2 | 0.97 | 12.0 | 0.93 | 13.6 | 0.98 | 14.0 | 1.00 | 15.8 | 1.04 |
| | 65 | 6.8 | 0.66 | 8.6 | 0.81 | 10.7 | 0.94 | 12.4 | 0.91 | 14.0 | 0.96 | 14.4 | 0.97 | 16.2 | 1.02 |
| **MUZ-FE18NA** | 75 | 9.5 | 0.91 | 12.5 | 1.15 | 15.7 | 1.35 | 18.7 | 1.50 | 21.1 | 1.58 | 21.7 | 1.60 | 24.6 | 1.66 |
| | 70 | 10.3 | 0.87 | 13.3 | 1.11 | 16.2 | 1.32 | 19.1 | 1.46 | 21.6 | 1.54 | 22.2 | 1.57 | 25.2 | 1.63 |
| | 65 | 10.8 | 0.83 | 13.6 | 1.06 | 17.0 | 1.27 | 19.8 | 1.42 | 22.2 | 1.50 | 22.9 | 1.52 | 25.7 | 1.60 |

**NOTE**: 1. IDB : Intake air dry-bulb temperature
TC : Total Capacity (x$10^3$ Btu/h) TPC : Total Power Consumption (kW)
2. Above data is for heating operation without any frost.

Unlike conventional heat pumps, another variable has to be considered: the compressor frequency. Indeed, a VCHP rarely operates at rated speed, and the table presented above can change significantly with the unit compressor frequency. Figure 3-23 presents the capacity and power input correction curves extracted from the user manual.

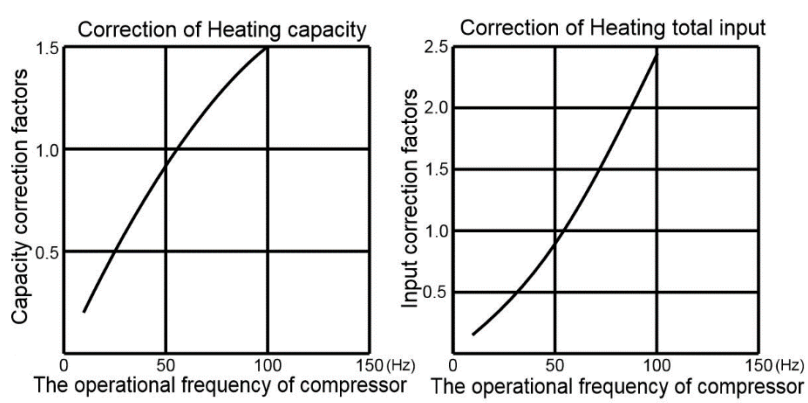


Figure 3-23: Example of capacity (left) and power input (right) correction curves for frequency (Mitsubishi Electric Corporation 2009a)

Multiplying the rated capacity and power input by the correction factor allows to extrapolate error-induced manufacturer curves for comparison with tests results at different compressor speeds.

### 3.4.3 Analysis

As explained previously, measured capacity, power input and COP are approximated by polynomial curve fits for every 5 Hz wide frequency bin. Figure 3-24 presents a comparison between measured and manufacturer published (dashed lines) heating capacity for a variety of chosen frequencies.

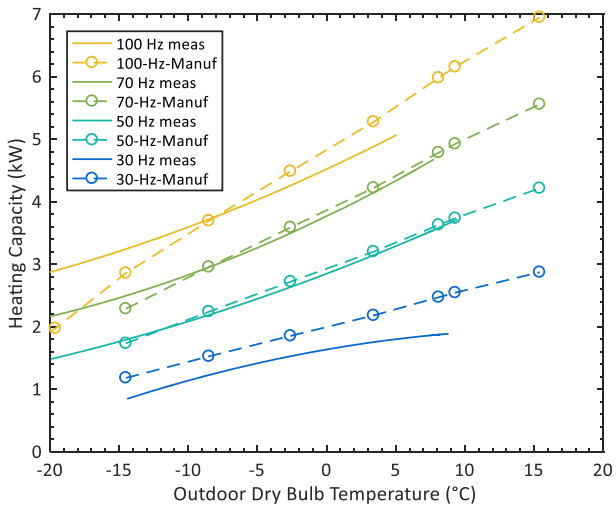


Figure 3-24: Steady state - Measured and manufacturer published heating capacity vs outdoor shed dry-bulb temperature for a variety of chosen frequencies

Measured heat output is generally close to manufacturer data (and even seems better than predicted at very low temperatures). Comparison at very low frequencies is impossible since the 10 Hz and 20 Hz bins are empty, while the 30 Hz frequency bin shows the greatest gap with manufacturer published capacity.

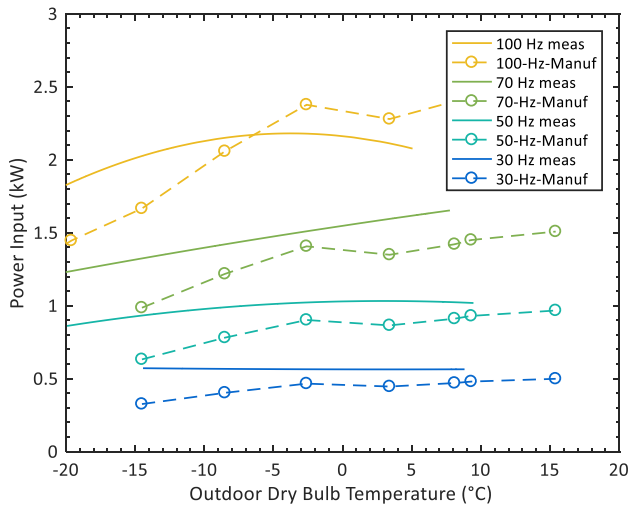


Figure 3-25: Steady state - Measured and manufacturer published power input vs outdoor dry-bulb temperature for a variety of chosen frequencies

In a similar fashion, comparison between measured and manufacturer published power input in Figure 3-25 revealed a larger power consumption than expected for every frequency, especially at lower outdoor temperatures. This situation leads to substantially lower than predicted manufacturer COP values for every frequency bin, as shown in Figure 3-26. The gap between measured and manufacturer data seems to increase as outdoor temperatures and frequencies decrease.

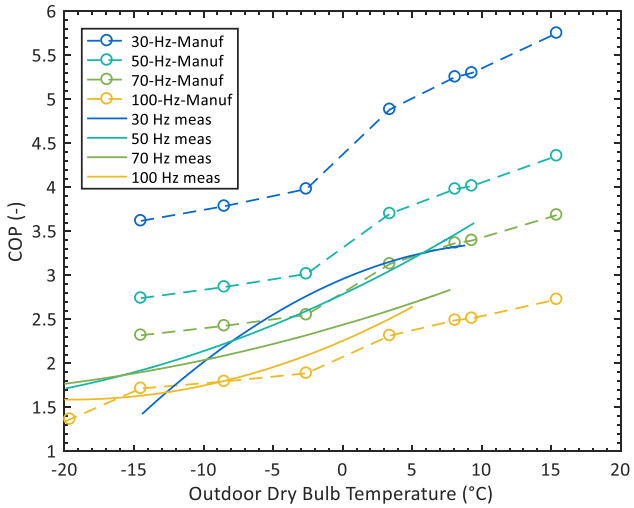


Figure 3-26: Steady state - Measured and manufacturer published COP vs outdoor shed dry-bulb temperature for a variety of chosen frequencies

### 3.4.4 Coefficients of determination

The coefficient of determination (R-squared) can help evaluate the accuracy of the polynomial linear regressions previously obtained for each frequency bin. It is defined in Equation (3.1), where $y_i$ is the measured dependent variable, $y_{mean}$ is the mean and $f_i$ is the estimated dependent variable with the curve fit.

$$R^2 = 1 - (SS_{res} - SS_{tot}) = 1 - (\sum(y_i - f_i)^2 / \sum(y_i - y_{mean})^2) \quad (3.1)$$

Data can be insufficient and/or too sparse in certain frequency bins, yielding a low r-squared value. Table 3-2 presents the r-squared capacity, power input and COP values for every frequency bin.

Table 3-2: Coefficients of determination for capacity and power input for every frequency bin.

| | | **Capacity** | **Power** | | | **Capacity** | **Power** |
|---|---|---|---|---|---|---|---|
| **Freq bin** | % data | R-square | R-square | **Freq bin** | % data | R-square | R-square |
| **20** | 0.0 % | NaN | NaN | **70** | 5.1 % | 0.9625 | 0.6250 |
| **25** | 8.3 % | 0.7420 | 0.0056 | **75** | 2.8 % | 0.9429 | 0.6248 |
| **30** | 6.7 % | 0.8877 | 0.0016 | **80** | 4.9 % | 0.8634 | 0.5775 |
| **35** | 4.4 % | 0.5950 | 0.0178 | **85** | 1.5 % | 0.8440 | 0.5313 |
| **40** | 5.8 % | 0.6632 | 0.0022 | **90** | 3.9 % | 0.8167 | 0.5948 |
| **45** | 4.5 % | 0.8991 | 0.0973 | **95** | 2.7 % | 0.7886 | 0.5185 |
| **50** | 5.6 % | 0.9382 | 0.214 | **100** | 3.3 % | 0.7084 | 0.5528 |
| **55** | 5.9 % | 0.9264 | 0.222 | **105** | 5.7 % | 0.5544 | 0.6009 |
| **60** | 7.7 % | 0.9328 | 0.4825 | **110** | 17.0 % | 0.5479 | 0.6432 |
| **65** | 4.2 % | 0.9215 | 0.2257 | **115** | 0.1 % | 0.0068 | 0.6212 |

Coefficients of determination are much too low in some frequency bins. A simpler and more accurate method is therefore required to express the test results in a form that could help build the VCHP model.

## 3.5 Multiple polynomial regressions

Instead of artificially grouping data points in frequency bins, multiple polynomial regressions can be used as previously described in Tang (2005). Curve fits with respect to outdoor shed temperature and frequency are obtained for capacity and power input (Equations 3.2 and 3.3).

$$Capacity\ (kW) = -0.864931 - 4.93855 * 10^{-5} * T_{out} + 9.94121 * 10^{-4} * {T_{out}}^2 + 9.23892 * 10^{-2} * freq - 3.69149 * 10^{-4} * freq^2 + 2.09704 * 10^{-3} * T_{out} * freq - 4.46009 * 10^{-7} * {T_{out}}^2 * freq - 9.79582 * 10^{-6} * T_{out} * freq^2 \quad (3.2)$$

$$Pwr\ input\ (kW) = 0.115655 + 6.11452 * 10^{-3} * T_{out} - 2.57571 * 10^{-5} * {T_{out}}^2 + 1.20659 * 10^{-2} * freq + 1.16796 * 10^{-4} * freq^2 - 3.63099 * 10^{-4} * T_{out} * freq + 7.71952 * 10^{-7} * {T_{out}}^2 * freq + 6.66687 * 10^{-6} * T_{out} * freq^2 \quad (3.3)$$

The mesh shown in Figure 3-27 represents the multiple polynomial regression for heat output with respect to outdoor shed temperature and compressor frequency. A similar figure is obtained for power input in Figure 3-28.

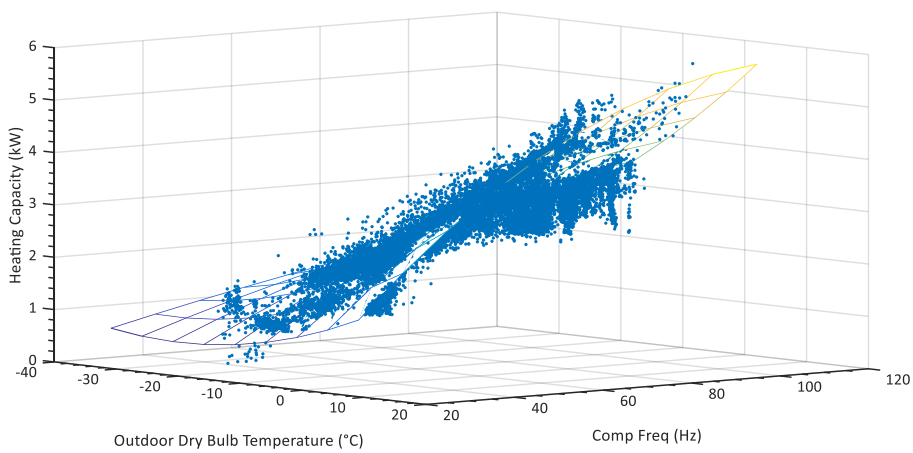


Figure 3-27: Multiple polynomial regression for heat output vs outdoor shed temperature and compressor frequency

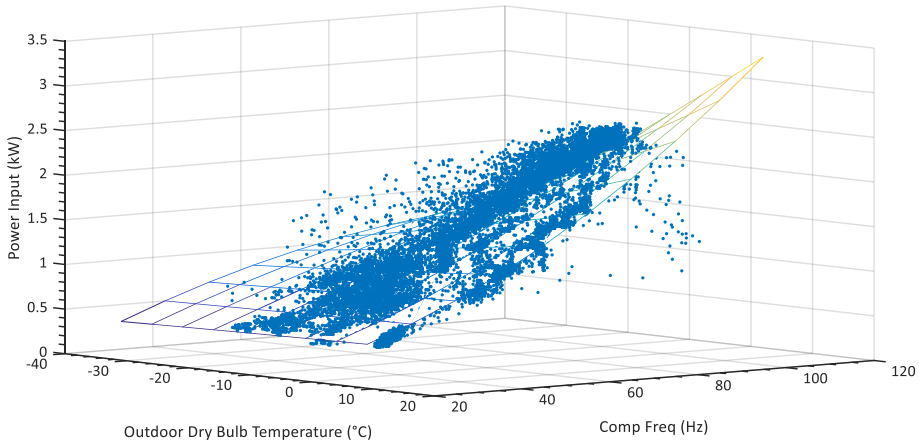


Figure 3-28: Multiple polynomial regression for power input vs outdoor shed temperature and compressor frequency

In both cases, it appears that the majority of data points can be reasonably approximated by the meshes, leading to much better r-squared ratios for capacity and power input (0.9299 and 0.9527, respectively). Moreover, this method is simpler than the frequency bins since only two multiple polynomial curve fits can reasonably estimate the VCHP performance for all data points.

Therefore, these multiple polynomial regressions are used to build the new model.

## 3.6 Conditions that trigger defrost cycles

The reverse cycle defrost control strategy of the observed unit is not fully understood at this stage. However, the manufacturer confirms it is related to outdoor temperature, outdoor unit temperature, humidity and a timer. Focusing on the last 5 min before each defrost cycle can help to learn about the conditions triggering this phenomenon. The average suction temperature 5 min before each defrost cycles is plotted against average temperature of the outdoor shed 5 min before each defrost cycles in Figure 3-29 (left), suggesting that a suction temperature close to the outdoor shed temperature might contribute to trigger a defrost cycle.

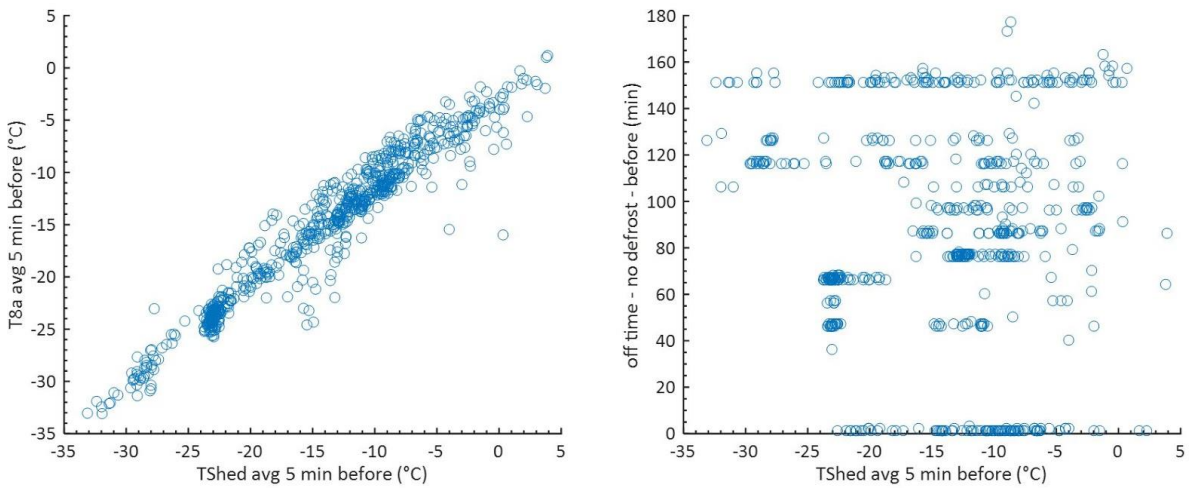


Figure 3-29: Influence of outdoor air and unit temperature (left) and timer (right) on defrost cycles

On the right of Figure 3-29, the potential role of a timer as a trigger for defrost cycle is also investigated. The vertical axis shows the number of minutes since the previous defrost, while the horizontal axis is once again the average temperature of the outdoor shed 5 min before each defrost cycles. It seems that the dots are regrouped on horizontal lines approximately every 10 min, with a minimal interval of 40 min and a maximum interval of 150 min between two defrost cycles. However, the influence of the outdoor shed temperature on the time span between defrost cycles remains unclear. Finally, dots that fall on the horizontal axis account for the second, third and fourth minutes of a defrost cycle. At these points, the number of minutes since the previous defrost is indeed zero.

The potential role of the humidity as a trigger for defrost cycles could not be investigated. Future work should include humidity monitoring in the test sheds.

## 3.7 Comparison with conventional heat pumps

Confronting VCHP and conventional heat pump performance can provide useful insights. Even though the accuracy of the frequency bin method remains debatable, it allows to compare test results with manufacturer data from four commercially available conventional heat pumps.

Once again, measured heat output and COP are approximated by polynomial curve fits for various 5 Hz wide frequency bins. Figure 3-30 presents the heating capacity - obtained from manufacturer data - of a 0.75 ton, 1.0 ton, 1.5 ton and 2.0 ton conventional heat pumps (dashed) opposed to measured VCASHP capacity at different frequencies.

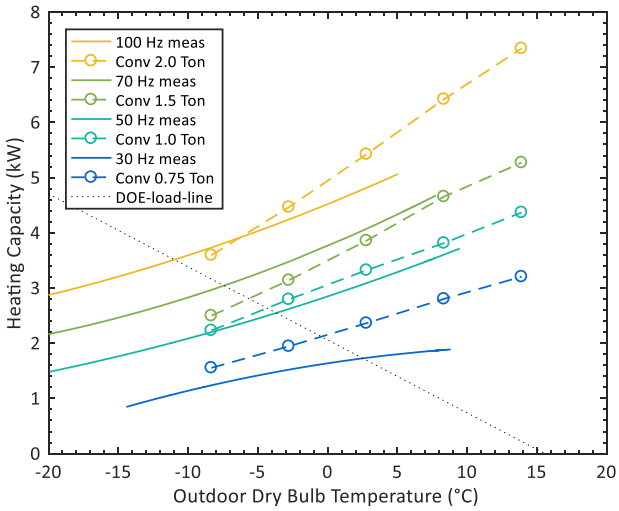


Figure 3-30: Comparing heating capacity between different sizes of conventional ASHPs and a VCASHP at different compressor frequencies (adapted from Kegel & McDonald 2015)

The alternative DOE load line from Rice et al. (2015) is the same as presented earlier in Equation (1.8).

Results show that the VCASHP can operate at much lower outdoor temperatures than the conventional heat pumps. Moreover, heating capacity at 100 Hz appears to be equivalent to a 2.0 ton conventional heat pump, while a mid-range frequencies can replicate the heat output of a 1.5 ton or 1.0 ton conventional heat pump. The VCASHP also shows a balance point at -11 °C (at 100 Hz), significantly lower than the four conventional heat pumps.

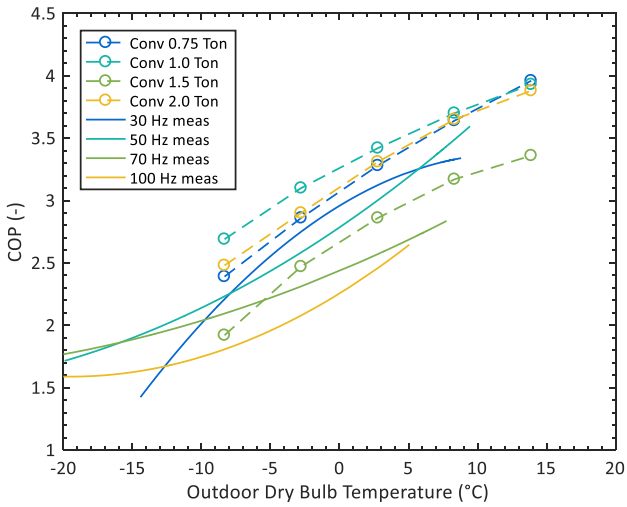


Figure 3-31: Comparing COP between different sizes of conventional ASHPs and a VCASHP at different compressor frequencies (adapted from Kegel & McDonald 2015)

Figure 3-31 compares VCHP performance to the conventional heat pumps in terms of COP. Below the balance point, COP ranges from 1.4 to 2.1, providing better energy saving potential than electric resistance heating.

For outdoor temperatures between -11 °C and -4 °C, VCHP compressor frequency decreases from 100 Hz to 60 Hz (according to the load line in Figure 3-30), raising the COP up to 2.5. This efficiency is comparable to - or slightly lower than - conventional heat pumps (except the 1.5 ton) at -4 °C.

For outdoor temperatures between -4 °C and 3 °C, compressor frequency decreases from 60 Hz to 30 Hz. The VCASHP is able to meet the load without cycling at a lower heating output than a 0.75 ton conventional heat pump. Again, conventional heat pumps (0.75 ton, 1.0 ton, 2.0 ton) offer a slightly better COP (from 2.3 to 3.4) than the VCASHP (from 2.0 to 3.1) for this temperature range.

Moreover, conventional heat pumps (0.75 ton, 1.0 ton, 2.0 ton) generally show a COP that is 0.3 higher than VCASHPs for mild outdoor temperatures.

In summary, the VCHP can operate with a COP higher than 1.0 at much lower outdoor temperatures than conventional heat pumps, which can be especially interesting in cold climate

and/or where electricity rates are generally high. However, for temperatures over -8 °C, the VCHP does not outperform the manufacturer data for conventional heat pumps (except the 1.5 ton).

## 3.8 Uncertainty analysis

The uncertainty of the main instruments - as detailed in Kegel & McDonald (2015) - is presented in Table 3-3.

Table 3-3: Uncertainty of main instruments

| **Instrument** | **Error** |
|---|---|
| Pressure transducers | ± 0.08 % |
| Thermocouple | ± 1 °C |
| Refrigerant mass flow rate | ± 0.2 %<br>± 1.5 % (below 25 % rated flow) |
| Power input Wattnode transducer | 0.5 % |
| Air flow meter | (Assumed ± 20 %) |

As explained previously in section 2.2.2 – “Air side”, the rudimentary method used to measure the air volumetric flow during the last week of testing induced a considerable uncertainty that is estimated at ± 20 %.

Figure 3-32 shows the evolution of enthalpy and refrigerant temperature at the indoor heat exchanger inlet and outlet ($h_4$, $h_6$, $T_4$, $T_6$, respectively) during a typical night of testing.

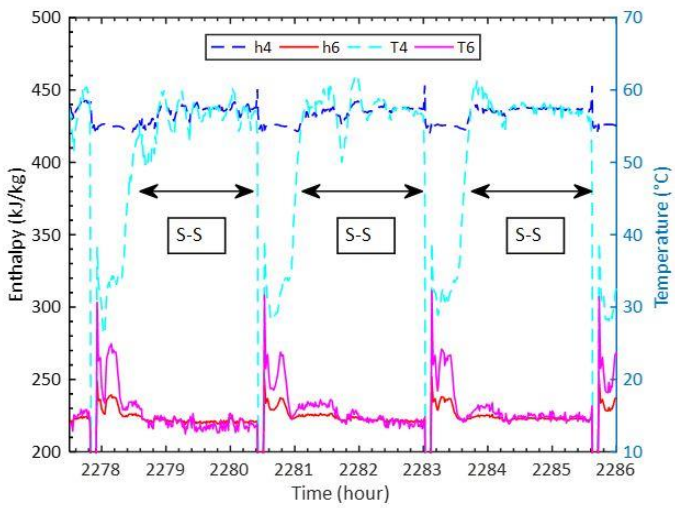


Figure 3-32: Evolution of enthalpy and refrigerant temperature at the indoor exchanger inlet and outlet

For steady-state data (S-S), the largest variations in refrigerant temperature (approximately 10 °C) yield a relatively small variation in enthalpy of approximately 15 kJ/kg. Therefore, it can be safely assumed that an uncertainty of ± 1 °C on temperature is equivalent to an uncertainty of ± 5 kJ/kg on enthalpy for $h_4$ and $h_6$, if we also account for the fact that temperature sensors are measuring the pipe surface temperature and not the refrigerant temperature. Absolute uncertainty on indoor HX refrigerant enthalpy difference between inlet and outlet is determined as follows:

$$u\,(\Delta h_{indoorHX}) = \sqrt{u(h_4)^2 + u(h_6)^2} \tag{3.5}$$

$$= \sqrt{5^2 + 5^2} = \pm\, 7.1\ kJ/kg$$

Based on Equation (2.1) and Table 3-3, relative uncertainty on heat output calculated on the refrigerant side can be estimated by Equation (3.).

$$\delta Q_{ref\ side} = \sqrt{\delta \dot{m}_{ref}{}^2 + \delta \Delta h_{indoorHX}{}^2} \tag{3.6}$$

$$= \sqrt{0.015^2 + \left(\frac{7.071}{425 - 225}\right)^2} = \pm 3.8\ \%$$

The steady state heat output results previously presented in section 3.4.3 – "Analysis" are updated with their uncertainty in Figure 3-33. Error boxes are arbitrarily added on regression results at every 5 °C outdoor temperature interval. Results show good agreement with manufacturer data at intermediate compressor speeds. However, measured heat output at 30 Hz is significantly lower than manufacturer data. The advertised heating capacity at 100 Hz also seems overestimated, except at low outdoor temperatures where the measured data actually exceeds manufacturer data.

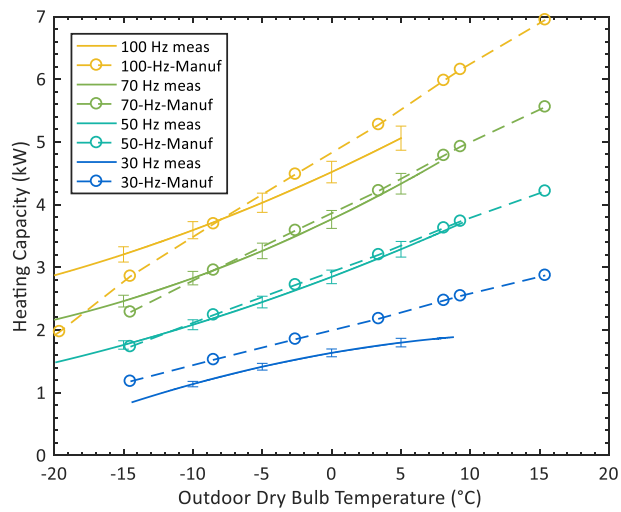


Figure 3-33: Steady state - Measured (with uncertainty) and manufacturer published heating capacity vs outdoor shed dry-bulb temperature for a variety of chosen frequencies

A similar approach is used for steady state COP in Figure 3-34. The highest compressor speed (100 Hz) is the only one for which the manufacturer value is partly contained within the uncertainty limits of the measured COP.

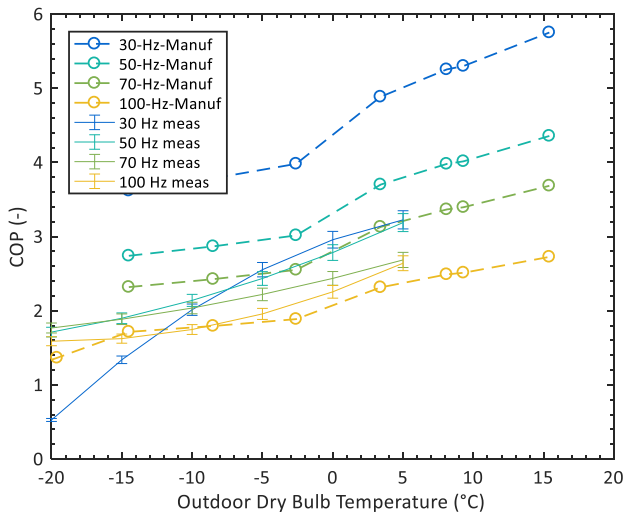


Figure 3-34: Measured (with uncertainty) and manufacturer published COP vs outdoor shed dry-bulb temperature for a variety of chosen frequencies

## 3.9 Influence of indoor temperature

Figure 3-35 shows the COP for low compressor frequency (30-50 Hz, identified as ‘o’) and high compressor frequency (90-112.5 Hz, identified as ‘+’) steady state data points with respect to outdoor dry-bulb temperature. The color bar indicates the indoor temperature distribution. As expected, most of the points are contained within a one degree margin of the chosen indoor setpoint for all the tests (21 °C). In some occasions - mostly at higher compressor speeds - the VCHP is unable to meet the load and reach the setpoint. This can be caused by higher loads than the maximum available capacity and/or the protection mechanisms described previously (see section 3.2.5 – “Protection mechanisms”). The highest indoor temperatures are generally recorded at lower compressor speeds and higher outdoor shed temperatures.

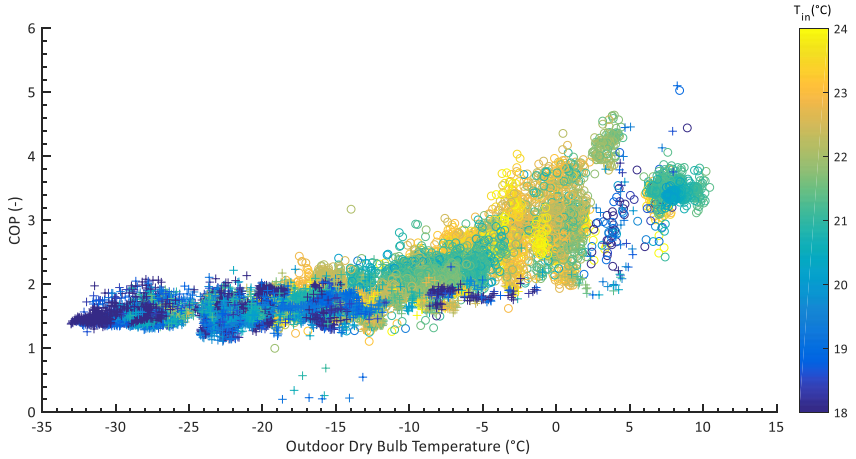


Figure 3-35: COP of low frequency (30-50 Hz, ‘o’) and high frequency (90-112.5 Hz, ‘+’) steady state data points with respect to outdoor shed dry-bulb temperature

# CHAPTER 4 THE MODEL

As mentioned previously, the objective is to use the test results to build a simple, effective and accessible VCHP model to help the market better understand the real potential of the technology. This chapter describes the approach behind this new VCHP model.

## 4.1 General approach

The modeling approach is inspired by Bouheret & Bernier (2018), as described earlier. A VCHP performance table based model is built in TRNSYS and relies on a PI controller. However, contrary to Bouheret & Bernier (2018), the model is meant for air-source VCHPs, which allows to trade the distributed approach for a new dedicated VCASHP type.

The existing TRNSYS conventional ASHP Type 954 (TESS 2012) is used as a starting point and modified in accordance with tests results to achieve a better mapping of VCASHP performance. Indeed, results show the clear impact of compressor frequency on VCASHP capacity and power. Therefore, frequency is introduced as a key variable to the new model.

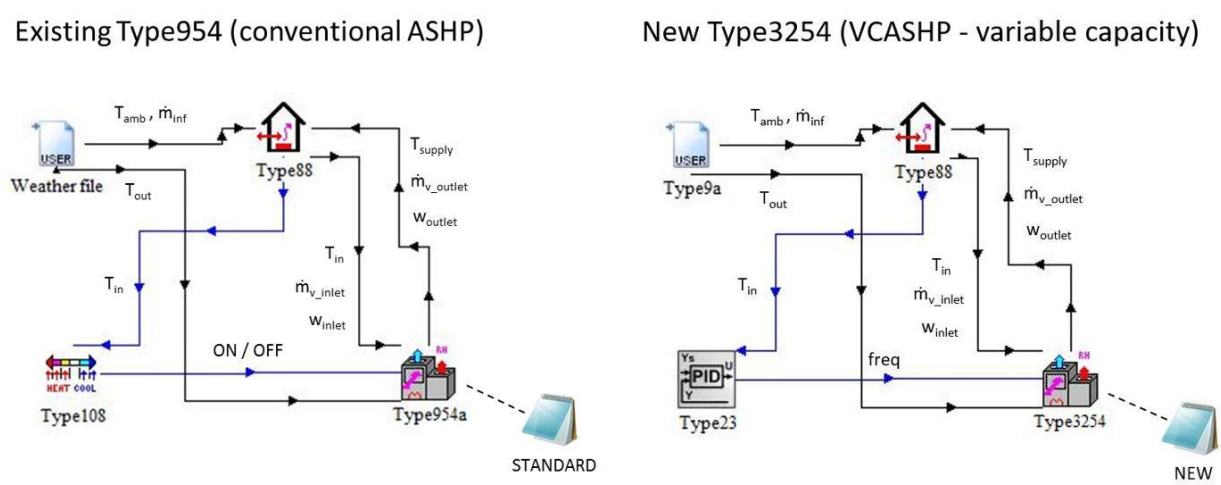


Figure 4-1: Typical ASHP model (left) compared to a typical new VCASHP model (right)

Figure 4-1 compares a conventional ASHP model (left) with a typical new VCASHP model (right). Type 108 ON/OFF controller (left) is replaced by a Type 23 PID controller (right) which sends a frequency signal that is received as an input by the new Type 3254. This frequency, divided by the

new rated frequency parameter, becomes a normalized frequency value that is used to interpolate in the new performance file to obtain the normalized capacity ratio. Multiplying it by the rated capacity of the VCASHP provides the heat output supplied to the building (Type 88 in this example). The updated indoor temperature of the building is then sent back to the Type 23 PID controller and compared to the setpoint to adjust the frequency. The same cycle is then repeated for every time step of the simulation. Note that for the specific case of this project, the outdoor temperature ($T_{out}$) is equivalent to $T_{outdoor_shed}$, and the indoor temperature ($T_{in}$) is equivalent to $T_{indoor_shed}$.

## 4.2 New performance file

The new Type 3254 uses a modified version of an existing standard TRNSYS performance file. User can refer to the Type 954 (TESS 2012) documentation for more information about this "standard" performance table, which contains normalized capacity and power ratios only at rated frequency. Furthermore, a handy Excel program is proposed to help users convert the standard performance file into a new performance file adapted for Type 3254 (see companion software provided with this thesis).

Figure 4-2 details the evolution from the standard to the VCHP performance table, adding one extra header row for normalized frequency steps, and numerous extra lines for normalized capacity and power ratios at each of these frequency steps.

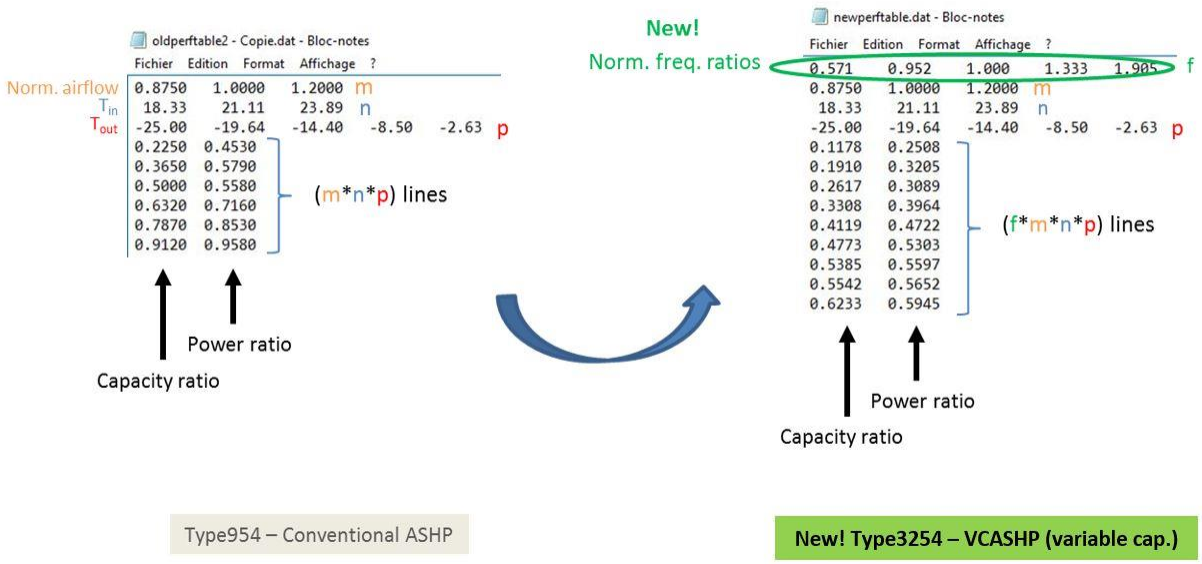


Figure 4-2: Conventional ASHP (left) compared to new VCASHP performance file (right)

The frequency correction factors needed for each of these steps can be obtained from detailed manufacturer data or experimental multiple polynomial regressions.

### 4.2.1 Manufacturer data based VCHP performance file

The simplest scenario ("Option 2") was described previously in section 3.4.2 – "How manufacturer data is obtained". Some manufacturers publish capacity and power input correction curves with respect to compressor speed (Figure 3-23). From these, the user can extrapolate a capacity and power input correction factor for each of the chosen frequency steps (Table 4-1). Adding these factors to the "Option_2" tab then allows the Excel program to multiply them by manufacturer data at rated speed to generate the new VCHP performance table.

Table 4-1: Capacity and power input correction factor vs frequency

| **Freq (Hz)** | **Capacity correction factor (-)** | **Power correction factor (-)** |
|---|---|---|
| 20 | 0.4 | 0.32 |
| 30 | 0.62 | 0.48 |
| 40 | 0.77 | 0.68 |
| 50 | 0.91 | 0.93 |
| 52.5 | 1 | 1 |
| 60 | 1.07 | 1.16 |
| 70 | 1.2 | 1.45 |
| 80 | 1.32 | 1.8 |
| 90 | 1.42 | 2.14 |
| 100 | 1.5 | 2.45 |

Other manufacturers only provide performance data at rated frequency (“Option_1”). In this case, the user can estimate the effect of frequency based on the unit tested in this study. Converting manufacturer curves to normalized frequency curve fits (Figure 4-3) allows to estimate the correction factors for different VCASHP sizes and compressor speeds. Indeed, the Excel program only needs the rated frequency of the unit, two or more frequency steps, and manufacturer data at rated speed to create the VCHP performance table.

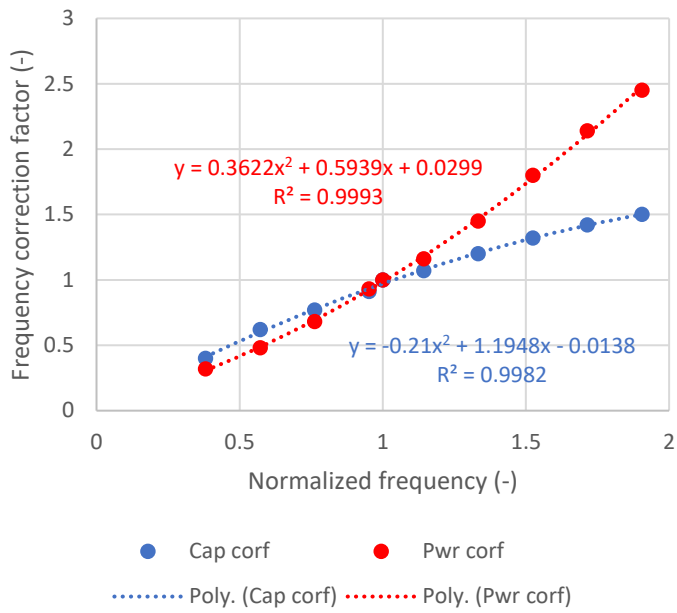


Figure 4-3: Frequency correction factors vs normalized frequency curve fits for capacity (blue) and power (red)

### 4.2.2 Regression-based VCHP performance file

In some cases, it can be more convenient to use multiple polynomial regression coefficients. As seen before in section 3.5 – "Multiple polynomial regressions", the user can express the VCHP capacity and power input as functions of outdoor temperature and compressor frequency. The Excel program included in the companion software will then use the multiple polynomial equations to calculate the normalized capacity and power ratios in the performance table for every combination of outdoor temperature and frequency.

Once again, two scenarios exist. User-specified coefficients can be added to the "Option_3b" tab of the Excel file. If these coefficients are not available, the user can also rely on the coefficients found in the tab "Option_3a". These were obtained in section 3.5 – "Multiple polynomial regressions" from the unit tested in this study, and can help to grossly estimate the performance of other VCHP units.

The regression approach has one important limitation, as it currently does not consider the effect of indoor temperature and air flow on VCHP performance. Indeed, since the normalized capacity

and power input ratios are only calculated as functions of the outdoor temperature and frequency, they remain the same for every indoor temperature and air flow steps found in the performance table header rows.

Future work should focus on the impact of these variables on VCHP performance, knowing that the manufacturer data table presented in section 3.4.2 – "How manufacturer data is obtained" showed variations of up to 10 % depending on the indoor temperature.

### 4.2.3 Fortran executable

A Fortran executable is also included in the companion software to help generate the VCHP performance files. The approach is similar to what has been described previously for the Excel program. The main difference is that both inputs and outputs are text files. The Fortran executable can therefore be useful if a standard TRNSYS text file with performance data at rated frequency already exists. This can save the user the elaborate task of manually (re)entering all the normalized capacity and power ratios in Excel. Instead, the Fortran executable combines a short text preprocessor with the standard TRNSYS text file to generate the VCHP performance table.

## 4.3 Two options to simulate defrost cycles

Multiple polynomial regressions - section 3.5 - were obtained with steady state data. However, as mentioned previously, global VCASHP performance is affected by defrost cycles. The user has the option of using the defrost integrated performance data given by a manufacturer if available (Type 3254b) or a second option of better taking into account the defrost cycles (Type 3254a), such as duration, frequency and recovery period.

## 4.4 Type 3254a – Dynamic model

To reproduce the dynamics of these defrost cycles, Type 3254a integrates new variables, as shown in Figure 4-4.

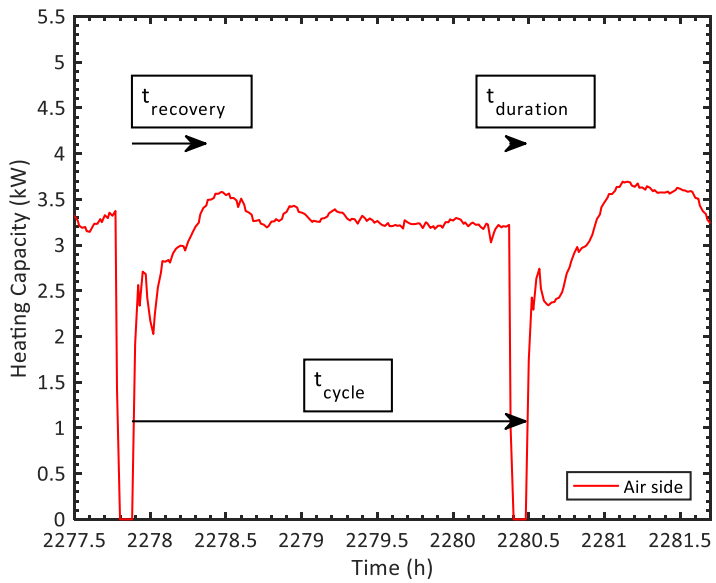


Figure 4-4: Reproducing the dynamics of defrost cycles with new variables $t_{cycle}$, $t_{recovery}$ and $t_{duration}$

The variable $t_{cycle}$ represents the length of a complete cycle, including the defrost phase ($t_{duration}$), while $t_{recovery}$ is the time following defrosts over which the transitory effects described previously occur. The user can set these variables manually to constant values, obtain them by linear regression with respect to outdoor temperature, or rely on default values based on experimental data. Type 3254a is recommended for small time steps – ideally 1 min – that should not exceed $t_{duration}$. It should obviously be used with performance data obtained in steady state conditions (outside of defrost periods).

As soon as the simulation time since last defrost is greater than the difference between $t_{cycle}$ and $t_{duration}$, the component operates in defrost mode. For the next $t_{duration}$ minutes, the VCASHP capacity is assumed to be zero, since the indoor fan is switched off. A correction factor of 0.6 is also applied on power input (not shown). Indeed, experimental data showed that adjusting power input at 60 % of its steady state value is a reasonable assumption during this period.

For $t_{recovery}$ minutes after defrost, the transient effects are modeled by an exponential penalty factor (Equation 4.1), similar to what was previously described with US DOE (2017, chap. 17.7.1.12).

$$RecovPnlty = 1 - \exp\left(\frac{-(t + \tau)}{\tau}\right) \tag{4.1}$$

$$\dot{Q}_{cond} = RatedCap * CapRatio * RecovPnlty \tag{4.2}$$

Indeed, this penalty factor (RecovPnlty) gets closer to 1 as 't' – current time step, in minutes – increases after defrost. Data suggests that selecting a time constant (τ) close to the difference between $t_{recovery}$ and $t_{duration}$ provides a good approximation of the transient effects. The penalty factor regulates the heat output for all time steps between 0 and $t_{recovery}$ minutes after defrost, as shown in Equation (4.2). The variable 'CapRatio' is the normalized capacity ratio extracted from the VCASHP performance table.

The default defrost cutoff temperature is set at 6 °C for the outdoor temperature. Figure 4-5 details the defrost simulation control strategy at every time step, including a special case where the cutoff temperature conflicts with the timer ($t_{cycle}$). Every simulation that has completed more than 50 % of a complete cycle at an outdoor temperature of less than 6 °C is automatically forced into defrost mode when the outdoor temperature raises over the cutoff temperature. This is meant to avoid a situation where the outdoor temperature would cycle around the cutoff temperature - each time resetting the counter $t_{cycle}$ - without ever getting the simulation into defrost mode. In reality, an ice layer would form on the evaporator under these conditions and would need to be removed by a defrost cycle.

Future work should also consider the influence of outdoor relative humidity in this defrost simulation control strategy.

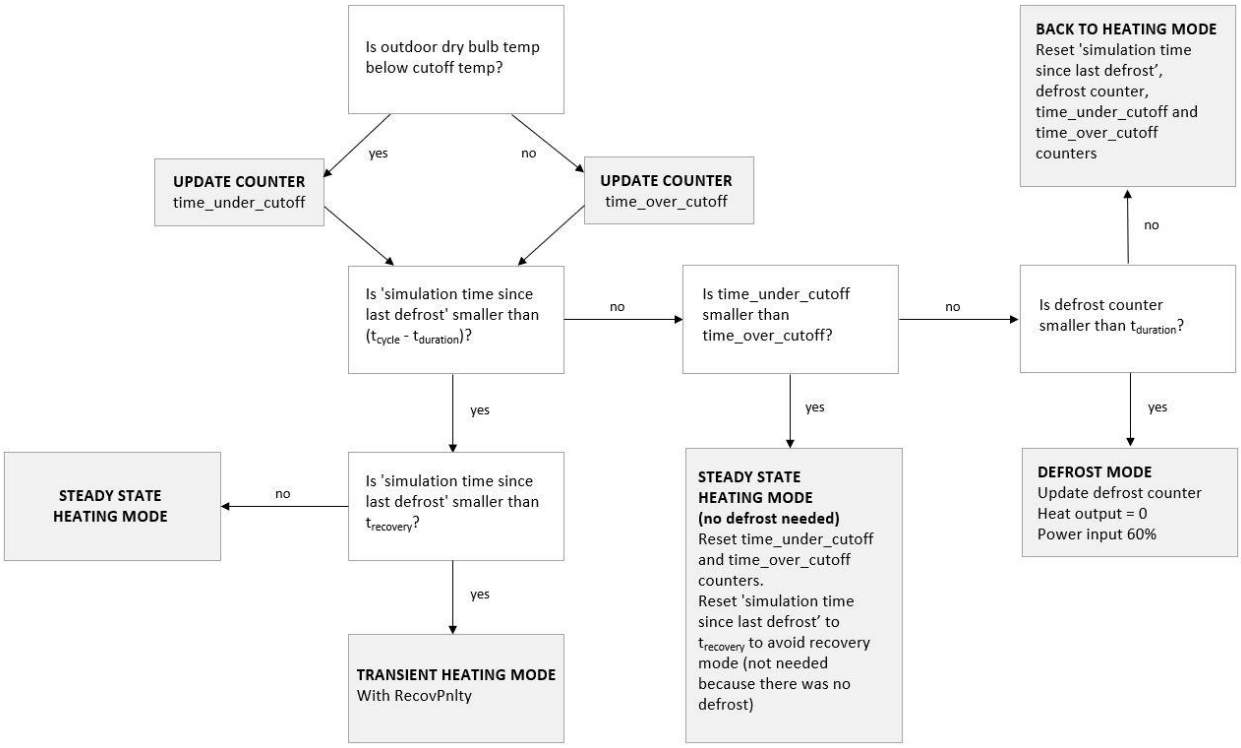


Figure 4-5: Defrost simulation control strategy at every time step

## 4.5 Type 3254b – Pseudo-steady-state model

This model is recommended for larger time steps and hourly simulations. As explained previously, Type 3254b applies a defrost penalty ratio to the simulated heat output at every time step to compensate the energy lost during defrost (Equation 4.3).

$$\dot{Q}_{cond} = RatedCap * \ CapRatio * DefrostPnlty \tag{4.3}$$

User can set the penalty (DefrostPnlty) manually, obtain it by linear regression with respect to outdoor temperature, or rely on a default value based on experimental data.

This model can also be used if manufacturer data capacity and power ratios already take defrost cycles into account. In that case, this (additional) defrost penalty ('DefrostPnlty') would be set to 1.0.

This penalty ratio is similar to the degradation coefficient proposed by Filliard (2009). And as in Type 3254a, the default defrost cutoff temperature is set at 6 °C for the outdoor temperature.

## 4.6 From Type 954 to Type 3254: modifications to the TRNSYS Proforma (tmf file) and Fortran code

The new parameters and inputs presented earlier are introduced in the VCASHP tmf file (Simulation Studio visual interface), using the conventional ASHP Type 954 as the foundation. The additions for Type 3254a and Type 3254b are shown in Table 4-2 and Table 4-3, respectively.

Table 4-2: New parameters and inputs for Type 3254a

| # | Name | Role | Unit |
|---|---|---|---|
| **24** | # of compressor frequency steps | Parameter | - |
| **25** | Rated compressor frequency | Parameter | $s^{-1}$ |
| **26** | Defrost simulation mode | Parameter | - |
| **27** | Defrost cutoff temperature | Parameter | °C |
| **28** | Duration of cycle | Parameter | min |
| **29** | Duration of recovery | Parameter | min |
| **30** | Duration of defrost | Parameter | min |
| **31** | Recovery time constant | Parameter | min |
| **32** | 1st-order Duration of cycle | Parameter | min * $°C^{-1}$ |
| **33** | 1st-order Duration of recovery | Parameter | min * $°C^{-1}$ |
| **34** | 1st-order Duration of defrost | Parameter | min * $°C^{-1}$ |
| **35** | 1st-order Recov. time constant | Parameter | min * $°C^{-1}$ |
| **23** | Compressor frequency | Input | $s^{-1}$ |

Table 4-3: New parameters and inputs for Type 3254b

| # | Name | Role | Unit |
|---|---|---|---|
| **24** | # of compressor frequency steps | Parameter | - |
| **25** | Rated compressor frequency | Parameter | $s^{-1}$ |
| **26** | Defrost simulation mode | Parameter | - |
| **27** | Defrost cutoff temperature | Parameter | °C |
| **28** | Defrost penalty | Parameter | - |
| **29** | 1st-order Defrost penalty | Parameter | $°C^{-1}$ |
| **23** | Compressor frequency | Input | $s^{-1}$ |

Parameter #26 allows to set the defrost simulation mode, where "1" is the dynamic (Type3254a) and "2" is the derating (Type3254b) approach. The defrost cutoff temperature sets the outdoor temperature limit under which defrost cycles occur.

The new defrost variables - $t_{cycle}$, $t_{recovery}$, $t_{duration}$, $\tau$ (Type 3254a) and *DefrostPnlty* (Type 3254b) - can be expressed as a 1st degree polynomial equation. Parameters #32 to #35 (Type3254a) and parameter #29 (Type3254b) are equivalent to the 1st order coefficient 'a' in Equation (4.4), while parameters #28 to #31 (Type3254a) and parameter #28 (Type3254b) are equal to 'b'. The user can set the 1st order coefficient to zero to express the new defrost variables as constant values.

$$New\ defrost\ variable = a * T_{out} + b \tag{4.4}$$

The complete Fortran code for Type 3254a and Type 3254b is available within the companion software provided with this thesis. The main additions to the Type 954 code concern the new VCASHP performance file - the interpolation vector now has a fourth variable, labelled as x(4) = freq/Rated_freq - and the defrost simulation control strategy detailed earlier in this chapter.

# CHAPTER 5 SIMULATION RESULTS

With Type 3254 and its new performance file in hand, it is now possible to perform simulations with the new VCASHP model. Using the outdoor temperature as the only measured input to the model, the result of these simulations is compared to the measurements to evaluate the accuracy of the new VCASHP model.

The TRNSYS simulation studio file is assembled exactly as shown previously in Figure 4-1. Data for the following simulation results is obtained on April 4-5th 2017 during a typical night of testing. Figure 5-1 reveals that ambient temperature ranges between 1 °C and 3 °C, and the temperature of the outdoor shed - seen by the evaporator - is maintained between -18 °C and -15 °C during steady-state operation (outside defrost).

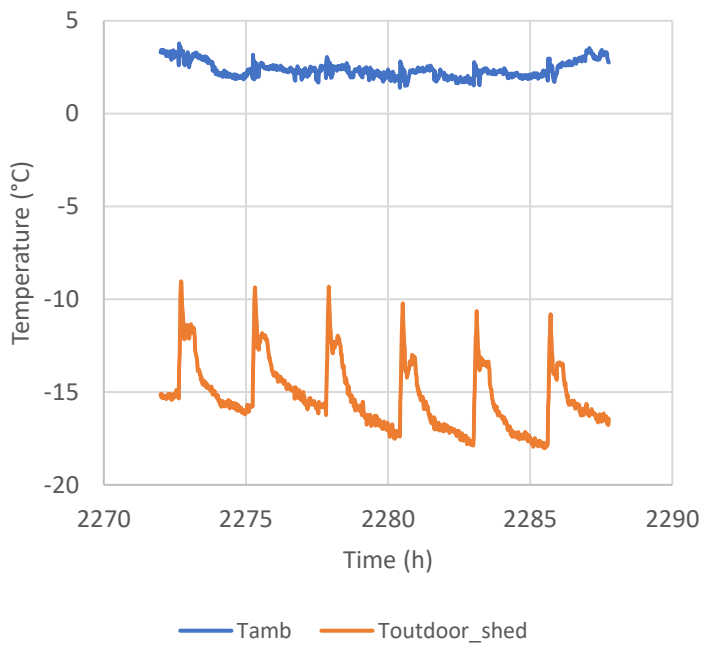


Figure 5-1: Ambient and outdoor shed temperature on April 4-5th, 2017

The indoor shed fresh air fan speed is controlled by the Raspberry Pi to maintain a load of approximately 10 000 Btu/h throughout the test. Previous results showed that this heating load is equivalent to the maximum heat output of the tested VCASHP unit under these conditions.

This dataset is selected for analysis because it is one of the very few where both heat output on refrigerant and air side were monitored, since the air flowmeter presented in the Methodology chapter was only introduced during the last week of testing.

## 5.1 Type 3254a – Dynamic model

Simulations use a time step of 1 min and an indoor setpoint of 21 °C. The variables $t_{cycle}$, $t_{recovery}$, $t_{duration}$ and the time constant ($\tau$) are set manually to constant values matching the results (156 min, 30 min, 6 min and 24 min, respectively), since experimental data does not provide reliable linear regressions with respect to outdoor temperature. The controller gain constant and integral time are respectively set to 10 min and 1 min.

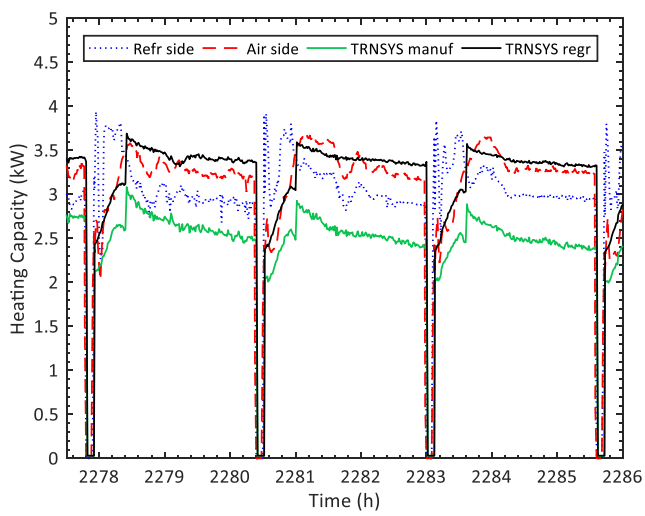


Figure 5-2: Type 3254a: Comparing measured (refrigerant and air side) to simulated heat output (manufacturer and regression performance table)

The measured heat output is compared to simulation results in Figure 5-2. The first simulation relies on a new VCASHP performance table based on manufacturer data, while the second one uses a performance table developed with the multiple polynomial regressions obtained previously.

The dataset and time frame are the same as in Figure 3-4. For both simulations, Type 3254a is able to simulate defrost cycles dynamically. Moreover, the simulation based on regressions provides the best estimation of the VCASHP heat output.

Discrepancies with the manufacturer data simulation are partially caused by what was seen previously in Figure 3-33. Indeed, measured heat output is higher than predicted by manufacturer data at very low temperatures (i.e., -15 °C outdoor and below). Incomplete manufacturer data can also explain the discrepancies with regression-based simulations. No performance data is provided over 100 Hz, while test results show that the unit can operate at a maximum compressor speed of 112.5 Hz. Since TRNSYS does not extrapolate over the limits of the performance table, simulated VCASHP performance at maximum speed is the same as at 100 Hz. However, test results and multiple polynomial regressions show that the VCASHP capacity and power input can increase significantly from 100 Hz to 112.5 Hz. Simulations close to maximum compressor speed like this one (more details concerning frequency will follow) are therefore susceptible to create wider performance gaps between the manufacturer data and the regression-based performance files.

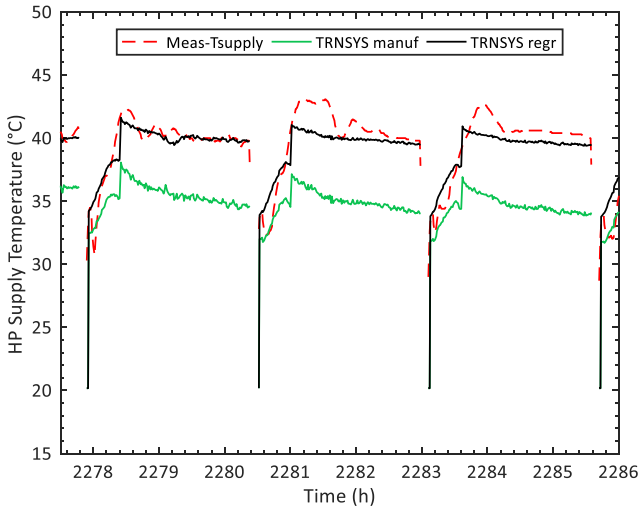


Figure 5-3: Type 3254a: Comparing measured to simulated supply temperature (manufacturer and regression performance table)

In a similar fashion, the measured VCASHP supply temperature is compared to simulation results in Figure 5-3. The performance table based on regressions seems to provide a better estimation of

the supply temperature than manufacturer data. Moreover, evaluation of the supply temperature is considered irrelevant during defrost cycles, since the indoor fan is temporarily turned off.

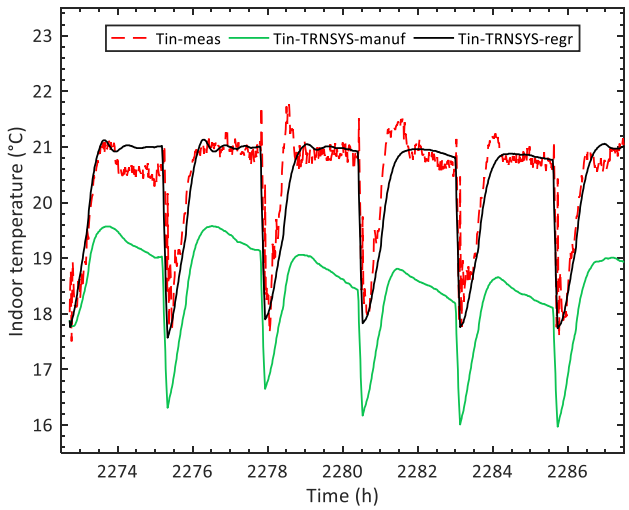


Figure 5-4: Type 3254a: Comparing measured to simulated indoor temperature (manufacturer and regression performance table)

Figure 5-4 compares measured indoor temperature to simulation results for Type 3254a. A wider time frame is introduced to provide an overview of the different measured indoor temperature profiles for each cycle. In general, the regression-based performance table allows to adequately simulate the measured indoor temperature, consistently reaching the 21 °C setpoint at steady state.

As expected, the simulation using the published manufacturer data leads to a much lower indoor temperature. Indeed, its underestimation of the heat output and supply temperature – as seen previously in Figure 5-2 and Figure 5-3 – prevent the model from maintaining the building temperature closer to the indoor setpoint.

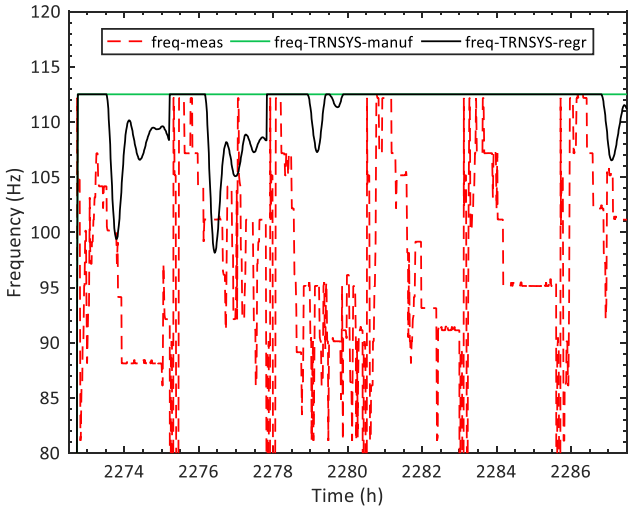


Figure 5-5: Type 3254a: Comparing measured to simulated frequency (manufacturer and regression performance table)

Moreover, the different measured indoor temperature profiles for each cycle seem to be linked with variations in measured compressor frequency. Figure 5-5 reveals significant discrepancies between measured and simulated compressor frequency. This seems to be caused by a protection mechanism limiting the VCASHP frequency. As explained earlier (section 3.2.5 – "Protection mechanisms"), the control strategy and the implications of this operation are not fully understood at this stage. However, the manufacturer service manual and previous work (Bertsch and Groll 2008) do confirm that a high discharge temperature - generally around 110-120 °C - can trigger a drastic reduction in frequency to prevent the compressor from overheating.

The surprising part is mostly that the VCASHP is able to reduce the compressor speed in steady state with little impact on the measured heat output, supply temperature and indoor temperature. Since the model does not simulate refrigerant temperature, it does not take this protection mechanism into account. This leads to a slight overestimation of the VCASHP power input in steady state, as seen in Figure 5-6.

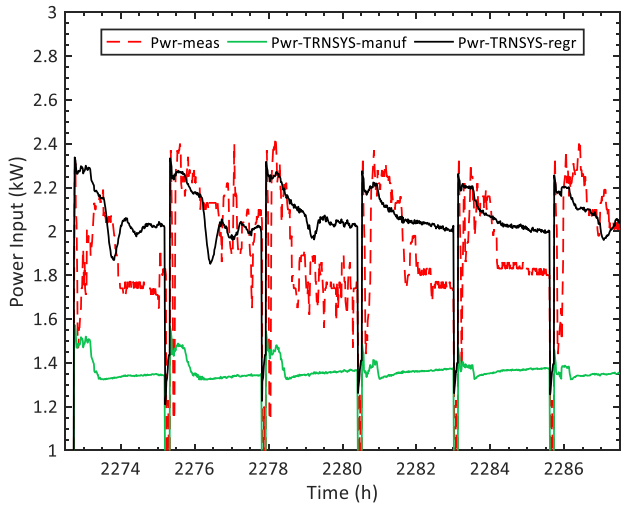


Figure 5-6: Type 3254a: Comparing measured to simulated power input (manufacturer and regression performance table)

Finally, another simulation is performed with a time step and a controller integral time of 5 min. Figure 5-7 compares measured heat output to simulation results. As expected, a time step that is not sufficiently smaller than the duration of defrost ($t_{duration}$) induces an increasing offset at every cycle. This suggests that the use of the pseudo-steady-state model (Type 3254b) is more suitable for larger time steps, especially if the dynamic behaviour of the defrost does not need to be modeled.

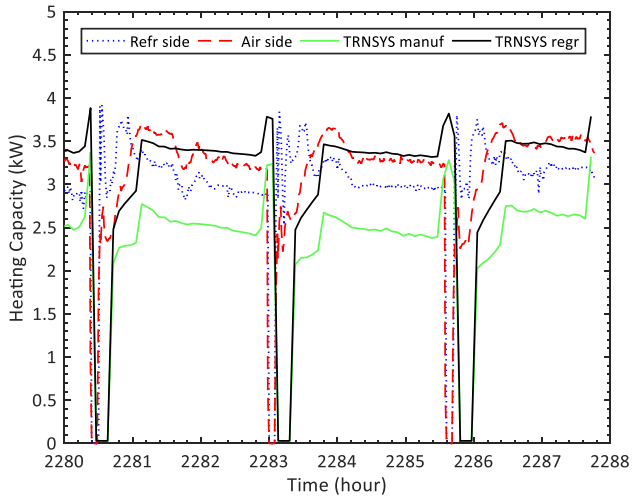


Figure 5-7: Type 3254a: Simulation of heat output with a timestep of 5 min

## 5.2 Type 3254b – Pseudo-steady-state model

A simulation is performed with a time step and controller integral time of 10 min, and with an indoor setpoint of 21 °C. Experimental data is not suitable to apply a linear regression to take into account the defrost penalty. It is therefore manually set to 0.9. Indeed, as shown by the area under the curve in Figure 5-2, the energy lost during defrost cycles can be approximated to 10 % of the steady state energy provided by the VCASHP.

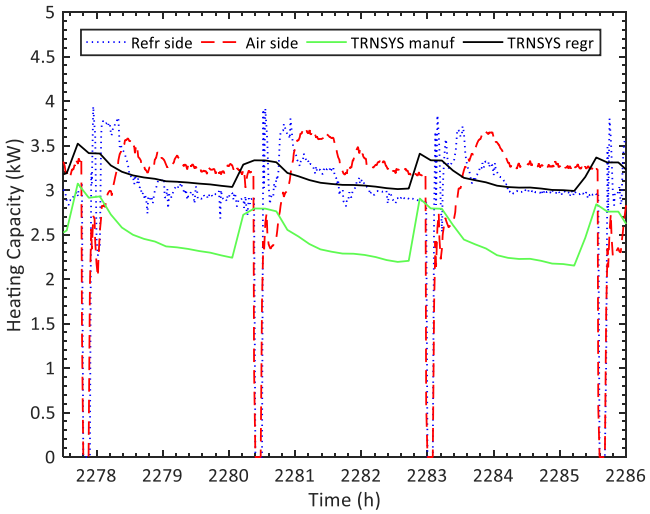


Figure 5-8: Type 3254b: Comparing measured (refrigerant and air side) to simulated heat output (manufacturer and regression performance table)

The measured heat output is compared to simulation results in Figure 5-8. The regression-based performance table provides a mostly constant simulated heat output, that remains slightly lower than the measured heat output because of the defrost penalty. More importantly, the area under the simulated and measured curves is equivalent, meaning that the total energy delivered to the building is adequately simulated. The small simulation peaks over each defrost cycle should be ignored, since they are caused by a temporary increase of the outdoor temperature in the testing chamber during the defrost process. This behavior is unlikely to be encountered through normal usage. As seen previously with Type 3254a, the performance table based on manufacturer data leads to an underestimation of the heat output under these conditions.

Figure 5-9 compares measured indoor temperature to simulation results for Type 3254b. Once again, the regression-based simulation provides a closer approximation of the indoor temperature than the manufacturer data performance table.

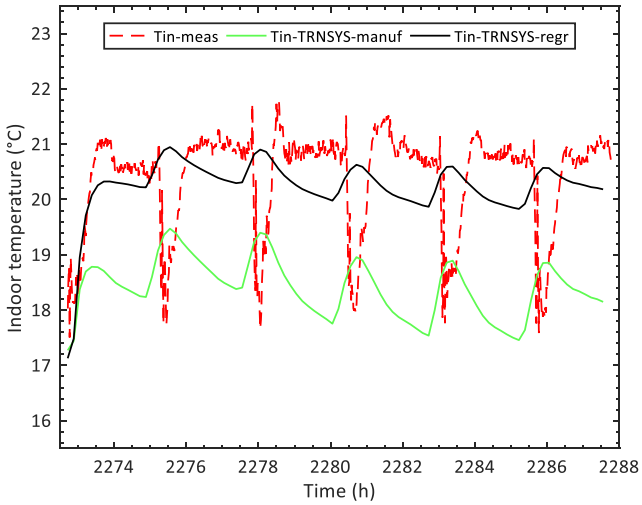


Figure 5-9: Type 3254b: Comparing measured to simulated indoor temperature (manufacturer and regression performance table)

The temporary increase of the outdoor shed temperature described previously also leads to an overestimation of the building indoor temperature during defrost cycles. As expected, the regression-based simulated indoor temperature remains slightly lower than the measured indoor temperature because of the defrost penalty.

# CHAPTER 6 CONCLUSION AND RECOMMENDATIONS

Although performance data published by manufacturers suggests that Variable Capacity Air-Source Heat Pumps (VCASHPs) can deliver much improved heating capacity and coefficient of performance compared to single-speed machines, laboratory and field tests have shown that the performance is not always matching the expectations. There is also a lack of flexible simulation models to allow designers to estimate energy savings. This thesis presents a simulation model that was developed using experimental data collected on a ductless (mini-split) VCASHP at the CanmetENERGY laboratory in Varennes.

Better mapping of VCHP performance was achieved by varying heating loads and user-defined outdoor temperatures, in addition to explicitly measuring the impact of compressor frequency. The multiple polynomial regressions obtained from this process allowed to build the new VCASHP model. The developed TRNSYS component can use a modified performance table including data at different compressor frequencies, or rely on multiple regressions to model the heating capacity, power input and coefficient of performance under different operating conditions. Defrost cycles are taken into account using a steady-state “derating” approach which is well adapted to long time steps (e.g. hourly), or using an original approach that models the defrost cycles dynamically, which is well adapted to short time steps (e.g. 1 min).

## 6.1 Contributions

The main contributions of this project are:

- A complete VCHP performance map was obtained by explicitly measuring compressor speed and performing tests for a variety of heating loads and on a large range of outdoor temperatures (including cold climate performance at very low temperatures)
- A simple and flexible model - specific to VCASHPs - accessible in TRNSYS, a renowned and widespread building simulation software.
- The possibility to dynamically model defrost cycles, to better help predict and understand their impact of VCASHP performance

## 6.2 Limitations

Despite the contributions listed above, this work also has some limitations:

- Heat output was only obtained on refrigerant side for most of the testing phase, yielding a high level of uncertainty on these values. Heat output validation on air side was only introduced during the last week of testing, with an approximation of the flowrate (only air speed was measured).
- This constraint limited the number of tests and the conditions (outdoor temperature, heating load) for which it was possible to validate the model. Indeed, the new component could only be validated in TRNSYS at high compressor speed, and at an outdoor shed temperature of -15 °C.
- Test results were only obtained in heating mode, for a single indoor setpoint (21 °C) and for one indoor unit fan speed (high)
- Wet-bulb outdoor temperatures provided by the manufacturer were converted to dry-bulb temperatures assuming a constant and arbitrary outdoor relative humidity, which might have affected the accuracy of the performance file. Humidity (indoor or outdoor) was not measured during the tests.
- The defrost cycle control strategy could not be fully understood, in part due to the fact that humidity was not monitored during the testing phase.
- Conditions triggering protection mechanisms and their implications on VCASHP performance remain unclear and introduced occasional noise that could not be removed from the steady state dataset.
- Although they can be used as a general indicator of VCASHP unit performance, the multiple polynomial regressions obtained in this study are technically only valid for the tested unit and its inherent characteristics. Moreover, the equations do not consider the influence of indoor temperature and indoor unit air flow on VCASHP performance.

## 6.3 Recommendations for future work

Future work should aim at replicating the explicit compressor speed methodology to validate the test results and performance curves in ASHRAE standard psychometric chambers, and with other ductless/ducted VCASHP systems (different manufacturers or sizes).

Heat output validation on air side should be obtained with an indoor unit air flow measurement nozzle, as described in Alexander et al. (1987). If not possible, high sensitivity measurement of the indoor unit fan power consumption and/or RPM could at least help to estimate the evolution of air flow.

Monitoring the relative humidity could also help to better understand the defrost cycle strategy, which could allow to express defrost length and off-time between defrost cycles in the VCASHP model as a function of outdoor temperature and/or humidity.

Tests should be performed in cooling mode, and for a variety of indoor setpoints and indoor unit fan speeds. Moreover, additional information could be gathered on protection controls - especially their triggers and implications - to find ways to incorporate them in the VCASHP model and better replicate the actual VCASHP performance under these conditions.

Multiple polynomial regressions should preferably be expressed in a non-dimensional form - as described in Tang (2005) - to facilitate their application to other VCASHP units. The indoor temperature could also be added as a third independent variable to calculate capacity and power input, so that multiple polynomial regressions would become a function of outdoor temperature, compressor frequency and indoor temperature. Indoor humidity should also be considered in cooling.

Finally, the accuracy of the model could be improved by offering the user the option to enter wet-bulb outdoor temperatures in heating, and avoid risky assumptions on relative humidity to convert values to dry-bulb temperatures. The new VCASHP model should also be validated for a wide variety of outdoor conditions and heating loads (or compressor speeds), leading to a more robust model that could provide engineers a reliable simulation tool to assess the appropriateness of widespread adoption of VCASHPs in Canada’s residential sector.

# BIBLIOGRAPHY

Air-Conditioning & Refrigeration Institute (ARI). 2005. *Unitary Air-Conditioning and Air-Source Heat Pump Equipment*. *Standard 210/240*. Vol. 552. Arlington, VA, USA: Air-Conditioning and Refrigeration Institute.

Air-Conditioning Heating and Refrigeration Institute. 2012. *Standard, Performance Rating of Unitary Air-Conditioning & Air-Source Heat Pump Equipment, ANSI/AHRI Standard 210/240 with Addenda 1 and 2*. *ANSI/AHRI Standard 210/240*. Vol. 2. Arlington, VA, USA: Air-Conditioning, Heating, and Refrigeration Institute.

Alexander, Linda L, Frederick J Reed, Alberto A DeRosa, Eugene L Valerio, Earl J Gmoser, Goerge S Yamamoto, Gerald P Jollette, et al. 1987. *Standard Methods for Laboratory Airflow Measurement*. Atlanta, GA, USA: American Society of Heating, Refrigerating and Air-Conditioning Engineers (ASHRAE).

Aye, Lu. 2007. "Heat Pumps." In *Encyclopedia of Energy Engineering and Technology - 3 Volume Set (Print Version)*, edited by BL Capeheart, 1st Ed., 814–821. Boca Raton, FL, USA: Taylor & Francis Group, vol. 2. doi:10.1201/9780849338960.ch96.

Bagarella, Giacomo, Renato M. Lazzarin, and Biagio Lamanna. 2013. "Cycling Losses in Refrigeration Equipment: An Experimental Evaluation." *International Journal of Refrigeration* 36 (8). Elsevier Ltd and IIR: 2111–2118. doi:10.1016/j.ijrefrig.2013.07.020.

Bell, Ian H, Jorrit Wronski, Sylvain Quoilin, and Vincent Lemort. 2014. "Pure and Pseudo-Pure Fluid Thermophysical Property Evaluation and the Open-Source Thermophysical Property Library CoolProp." *Industrial & Engineering Chemistry Research* 53 (6). American Chemical Society: 2498–2508. doi:10.1021/ie4033999.

Bertsch, Stefan S., and Eckhard A. Groll. 2008. "Two-Stage Air-Source Heat Pump for Residential Heating and Cooling Applications in Northern U.S. Climates." *International Journal of Refrigeration* 31 (7): 1282–1292. doi:10.1016/j.ijrefrig.2008.01.006.

Big Ladder Software LLC. 2014. "Performance Curves." https://bigladdersoftware.com/epx/docs/8-0/engineering-reference/page-114.html.

Blervaque, Hubert, Pascal Stabat, Sila Filfli, Mathieu Schumann, and Dominique Marchio. 2016.

"Variable-Speed Air-to-Air Heat Pump Modelling Approaches for Building Energy Simulation and Comparison with Experimental Data." *Journal of Building Performance Simulation* 9 (2): 210–225. doi:10.1080/19401493.2015.1030862.

Bouheret, Samuel, and Michel Bernier. 2018. "Modelling of a Water-to-Air Variable Capacity Ground-Source Heat Pump." *Journal of Building Performance Simulation* 11 (3): 283–293. doi:10.1080/19401493.2017.1332686.

Brandemuehl, M. J., S. Gabel, and I. Andresen. 1993. *HVAC 2 Toolkit: A Toolkit For Secondary HVAC System Energy Calculations*. Atlanta, GA, USA: American Society of Heating, Refrigerating and Air-Conditioning Engineers, Inc.

BSRIA. 2017. "BSRIA Global Air Conditioning Study Shows Contraction in 2016." https://www.bsria.co.uk/news/article/bsria-global-air-conditioning-study-shows-contraction-in-2016/.

Canadian Standards Association. 2017. *CSAEXP07 – Stakeholder Draft: Energy Performance of Split-System and Single-Package Air Conditioners and Heat Pumps, Draft Version April 24, 2017*. Mississauga, ON, Canada: CSA Group.

Cheung, H., S. Nyika, and J.E. Braun. 2011. *Performance Testing of Ductless Heat Pumps: Progress Report for February*. West Lafayette, IN, USA: Perdue University.

Cheung, Howard, and James E. Braun. 2014. "Performance Mapping for Variable-Speed Ductless Heat Pump Systems in Heating and Defrost Operation." *HVAC&R Research* 20 (5): 545–558. doi:10.1080/10789669.2014.917934.

Christensen, D, X Fang, J Tomerlin, J Winkler, and E Hancock. 2011. *Field Monitoring Protocol: Mini-Split Heat Pumps*. Oak Ridge, TN, USA: US Department of Energy.

Corberán, J. M., D. Donadello, I. Martínez-Galván, and C. Montagud. 2013. "Partialization Losses of ON/OFF Operation of Water-to-Water Refrigeration/heat-Pump Units." *International Journal of Refrigeration* 36 (8): 2251–2261. doi:10.1016/j.ijrefrig.2013.07.002.

Cummings, James B, and Charles R Withers. 2014. "Making the Case for Oversizing Variable-Capacity Heat Pumps Research Findings." In *Proceedings of the 18th ACEEE Biennial Summer Study on Energy Efficiency in Buildings, Pacific Grove, California, USA, August 17-22*, 42–54. Pacific Grove, CA, USA.

Cummings, James B, Charles R Withers, and Jamie Kono. 2015. *Cooling and Heating Season Impacts of Right-Sizing of Fixed and Variable-Capacity Heat Pumps With Attic and Indoor Ductwork*. Oak Ridge, TN, USA: US Department of Energy.

Davis, Robert, and Ben Larson. 2016. "Performance Testing of Variable Capacity Heat Pumps in the Pacific Northwest." In *Proceedings of the 19th Biennial ACEEE Conference on Energy Efficiency in Buildings, Pacific Grove, CA, USA, August 21-26*, 1–14.

Domanski, Piotr A. 1988. *Recommended Procedure for Rating and Testing of Variable Speed Air Source Unitary Air Conditioners and Heat Pumps*. Gaithersburg, MD, USA: U.S. Department of Commerce.

Ecotope Inc. 2014. *Final Summary Report for the Ductless Heat Pump Impact and Process Evaluation*. Portland, OR, USA: Northwest Energy Efficiency Alliance.

Energy Star. 2018. "Ductless Heating & Cooling." https://www.energystar.gov/products/heating_cooling/ductless_heating_cooling.

EPRI. 2014. *Variable-Speed Heat Pumps for Energy Efficiency and Demand Response - Field Testing High-Efficiency Systems in a Simulated-Occupancy Home in Knoxville, Tennessee*. Palo Alto, CA, USA: Electric Power Research Institute.

European Commission. 2016. "Renewable Energy Directive." https://ec.europa.eu/energy/en/topics/renewable-energy/renewable-energy-directive.

Filliard, Bruno. 2009. "Performance Evaluation of an Air-to-Air Heat Pump Coupled with Temperate Air-Sources Integrated into a Dwelling." In *Proceedings of the 11th International IBPSA Conference, Glasgow, Scotland, July 27-30*, 2266–2273. Glasgow, Scotland.

Francisco, Paul W, Larry Palmiter, and David Baylon. 2004. "Understanding Heating Seasonal Performance Factors for Heat Pumps." In *Proceedings of the 13th ACEEE Biennial Summer Study on Energy Efficiency in Buildings, Pacific Grove, California, USA, August 22-27*, 1.82–1.94. Pacific Grove, California, USA.

Gomes, A., C. Henggeler Antunes, and J. Martinho. 2013. "A Physically-Based Model for Simulating Inverter Type Air Conditioners/heat Pumps." *Energy* 50: 110–119. doi:10.1016/j.energy.2012.11.047.

Hamam, Y, and F Rocaries. 1983. “Mathematical Model of a Variable Capacity Heat Pump.” In *Proceedings of the 6th Miami International Conference on Alternative Energy Sources, Miami, Florida, USA, December 12–14*. Miami Beach, FLA, USA.

Hunt, Walter, Ron Domitrovic, and Jack Callahan. 2015. “Performance Characteristics of Residential Variable Capacity Heat Pump.” In *Proceedings of the 2015 ASHRAE Winter Conference, Chicago, IL, USA, January 24–28*, 1–9. Chicago, IL, USA.

Hunt, Walter, George Gurlaskie, and Ron Domitrovic. 2014. “Residential Heating Efficiency Comparison for Differing Heat Pump Types and Sizing Methods.” In *Proceedings of the 2014 ASHRAE Winter Conference, New York City, NY, USA, January 18-22*. New York City, NY, USA.

IEA Heat Pumping Technologies Program. 2017. “High Interest for Heat Pumps in China.” http://heatpumpingtechnologies.org/news/1/53323/.

Janssen, John E. 1999. “The History of Ventilation and Temperature Control.” *ASHRAE Journal* 41 (October): 48–70.

Jeon, Jongug, Sunil Lee, Daehie Hong, and Yongchan Kim. 2010. “Performance Evaluation and Modeling of a Hybrid Cooling System Combining a Screw Water Chiller with a Ground Source Heat Pump in a Building.” *Energy* 35 (5): 2006–2012. doi:10.1016/j.energy.2010.01.016.

Jin, Hui, and Jeffrey D. Spitler. 2002. “A Parameter Estimation Based Model of Water-To-Water Heat Pumps for Use in Energy Calculation Programs.” *ASHRAE Transactions* 108 (1). Atlantic City, NJ, USA: 3–17.

Karlsson, Fredrik. 2007. “Capacity Control of Residential Heat Pump Heating Systems.” Göteborg, Chalmers University of Technology.

Karlsson, Fredrik, Peter Lidbom, and Monica Axell. 2006. “Air-to-Air Heat Pumps Evaluated for Nordic Circumstances.” *IEA Heat Pump Centre Newsletter*.

Kegel, Martin, and Eric McDonald. 2015. *Cold Climate Ductless Split Heat Pump Preliminary Test Report*. Varennes, QC, Canada: Natural Resources Canada.

Kegel, Martin, Jeremy Sager, Martin Thomas, Daniel Giguere, and Roberto Sunye. 2017.

"Performance Testing of Cold Climate Air Source Heat Pumps." In *Proceedings of the 12th IEA Heat Pump Conference, Rotterdam, Netherlands, May 15-18*. Rotterdam, NLD.

Kegel, Martin, Roberto Sunye, and Justin Tamasauskas. 2012. "Life Cycle Cost Comparison and Optimisation of Different Heat Pump Systems in the Canadian Climate." In *Proceedings of eSim 2012 : The Canadian Conference on Building Simulation, Halifax, Nova Scotia, Canada, May 1-4*, 492–505. Halifax, NS, CAN.

Kegel, Martin, Justin Tamasauskas, Roberto Sunye, and Daniel Giguère. 2014. "Heat Pumps in the Canadian Residential Sector." In *Proceedings of the 11th IEA Heat Pump Conference, Montréal, QC, Canada, May 12-16*. Montréal, CAN.

Kim, Young Jin, Elena Fuentes, and Leslie K. Norford. 2016. "Experimental Study of Grid Frequency Regulation Ancillary Service of a Variable Speed Heat Pump." *IEEE Transactions on Power Systems* 31 (4): 3090–3099. doi:10.1109/TPWRS.2015.2472497.

Klein, S.A. 2016. *EES, Engineering Equation Solver, V10.190*. V10.190. F-Chart Software.

Lapsaa, Melissa, Gannate Khowailedb, Karen Sikesb, and Van Baxtera. 2017. "Heat Pumps in North America – 2017 Regional Report." In *Proceedings of the 12th IEA Heat Pump Conference, Rotterdam, Netherlands, May 15-18*. Rotterdam, NLD.

Larson, Ben, Bob Davis, Jeffrey Uslan, and Lucinda Gilman. 2013. *Residential Variable Capacity Heat Pump Field Study*. Portland, OR, USA: Bonneville Power Administration.

Le Lostec, Brice, and Hervé-Frank Nouanegue. 2014. "On-Site Performance of Air Source Heat Pumps." In *Proceedings of the 11th IEA Heat Pump Conference, Montréal, QC, Canada, May 12-16*, 1–13. Montréal, CAN.

Madani, Hatef, Joachim Claesson, and Per Lundqvist. 2011. "Capacity Control in Ground Source Heat Pump Systems: Part I: Modeling and Simulation." *International Journal of Refrigeration* 34 (6). Elsevier Ltd and IIR: 1338–1347. doi:10.1016/j.ijrefrig.2011.05.007.

Manteufel, Randall. 2014. "Intro Refrigeration Cycle, Vapor Compression." https://www.youtube.com/watch?v=QKQXd6taWak.

McDonald, Eric, and Martin Kegel. 2017. *Performance Standard Testing of Variable Speed Heat Pumps*. Varennes, QC, Canada: Natural Resources Canada.

Messmer, Craig. 2013. *Residential Cold Climate Heat Pump (CCHP) w/Variable Speed Technology*. Arnold, MO, USA: UNICO, Inc.

Mitsubishi Electric. 2013. *M-Series Contractor Guide*. Suwanee, GA, USA: Mitsubishi Electric Cooling & Heating.

Mitsubishi Electric Corporation. 2009a. *Outdoor Unit Service Manual for Models MUZ- FE09NA, MUZ-FE12NA & MUZ-FE18NA. No OBH543 REVISED EDITION-F*. Tokyo, JP: Mitsubishi Electric Corporation.

Mitsubishi Electric Corporation. 2009b. *Indoor Unit Service Manual for Models MSZ- FE09NA, MSZ-FE12NA & MSZ-FE18NA. No OBH542 REVISED EDITION-B*. Tokyo, JP: Mitsubishi Electric Corporation.

Mueller, Dale A., and Stephen L. Serber. 1980. *Heat Pump System Defrost Control*. USA: US Patent 4209994A, filed July 1.

Munk, Jeffrey, Christopher Halford, and Roderick Jackson. 2013. *Component and System Level Research of Variable Capacity Heat Pumps*. Oak Ridge, TN, USA: US Department of Energy.

Munk, Jeffrey, Adewale Odukomaiya, Roderick Jackson, and Anthony Gehl. 2014. *Residential Variable-Capacity Heat Pumps Sized to Heating Loads*. Oak Ridge, TN, USA: US Department of Energy.

Nakos, Helena, Haglund Stignor, Peter Lidbom, and Stefan Thyberg. 2014. "Air-to-Air Heat Pumps Evaluated for Nordic Climates- Trends and Standards." In *Proceedings of the 11th IEA Heat Pump Conference, Montréal, Québec, Canada, May 12-16*. Montréal, QC, CAN.

Nishihata, Hisashi. 2013. *Heat Pumps - Technology Policy Brief E19*. Masdar City, Abu Dhabi: IEA-ETSAP and IRENA.

Northeast Energy Efficiency Partnerships (NEEP). 2017a. *Cold Climate Air Source Heat Pump Specification-Version 2.0 Proposal*. Lexington, MA, USA.

Northeast Energy Efficiency Partnerships (NEEP). 2017b. *Guide To Sizing & Selecting Air-Source Heat Pumps in Cold Climates*. Lexington, MA, USA.

NRCan. 2004. *Heating and Cooling with a Heat Pump*. *EnerGuide*. Gatineau, QC, CAN: Natural Resources Canada's Office of Energy Efficiency.

NRCan-OEE. 2016. *Energy Efficiency Trends in Canada - 1990 to 2013*. Ottawa, ON, CAN: Natural Resources Canada, Office for Energy Efficiency.

Nyika, S, S O Holloway, W T Horton, and J E Braun. 2014. "Generalized Performance Maps for Variable-Speed, Ducted, Residential Heat Pumps." *ASHRAE Transactions* 120 (2): 80–89.

Quaschning, Volker. 2010. *Renewable Energy and Climate Change*. Chichester, UK: John Wiley & Sons. doi:10.1002/9781119994381.

Reay, D. A., and D. B. A. Macmichael. 1988. *Heat Pumps (2nd Ed)*. Oxford, England ; New York: Pergamon Press.

Rice, C. Keith, Jeffrey D. Munk, and Som S. Shrestha. 2015. *Review of Test Procedure For Determining HSPFs of Residential Variable-Speed Heat Pumps*. Oak Ridge, TN, USA: US Department of Energy.

Rice, C. Keith, Bo Shen, and Som S. Shrestha. 2015. *An Analysis of Representative Heating Load Lines for Residential HSPF Ratings*. Oak Ridge, TN, USA: US Department of Energy. doi:10.2172/1214506.

Sager, Jeremy, M Thomas, and Frank Szadkowski. 2014. *Cooling and Heating Season Performance Assessment of a Mini-Split Cold Climate Air Source Heat Pump*. Ottawa, ON, CAN.

Schoenbauer, Ben, Nicole Kessler, and David Bohac. 2016. "Field Assessment of Cold Climate Air Source Heat Pumps." In *Proceedings of the 19th Biennial ACEEE Conference on Energy Efficiency in Buildings, Pacific Grove, CA, USA, August 21-26*, 1–14. Pacific Grove, CA, USA.

SouthShore HVAC. 2017. "Why Bigger Isn't Better with Heat Pump Sizes." http://www.southshorehvac.ca/why-bigger-isnt-better-with-heat-pump-sizes/.

Standards Council of Canada. 2006. *Performance Standards for Split-System and Single- Package Central Air Conditioners and Heat Pumps*. Mississauga, ON, Canada: Standards Council of Canada, CAN/CSA- C656-05.

Tang, Chih Chien. 2005. "Modeling Packaged Heat Pumps in a Quasi-Steady State Energy Simulation Program." Oklahoma State University, OK, USA.

Tardif, Jalomi Maayan, Martin Kegel, John Scott, Justin Tamasauskas, and Michael Leonard. 2016. *Air Source Heat Pump Test Bench Operation and Maintenance Manual*. Varennes, QC, Canada: Natural Resources Canada.

TESS. 2012. *TESSLibs 17 - Component Libraries for the TRNSYS Simulation Environment*. Madison, WI, USA: Thermal Energy Systems Specialists.

The MathWorks Inc. 2016. *MATLAB Version 2016b*. Natick, MA, USA: The Mathworks Inc.

Transsolar. 2012. *TRNSYS 17 – A TRaNsient SYstem Simulation Program, User Manual. Version 17.1*. Madison, WI: University of Wisconsin-Madison.

U.S. Department of Energy. 1979. "Test Procedures for Central Air Conditioners." *Federal Register* 44 (249): 76,700-76,763.

US DOE. 2016. *Energy Conservation Program: Test Procedures for Central Air Conditioners and Heat Pumps*. 10 CFR Parts 429 and 430.

US DOE. 2017. *EnergyPlus Engineering Reference (v 8.8)*. Washington, DC, USA: US Department of Energy.

Waddicor, David A., Elena Fuentes, Marc Azar, and Jaume Salom. 2016. "Partial Load Efficiency Degradation of a Water-to-Water Heat Pump under Fixed Set-Point Control." *Applied Thermal Engineering* 106: 275–285. doi:10.1016/j.applthermaleng.2016.05.193.

Winkelmann, F.C., B.E. Birdsall, W.F. Buhl, K.L. Ellington, E. Erdem, J.J. Hirsch, and S. Gates. 1993. *DOE-2 Supplement (Version 2.1E)*. Berkeley, CA, USA: Lawrence Berkeley National Laboratory.

Winkler, J. 2011. *Laboratory Test Report for Fujitsu 12RLS and Mitsubishi FE12NA Mini-Split Heat Pumps*. Oakridge, TN, USA: US Department of Energy.

# APPENDIX A – COMPANION SOFTWARE PACKAGE

Description of the companion software package :

- Type 3254 : TRNYS component for VCHPs. Includes the Fortran code (Type3254.f90) for the dynamic version (Type 3254a) and the pseudo-steady-state version (Type 3254b), along with the tmf files, example files for both versions and the related external files.

- User manual for Type 3254

- Excel performance file generator : Excel program that generates a VCHP performance file based on manufacturer data and/or experimental results manually entered by the user. Instructions can be found on the first tab and on a separate README.pdf file.

- Fortran executable performance file generator : Fortran program (VCHPperf.exe) that converts an existing conventional HP performance text file (oldperftable3.dat) in a VCHP text file (newperftable.dat). If the conventional text file is available, this can save the user the elaborate task of manually (re)entering all the normalized capacity and power ratios in Excel. Instead, the Fortran executable combines a short text preprocessor (preprocessor3fmax.dat) with the standard TRNSYS text file to generate the VCHP performance table. Instructions are found on a separate README.pdf file. The Fortran code (Fortran_code_for_the_program.f90) that allowed to build the program is also part of the package.